Sudan University of Science and Technology
Graduate Studies

Effect of Magnetic Field Intensity on Dye Solar Cells

تأثير شدة المجال المغناطيسي على الخلايا الشمسية الصبغية

Thesis Submitted for the Degree "Doctor Philosophy"

Submitted by:

Nserdin Abdallah Ragab Abduelkreem

Supervised by:

Dr. Sawsan Ahmed Elhouri Ahmed

Co-Supervisor:

Dr. Ahmed Hassan Alfaki

August 2018

بسم الله الرحمن الرحيم

صدق الله العظيم

Dedication

I dedicate this thesis to the soul of

My Mother,

My Father,

To my Wife and my Son

To my all relatives and friends

Acknowledgment

Firstly Thanks to God to give me good health and doing well.I am greatly indebted to the following people, who made this thesis possible, I would like to express my deepest gratitude to my supervisor, Prof. Sawsan Ahmed Elhouri Ahmed for giving me the freedom of exploring my research interest, She has been very supportive and patience throughout this research despite my lack of knowledge on the subject. She also given me direction as to where my research should be focused on, for day-to-day supervision and guidance me. I must thank Dr. Ahmed Hassan Alfaki has endlessly given me advice and insightful ideas for my research. I would also like to thank Dr. Abdalsakhi. S. M. H for giving the support and guidance for laboratory part to my research, He has been kind enough to proofread this thesis and gave me valuable suggestions to improve this thesis. I am indebted to many of my colleagues to support me.

Abstract

In this work, we investigated the effect of magnetic field Intensity on Dye Solar Cells that made from 15 samples in three groups by three different dyes (Rhodamine B, Coumarin 500 and Eriochrome black T) when effect by magnetic field (0, 1, 2, 3 and 4) mT. The cells were fabricated from ITO which act as a cathode beside MEH PPV, (Rohadamin B, Coumarin 500 and Eriochrome black T) dye and anodes is (Ag). It was found that the efficiency of the solar cell increases with magnetic field increases by rated 1.5x10-4 %, 6.6x10-4 % and 7.4x10-7 % .mT-1 respectively, for Rhodamine B, Coumarin 500 and Eriochrome black T. Other effects on dye solar cells by magnetic field in the densities current, that increase of magnetic field increases densities current increase by conduction rated 7.8x10-4, 4.48x10-7 and 2.4x10-3 mA.cm-2 .mT-1, respectively for Rhodamine B, Coumarin 500 and Eriochrome black T. Otherwise detailed effect of energy band gaps on dye - sensitized solar cells (DSSCs) efficiency increase of energy band gaps decreases the efficiency of solar cell. This is since the energy band gaps increase enables electrons having lower excitation energy to become free electron in a conduction band thus decreasing the electric solar efficiency by rated 3% with 1 eV.

المستخلص

في هذا البحث، تمت دراسة تأثير شدة المجال المغناطيسي على الخلايا الشمسية الصبغية لعدد 15 عينة من الخلايا الشمسية الصبغية في ثلاث مجموعات صنعت بواسطة ثلاثة أصباغ مختلفة الرودامين ب، الكومارين 500 و إكروكورم الأسود تي، وتم تأثير عليها بواسطة المجالات التي تعمل كمهبط إلى جانب ITO المغناطيسية (0 ، 1 ، 2 و 3 و 4) ملي تسلا. صممت الخلايا من ،واحدى الصبغيات الرودامين ب، الكومارين 500 و إكروكورم الأسود تي، و أنود هو MEH PPV -x10وقد وجد أن كفاءة الخلية الشمسية تزداد مع زيادة المجال المغناطيسي بنسبة 1.5 (Ag) الفضة ملي على تسلا لكل من الرودامين ب، الكومارين 500 و % 7-x10و 7.4 % 4-6.6x10، % 4 إكروكورم الأسود تي، كما رصد تأثيرات أخرى على الخلايا الشمسية الصبغية عن طريق المغناطيسية المقدمة في كثافة التيار ، بحيث زيادة المجال المغناطيسي تزيد كثافة التيار بمقدار4 لكل من الرودامين ب، الكومارين mA.cm-2 .mT-1 3-x10و 2.4 7-4.48x10، -7.8x10 500 و إكروكورم الأسود تي. تمت دراسة تأثير فجوة الطاقة للصبغيات علي كفاءة الخلايا الشمسية زيادة فجوة الطاقة يقلل من كفاءة الخلية الشمسية، هذا لأن زيادة فجوة الطاقة لا (DSSCs)الصبغية تمكّن الإلكترونات ذات طاقة التهييج الأقل أن تصبح إلكترون حر في نطاق التوصيل وبالتالي تقلل من كفاءة الطاقة الشمسية الكهربائية بنسبة 3٪ لكل واحد الكترون فولت .

Table of Contents

Chapter One
Introduction

1.1 Prelude

Solar radiation is one of the alternatives available for the production of electrical power, that do not have traces or residues are injurious to the environment. They are convert incident light into electrical energy either by thermal conversion of the sun's energy in boilers solar and use the steam produced in the management of the turbine or by conversion light energy to electrical energy by solar cells [1, 2, and 3].

Solar cell is tool semiconductor that converts solar energy into electrical energy. Silicon is the best semiconductor material used today in the manufacture of the solar cell the wide spread of it is due to high ratio of the abundance of the silicon in the land cost of production is also reasonable and the efficiency is high compared to other cells, however silicon cells suffer from the high cost and difficulty of manufacturing beside complexity associated with the formation of crystals of silicon [4, 5 and 6].

This has led scientists to think in the manufacture of solar cells from other materials. So they veered scientists to mimic the way the plant do in converting the sun's energy across the chromosomes to useful energy. This resulted in their attempts for the manufacture of solar cells using polymers and dyes [7, 8, and 9].

1.2 Research Problem

The research problem comes from the fact that there are many factors that affect the performance and efficiency of solar cell. There are also factors concerned with the cost and manufacturing. Thus there is an urgent need to

know it. And study the effect of magnetic field intensity on dye solar cells efficiency.

1.3 Aim of the Work

The research aims to determine the impact of change of magnetic fields of dye solar cells on their performances and efficiency of the solar cell.

1.4 Presentation of the thesis

The thesis consists of the six chapters. Chapter one is the Introduction to Solar radiation, Solar cell, Aim of the Work and Problem and important of this Research, and since the first development of DSSCs in the early, different groups have introduced various methods of fabricating them. Chapter two is the theoretical background about solar cells and magnetic field. Chapter three the Literature Review. Chapter four consists of method, materials and Analysis explains the development of new polymer electrolytes based on DSSCs materials, the fabrication methods are described.

This involves the study of different electrolyte materials, titanium dioxide (TiO2) compact layers; a summary about the final working device is given. It also discusses the fabrication methods and characterization techniques used to evaluate the properties of polymer electrolytes and the final device structure. Chapter five Results and Analysis of this work was making three gropes of dye Solar cells with three different types of dyes (Rhodamine B, Coumarin 500 and Eriochrome black T). Chapter six is concerned about Conclusion and future works are presented. Further work is proposed with the hope of improving the ionic conductivity and thus the performance of DSSCs.

Chapter Two

Theoretical Background

2.1 Introduction

Photo electrochemical solar cells (PSCs), consisting of a photo electrode, a redox electrolyte, and a counter electrode, have been studied extensively. Several semiconductor materials, including single-crystal and polycrystalline forms of n- and p-Si, n- and p-GaAs, n- and p-InP, and n-CdS, have been used as photo electrodes. These materials, when used with a suitable redox electrolyte, can produce solar light-to-current conversion efficiency of approximately 10%. However, under irradiation, photo corrosion of the electrode in the electrolyte solution frequently occurs, resulting in poor stability of the cell, so efforts have been made worldwide to develop more stable PSCs [10]. Oxide semiconductor materials have good stability under irradiation in solution. However, stable oxide semiconductors cannot absorb visible light because they have relatively wide band gaps [11].Sensitization of wide band gap oxide semiconductor materials, such as TiO_2, ZnO, and SnO_2, with photo-sensitizers, such as organic dyes, that can absorb visible light has been extensively studied in relation to the development of photography technology since the late nineteenth century. In the sensitization process, photo-sensitizers adsorbed onto the semiconductor surface absorb visible light and excited electrons are injected into the conduction band of the semiconductor electrodes. Dye-sensitized oxide semiconductor photo electrodes have been used for PSCs [12].

2.2 Structure of Dye Sensitized Solar Cell

The main parts of DSSCs systems is composed of five elements, the transparent conducting oxides, counter conducting electrodes, the nano-structured wide band gab semiconducting layer, the dye molecules (sensitizer), and the electrolyte [13].

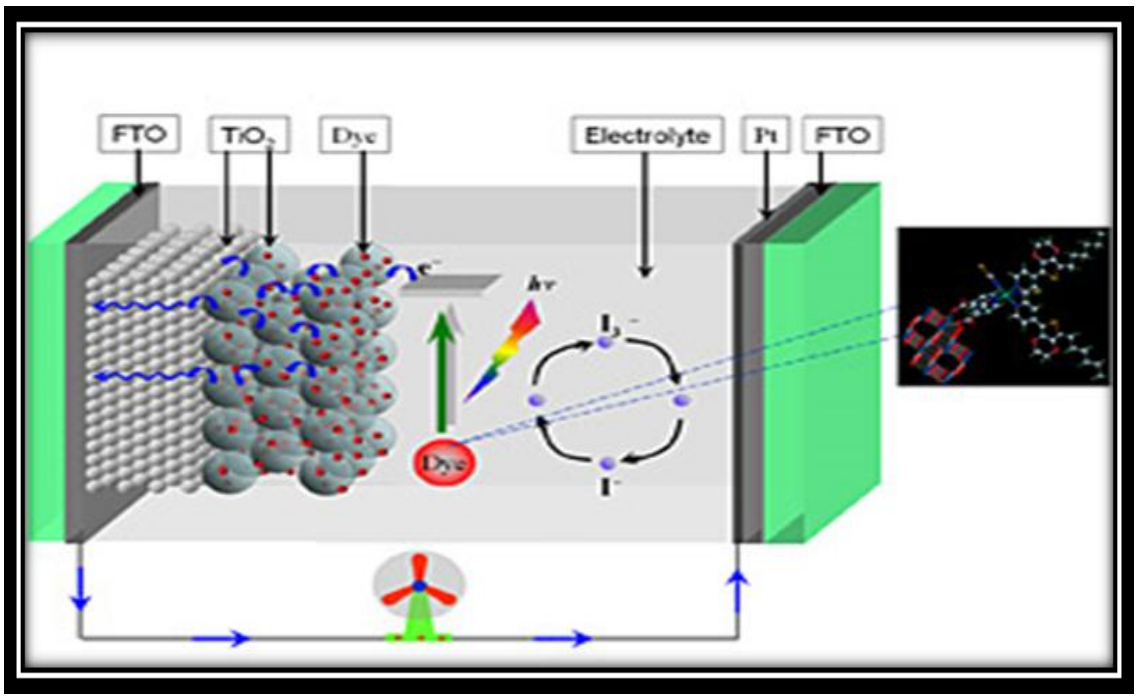

Figure (2.1) Dye sensitized solar cell diagram [1]

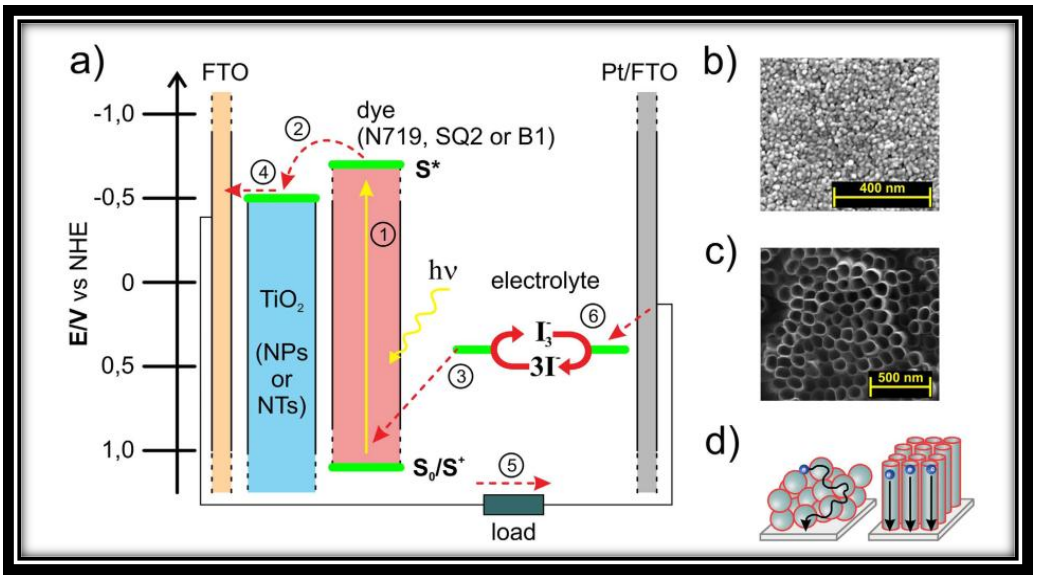

Figure (2.2) (a) Te structure of prepared DSSCs, SEM images of (b) TiO_2 NPs and (c) TiO_2 NTs photoanode, (d) Electron diffusion path through TiO_2 nanoparticles network (lef) and ordered nanotubes (right) [14].

2.2.1 Transparent Conducting Oxides (TCO) For both the Conducting Electrode and Counter Electrode

TCO coated glass is used as substrate for the TiO_2 photo electrode. For high solar cell performance, the substrate must have low sheet resistance and high transparency. In addition, sheet resistance should be nearly independent of the temperature up to 500°C, because sintering of the TiO_2 electrode is carried out at 450^0 C. Fluorine-doped tin oxide (FTO) coated glass is electrically conductive and ideal for use in a wide range of devices, including applications of thin film photo–voltaic devices, it has been recognized as a very promising material because it is relatively stable under atmospheric conditions, chemically inert, mechanically hard, Easily fabricated, has a high tolerance to physical abrasion and is less expensive than indium tin oxide [14].

2.2.2 TiO_2photo–electrode

Photo–electrodes made of such materials as Si, GaAs, InP, and CdS decompose under irradiation in solution owing to photo–corrosion. In contrast, oxide semiconductor materials, especially TiO_2, have good chemical stability under visible irradiation in solution; additionally, they are nontoxic and inexpensive. The TiO_2 thin-film photo–electrode is prepared by a very simple process. TiO_2 colloidal solution (or paste) is coated on a TCO substrate and then sintered at 450 to 500^oC, producing a TiO_2 film [15].

2.2.3 The Dye Molecules (Sensitizer)

Dye molecules of proper molecules structure are used to sensitized wide band gab nanostructure photo electrode [16].

2.2.4 Types of dyes

2.2.4.1 Inorganic dye

Includes metal complex, such as poly pridy (complex of ruthenium and osmium) [17].

2.2.4.2 Organic Dye

At the last years the efficiency of dye sensitized solar cell with organic dyes has increased comparable to the Ru-complex. Since organic dyes are not based on rare noble metal, the production costs mainly depend on the number of synthesis steps, thus they are potentially very cheap. The absorption coefficients are typically one order of magnitude higher comparable to Ru-complex making very thin TiO2 –layers feasible. At this point none of the

organic dyes have proven stability under evaluated temperature .the following examples is the most promising dye classes at the moment [17, 18].

2.2.4.3 Natural Dyes

Dyes derived from natural materials are exclusively used for educational purpose representing a low–cost and environmentally friendly alternative to conventional Ru-complex. Extracted dyes might also be a good starting point to evaluate, which dyes classes are potentially interesting for sensitization, example of natural dyes blackberries gave a conversion efficiency of 0.056% [19].

2.2.4.4 Organic Complex of Other Metals

Other metal complex have been securitized for their application in DSSC, among them Os- ,Pt ,and Fe-complex .however the overall conversion efficiency is only 50% of standard Ru-dye. Pt-complex gives modes efficiencies of 0.7% and iron-complex, which are very interesting due to the vast abundance of the metal and its non-toxicity, at a very low efficiency level at the moment 0.3% [19].

2.2.4.5 Electrolytes

Electrolyte containing I-/I-3 redox ions is used in DSSC to generate the oxidized dye molecules and hence completing the electric circuit by mediating electrons between the nanostructure electrode and counter electrode [20].

2.3 Dye–Sensitized Solar Cell Parameters

The percentage power conversion efficiency (P_{CE}) or of any solar cell device is simply the ratio of power output (P_{out}) versus power input ,(P_{in}) , power input (P_{in}) depend upon the incident light flux(I_o), and Power output implicit properties of the device itself ;namely the short- circuit current (I_{sc}) open-sir cut voltage (V_{oc}) and fill-factor (FF).the short-circuit current density (J_{sc})is typically reported to allow comparison between devices whose dimensions may vary (J_{sc}=I_{sc}/area). The FF is determined by the ratio maximum obtainable power/theoretical obtainable power where the theoretical obtainable power is the product I_{sc},V_{oc} (I_{sc} and V_{oc} being zero at open –circuit and short- circuit condition respectively with grade A solar –cells typically having (FF =0.7) [21].

$$FF = \frac{I_{max}V_{max}}{I_{sc}V_{oc}}\% \qquad (2.1)$$

$$P_{CE} = \eta = \frac{P_{out}}{P_{in}} \times 100 = \frac{I_{sc}V_{ov}FF}{I_0\,A} \times 100 \qquad (2.2)$$

2.4 Comparison of Common Types of PV modules

Silicon is a material commonly used in commercial PV modules. It is the second most abundant element in the Earth's crust, oxygen is the most abundant. Silicon occurs most frequently in nature as silicon dioxide (silica, SiO_2) and as silicates (compounds containing silicon, oxygen, metals, and maybe hydrogen). Sand and quartz are two of its most common forms. However, sand is generally too impure to be processed into silicon. High-

grade deposits of quartzite can be almost 99% pure silica, but will still be less than 90% silicon. The silica must be processed to become silicon. To become semiconductor grade silicon it must be processed and purified until it is 99.9999% pure silicon! This process, as you might expect, is very expensive. The computer industry uses purified silicon for manufacturing its computer chips [22].

2.4.1 Single crystal silicon (the Siemens modules on your roof are single crystal silicon)

❖ **Advantages**

• Well established and tested technology

• Stable conversion efficiencies over the life (20-30 years) of the module

• Highest efficiencies of silicon solar cells

❖ **Disadvantages**

• Expensive manufacturing process

• Uses expensive single crystal and other materials

• Round crystals have less packing density (single crystal silicon ingots are pulled from molten silicon as cylinders that are sawed into wafers)

Figure (2.3) Single crystal silicon (the Siemens modules on your roof are single crystal silicon)

2.4.2 Polycrystalline Silicon

❖ **Advantages**

• Well established and tested technology

• Stable conversion efficiencies over the life (20-30 years) of the module

• Square cells for better packing density

❖ **Disadvantages**

• Uses expensive materials (though less expensive than single crystal silicon)

• Expensive manufacturing process

• Slightly less efficient than single crystal silicon

Figure (2.4) Polycrystalline Silicon solar cell

2.4.3 Amorphous Silicon

❖ **Advantages**

• Low material use because the films are microns thick

• Potential for automated production

• Potential for low cost

• Less affected by shading due to long, thin cells – harder to shade a single cell

• Thinness contributes to use in specialized applications, i.e. calculators and watches (where small amount of power is required)

• Can be incorporated into windows and roofing tiles or shingles in building-integrated PV systems (the electrical generation system is part of the building skin)

❖ **Disadvantages**

• Lower efficiencies than single and polycrystalline silicon

• Larger areas needed for same power output as single or polycrystalline silicon due to lower efficiencies the cost per unit area (cost/area) of silicon solar cells increases with the size of the crystals. This means that a smaller area of single-crystal cells is required to generate 100 W of power. The cost of a panel that will generate a 100 W may be more constant than the size [22, 23].

Figure (2.5) Amorphous Silicon solar cells

2.4.4 Other Materials for PV Cells

Other materials are being researched for both their electrical generation potential and commercial feasibility, including: Copper Indium Dieseline, Cadmium Telluride, and Gallium Arsenide. These compounds may become the PV material of choice in the future [24].

2.5 Magnetic Fluid

Ferro fluid or magnetic fluid is a type of soft materials that typically consists of colloidal magnetic particles such as magnetite or manganese-zinc ferrites, dispersed with the aid of surfactants in a continuous carrier phase. The carrier phase could be hydrocarbons, fluorocarbons, water and liquid metals. The average diameter of the dispersed nano-particles ranges between 5 and 10 nm. Thermal agitation keeps the particles dispersed in the carrier because of Brownian motion, and the surfactant prevents the particles from sticking to each other. Each particle as a constant magnetic-dipole moment proportional to the size that can align with an external magnetic field, The Ferro fluid must be synthesized because that it is not found in nature. Up to now, two general methods for producing Ferro fluids have been used. The first method reduces a magnetic powder to a colloidal particle size by ball-milling grinding in the presence of a liquid carrier and a grinding aid which also serves as a dispersing agent. The second approach is a chemical co-precipitation technique in which the magnetite particles are coated with a surfactant and the dispersed in a continuous phase. Due to the advantages of the high production efficiency and preparing highly dispersed magnetite particles for the later method, the chemical co-precipitation is employed mainly at present. With the development in the manufacture processes, the Ferro fluid is applied widely, especially in engineering applications such as rotary seals [26], inertia dampers [25] and heat transfer devices [26].Due to their diverse phenomena, pattern forming systems of Ferro fluid films under external magnetic fields have attracted the interest of scientists and engineers. Many experimental results show that the columns agglomerated by magnetic particles occur in the

films under external magnetic fields [27, 28]. In Section 2, we will investigate the structural pattern formation in the magnetic fluid thin film under both parallel and perpendicular magnetic fields. The detailed description of the agglomeration of magnetic particles, the structural evolution is to be given. Also, the related physical mechanism is discussed in this section. On the other hand, owing to the rich structural patterns in the magnetic fluid films under external magnetic fields, the induced optical phenomena have put under extensive study. Those works were focused on birefringence, optical transmittance, and magneto chromatics. In Section 3, the magnet to optical and the magneto chromatic effect of the magnetic fluid films are further illustrated.

2.5.1 Structure in the Magnetic Fluid Films under External Magnetic Fields

To observe the structural patterns of magnetic fluids under external magnetic fluid fields, magnetic fluid is usually sealed in a glass cell of thickness of several to tens of micrometers. The applied magnetic field is either parallel (parallel field) or perpendicular (perpendicular field) to the plane of the film. The images of the structures in the magnetic fluid film are taken with an optical microscope and are recorded with a CCD video camera. In this section, we illustrate structure evolution in the magnetic fluid films under external magnetic fields [29].

2.5.2 Parallel Magnetic Fields

When a magnetic fluid film is subjected to parallel magnetic field, the magnetic nano-particles are aligned along the field and a portion of the magnetic particles in the fluid agglomerate to form needle-like chains in the magnetic fluid film. Some researchers suggest that the agglomeration of magnetic particles is due to phase separation, which results from the thermo-dynamical instability of the dispersion of magnetic particles [29, 30].As the field strength is further increased, more particles participate in the agglomeration and needle-like chains are distributed randomly in the film. Yusuf et al. showed that two separated chains merge and that the chains become longer under higher field [26]. It was also found that the chains elongate when the fluid concentration is raised. With the recent success in synthesizing highly homogeneous magnetic fluid [27], alone-dimensional periodic chain structure was obtained for magnetic fluid film under parallel magnetic fields [28, 29], as shown in Figure (2.2).Furthermore, the period Δx of the chain structurein the magnetic fluid film decreased as the H wasincreased. Figure 2 plots the Δx -H curve for various sweep rate of the external field. The curve is shifted to the region with lower Δx's as the sweep rate is raised. In addition to the sweep rate, the film thickness, fluid concentration, the cell width can also dominate the Δx -H curve of the magnetic fluid film under parallel magnetic fields [30]. It indicates that the period Δx can be manipulated from several to tens of micrometers.

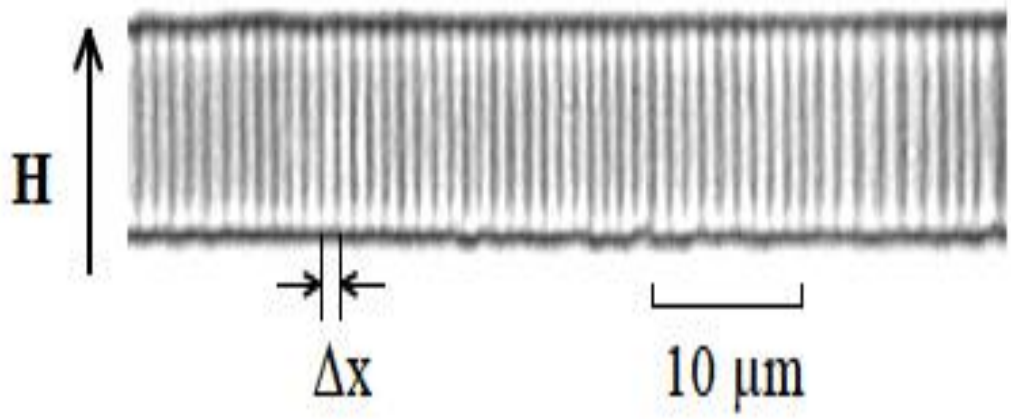

Figure (2.6) One-dimensional periodic chain structure in highly homogeneous agnetic fluid film under a parallel magnetic field, the field strength H is 200 Oe, the sweep rate dH/dt is100 Oe/s, the cell width w is 10 μm, the thickness L of the film is 1.5 μm, the concentration Ms is 17.6 emu/g, and the resultant Δx is 1.45 μm.

2.5.3 Perpendicular Magnetic Fields

In contrast to chains in magnetic fluid films under parallel fields, cylindrical magnetic columns were formed in the film under perpendicular fields [28, 29]. Through an observation for the time evolution of the formation of columns under given field exceeding some critical field strength, the diameter a of a column became larger and then saturated when the system reached an equilibrium state [30, 31]. Ytreberg and McKay give a theoretical relationship between the saturated diameter and the applied magnetic field and the thickness of the film under perpendicular fields [32]. This predicted relationship could be fitted to the experimental data very well. In our previous work [33], the structure in highly homogeneous magnetic fluid films evolved

from a mono-dispersed state to a disordered one when the magnetic field H was increased from zero to a critical value. If the H was further increased, particles agglomerated to form new columns. Then, a hexagonal ordered structure of columns was constructed. The ordered structure in a magnetic fluid film can be characterized by the averaged distance d between two neighboring columns and the averaged diameter a of columns. The averaged column distance d is obtained by fast Fourier transformation of the image of an ordered structure. For the ordered state, the d was found to decrease under a higher H, whereas a remained almost constant. The physical mechanism governing the d(H) curve was found to be due to two main interactions one is the attractive interaction between the magnetic column and the external magnetic field, the other is the repulsive interaction between two magnetic columns with parallel magnetization [34].

2.5.4 Magnetism in Matter

The magnetic field produced by a current in a coil of wire gives a hint as to what might cause certain materials to exhibit strong magnetic properties. In general, any current loop has a magnetic field and a corresponding magnetic moment. Similarly, the magnetic moments in a magnetized substance are associated with internal currents on the atomic level. One can view such currents as arising from electrons orbiting around the nucleus and protons orbiting about each other inside the nucleus. However, as we shall see, the intrinsic magnetic moment associated with the electron is the main source of magnetism in matter.We begin with a brief discussion of the magnetic moments due to electrons. The mutual forces between these magnetic dipole

moments and their interaction with an external magnetic field are of fundamental importance to an understanding of the behavior of magnetic materials. We shall describe three categories of materials paramagnetic, ferromagnetic, and diamagnetic. Paramagnetic and ferromagnetic materials are those that have atoms with permanent magnetic dipole moments. Diamagnetic materials are those whose atoms have no permanent magnetic dipole moments [35].

2.5.5 Magnetic Moments of Atoms

As we learned the total magnetic moment of an atom has orbital and spin contributions. For atoms or ions containing many electrons, the electrons in closed shells pair up with their spins and orbital angular momentum opposite each other, a situation that results in a net magnetic moment of zero. However, atoms with an odd number of electrons must have at least one "unpaired" electron and a spin magnetic moment of at least one Bohr magnet on μ_B, where [36]

$$\mu_B = \frac{e\hbar}{2m_e} = 9.274x10^{-24} J/T \qquad (2.3)$$

The total magnetic moment of an atom is the vector sum of the orbital and spin magnetic moments, and an unpaired outer electron can contribute both an orbital moment and a spin moment. For example, if the unpaired electron is in an s state, L= 0 and consequently the orbital moment is zero. However, if the unpaired electron is in a p or d state, $L \neq 0$ and the electron contribute both an orbital moment and a spin moment. The orbital moment is about the same order of magnitude as the Bohr magnet on. The nucleus of an atom also has a magnetic moment associated with its constituent protons and neutrons.

However, the magnetic moment of a proton or neutron is small compared with the magnetic moment of an electron and can usually be neglected. Because the masses of the proton and neutron are much greater than that of the electron, their magnetic moments are smaller than that of the electron by a factor of approximately 10^3.

2.5.6 Magnetization and Magnetic Field Strength

The magnetization of a substance is described by a quantity called the magnetization vector, M. The magnitude of the magnetization vector is equal to the magnetic moment per unit volume of the substance. As you might expect, the total magnetic field in a substance depends on both the applied (external) field and the magnetization of the substance. Consider a region where there exists a magnetic field B_0 produced by a current-carrying conductor. If we now fill that region with a magnetic substance, the total magnetic field B in that region is $B = B_0 + B_m$, where B_m is the field produced by the magnetic substance. This contribution can be expressed in terms of the magnetization vector as $B_m = \mu_0 M$; hence the total magnetic field in the region becomes [37]

$$B = B_0 + \mu_0 M \qquad (2.4)$$

It is convenient to introduce a field quantity H, called the magnetic field strength. This vector quantity is defined by the relationship $H = (B/\mu_0) - M$, or

$$B = \mu_0 (H + M) \qquad (2.5)$$

In SI units, the dimensions of both H and M are amperes per meter. To better understand these expressions, consider the space enclosed by a solenoid that carries a current I. (We call this space the core of the solenoid.) If this space is a vacuum, then M = 0 and $B = B_0 = \mu_0 H$. Since $B_0 = \mu_0 n I$ in the core, where n is the number of turns per unit length of the solenoid, then

$$H = B_0/\mu_0 = \mu_0 nI/\mu_0,$$

Or

$$H = nI \qquad (2.6)$$

That is, the magnetic field strength in the core of the solenoid is due to the current in its windings. If the solenoid core is now filled with some substance and the current I is kept constant, H inside the substance remains unchanged and has magnitude nI. This is because the magnetic field strength H is due solely to the current in the solenoid. However, the total field B changes when the substance is introduced. From Equation (2.7), we see that part of B arises from the term $\mu_0 H$ associated with the current in the solenoid; the second contribution to B is the term $\mu_0 M$, due to the magnetization of the substance filling the core [38].

2.5.7 Classification of Magnetic Substances

In a large class of substances, specifically paramagnetic and diamagnetic substances, the magnetization vector M is proportional to the magnetic field strength H. For these substances we can write [39]

$$M = \chi^H \qquad (2.7)$$

Where χ, (Greek letter chi) is a dimensionless factor called the magnetic susceptibility.

If the sample is paramagnetic, χ is positive, in which case M is in the same direction as H. If the substance is diamagnetic, χ is negative and M is opposite H. It is important to note that this linear relationship between M and H does not apply to ferromagnetic substances. Substituting Equation (2.7) for M into Equation (2.5) gives

$$B = \mu_0(H + M) = \mu_0(H + \chi^H) = \mu_0(1 + \chi)H$$

Or

$$B = \mu_m H \qquad (2.8)$$

Where the constant m is called the magnetic permeability of the substance and has the value

$$\mu_m = \mu_0(1 + \chi) \qquad (2.9)$$

2.6 Maxwell's Equations

In this supplement we discuss the relation between the integral and differential forms of Maxwell's equations, derive the 3d wave equation for vacuum electromagnetic fields, find the general form of a plane wave solution, and discuss the field energy conservation theorem. The second section summarizes a few mathematical items from vector calculus needed

for this discussion, including the continuity equation. Maxwell's equations in differential form are the following equations[39,40]:

$$\nabla . E = \frac{\rho}{\epsilon_0} \qquad \text{Gauss' law (electric)} \qquad (2.10)$$

$$\nabla . B = O \qquad \text{Gauss' law (magnetic)} \qquad (2.11)$$

$$\nabla X E = -\partial_t B \qquad \text{Faraday's law} \qquad (2.12)$$

$$\nabla X B = \mu_0 \, (j + \epsilon_0 \, \partial_t E) \quad \text{Ampere-Maxwell law} \qquad (2.13)$$

The first two equations are scalar equations, while the last two are vector equations [37]. The notation ∂t stands for ∂/∂t. We now discuss how these differential equations are obtained from the integral equations.

2.7 Gauss' Law (Maxwell First Low)

The integral form of Gauss' law is R∂V E · $dS = {}^{q}/_{\epsilon_0}$. This can be written as equality between three dimensional volume integrals, by writing the total charge enclosed q as the integral of the charge density over the volume, and using the divergence theorem to express the flux integral as the volume integral of the divergence of E. Since the two volume integrals are equal for any integration volume V, we can equate the integrands, thus obtaining the differential form of Gauss' law (1). For the magnetic field there are no magnetic monopole charges, hence we have simply (2)[41].

2.8 Faraday's Law (Maxwell Second Low)

Faraday's law states that the loop integral of the induced electric field is minus the time rate of change of the magnetic flux through the loop, R∂S E ·

dl = −(d/dt)RS B· dS. We can use Stoke's theorem to write the loop integral of E as a surface integral of the curl of E. Equating integrands then yields the differential form of Faraday's law, eqn. (2.10). The divergence of the left hand side of Faraday's law, ∇· (∇× E), vanishes identically [2], so if Faraday's law is consistent it must be true that ∇· ∂t B also vanishes. Since the time and space partial derivatives commute, this is the same as ∂t ∇· B, which vanishes thanks to the magnetic version of Gauss' law (2). So the absence of magnetic charges is required for Faraday's law to be self-consistent[41].

2.9 Ampere's law (Maxwell thread low)

Ampere's law states that the loop integral of the magnetic field is μ0 times the current flowing though the loop, R∂S B · dl = μ_0i. We can use Stake's theorem to write the loop integral of B as a surface integral of the curl of B, and we can write the current i though the loop as the flux integral of the current density j though a surface spanning the loop, i = R_S j · ds. Equating integrands we obtain the field equation ∇× B = μ_0j. Now if we check for self-consistency we discover a problem: the divergence of the left hand side vanishes identically, but the divergence of the right hand side, ∇· j, does not. In fact, charge conservation implies the continuity equation (2.3), i.e., ∇· j = −∂t ρ. In a steady state situation, where all time derivatives vanish, Ampere's law is self-consistent as it should be, since it was after all discovered to apply in steady state situations. However in the presence of time dependent charge densities it cannot be correct. To ensure consistency of Ampere's law in a time dependent setting we must add something to the right hand side so that it will be divergence free. To see what should be added, note that $\nabla . j =$

$-\partial_t \rho = \epsilon_0 \partial_t \nabla . E = -\nabla . (\epsilon_0 \partial_t \nabla . E)$, where Gauss' law (1) was used in the second equality. Thus Gauss' law and the continuity equation imply that the vector j+$\epsilon_0 \partial_t E$ has vanishing divergence, hence is a suitable source term for the curl of the magnetic field. The resulting modified equation, (2.4), might be called the Ampere-Maxwell equation. The extra term, $\epsilon_0 \partial_t$E, is called the displacement current density [42, 43].

2.10 Electromagnetic wave equation (Maxwell froths low)

Maxwell's equations are first order, coupled partial differential equations for E and B. They can be uncoupled by taking another derivative. In vacuum, i.e. with vanishing charge and current densities, we have [50]

$$\partial_t^2 \mathrm{E} = \partial_t \frac{1}{\epsilon_0 \mu_0} \mathrm{xB} = -\frac{1}{\epsilon_0 \mu_0} \nabla \mathrm{x} (\nabla \mathrm{xE}) = -\frac{1}{\epsilon_0 \mu_0} \nabla^2 \quad (2.15)$$

In the first line we used the Ampere-Maxwell law (4), in the second line we used Faraday's law (3) together with the fact that partial derivatives commute, and in the last line we used Gauss' law (1), together with the identity (17). An identical equation results for B as well. Equation (2.8) is the three dimensional wave equation for each component of the electric field, with a wave speed $c = 1/\sqrt{\mu_0 \in_0}$ = 3×10^8 m/s, the speed of light.

2.10.1 Magneto-Acoustic and Electro-Optical Effect

Optical Activity A rotation in the plane of oscillation of a linearly polarized beam upon passage through a medium, it occurs in asymmetrical molecules

where the electrons are more easily accelerated in one orientation than another. The random orientation of molecules in the medium does not cancel the effect, since flipped molecules retain the same handedness (just as a right-handed helix remains right-handed upon turning it upside down). Optical activity is much more prominent in nature than would be normally expected due to the fact that almost all amino acids (the building blocks of life) are left-handed. The angle of rotation β is defined as positive when the electric field is rotated clockwise,

$$\beta = \frac{\pi d}{\lambda_o}(n_l - n_r) \tag{2.16}$$

Where d is the thickness of the medium, λ_0 is the vacuum wavelength, n_l is the index of refraction for parallel polarization and n_r is the index of refraction for perpendicular polarization. A medium in which $n_l > n_r$ is called d-rotary, and a medium in which $n_l < n_r$ is called l-rotary. A quantity called specific rotary power is defined as [50,51]

$$[\text{specificrotrypower}] = \frac{\beta}{d} \tag{2.17}$$

2.10.2 Magneto-Optic Effect

A magneto-optic effect is any one of a number of phenomena in which an electromagnetic wave propagates through a medium that has been altered by the presence of quasi-static magnetic field. In such a material, which is also called gyro tropic or gyro-magnetic, left- and right-rotating elliptical polarizations can propagate at different speeds, leading to a number of

important phenomena. When light is transmitted through a layer of magneto-optic material, the result is called the Faraday Effect: the plane of polarization can be rotated, forming a Faraday rotator. The results of reflection from a magneto-optic material are known as the magneto-optic Kerr effect not to be confused with the nonlinear Kerr effect. In general, magneto-optic effects break time reversal symmetry locally (i.e. when only the propagation of light, and not the source of the magnetic field, is considered), which is a necessary condition to construct devices such as optical isolators through which light passes in one direction but not the other. The other, less useful, way to break time reversal symmetry is to rely upon absorption loss [52].

Chapter Three
Literature Review

3.1 Introduction

The energy problem encourages scientists to search for cheap efficient solar cells. One of most promising ones are Nano solar cells [53, 54, 55, and 51].In this chapter caught some of this samples.

3.2 Molecular Doping Of Low –Band Gap – Polymer, Fullerene Solar Cells, Effects On Transport and Solar Cells

This work done by Ali VeyselTunc (Energy and Semiconductor Research Laboratory, Institute of Physics, Carl von Ossietzky University Oldenburg, Oldenburg 26111, Germany) PCPDTBT, supplied by Konarka Technologies GmbH (Nürnberg, Germany), was p-doped with F4-TCNQ (Sigma-Aldrich) and blended with PCBM, purchased from Solenne BV. F4-TCNQ and PCPDTBT were separately dissolved in chlorobenzene, in concentrations of 1 mg/mL and 10 mg/mL, respectively. For the field-effect measurements, the dopant solution was added to the polymer solution to achieve concentrations of 0%; 0.1%; 0.2% and 0.3% by weight with respect to the polymer. Solutions were left stirring overnight for the polymer. Fullerene solutions PCBM were added to obtain a weight ratio of 1:1 with respect to the polymer. The semiconducting layers were then spin coated onto pre-cleaned substrates. All solution processing was performed in a N_2-filled glove box. We show how molecular doping can be implemented to improve the performance of solution

processed bulk hetrojunction solar cells based on a low-band gap polymer mixed with a fullerene derivative. The molecular dopant 2,3,5,6-tetrafluoro-7,7,8,8-tetracyanoquinodimethane (F4-TCNQ) is introduced into blends of poly[2,6(4,4-bis-(2-ethylhexyl)4H-cyclopenta[2,1-b:3,4-b0]-dithiophene)-alt-4,7-(2,1,3-benzothiadiazole)] (PCPDTBT) and [6,6]-phenyl-C61-butyric acid methyl ester (PCBM) via co-solution in a range of concentrations from 0% to 1%. We demonstrate that the whole conductivity and mobility increase with doping concentration using field-effect measurements. Photo induced absorption (PIA) spectroscopy reveals that the polar on density in the blends increases with doping. We show that the open circuit voltage and short circuit current of the corresponding solar cells can be improved by doping at 0.5%, resulting in improved power conversion efficiencies. The increase in performance is discussed in terms of trap filling due to the increased carrier density, and reduced recombination correlated to the improvement in mobility.

We demonstrate that molecular doping using F4-TCNQ leads to an increase in the photocurrent in PCPDTBT PCBM solar cells. We investigate blends doped at 0; 0.1; 0.25, 0.5 and 1 wt % with respect to the polymer. Field-effect measurements demonstrate that doping increases the whole conductivity and mobility in both PCPDTBT films and PCPDTBT: PCBM blends. The conductivity of the pristine polymer increases by more than ten times and for the polymer fullerene blend by about four upon doping. The whole mobility was also observed to increase with doping concentrations between 0% and 0.3% by five times for the pure polymer and three for the blend. PIA spectroscopy revealed an increase in the polar on densities and a shift in the GSB band, corresponding to trap filling by the increase in charges introduced by doping. In solar cells, doping leads to increases in the photocurrent from

9.42 to 10.31 mA/ cm^2 and an overall increase in the solar cell efficiency from 3.28% to 3.62 %. From the EQE data it is apparent that doping increases the efficiency in collecting photogene rated charges in spectral regions attributed to the PCPDTBT absorption. These results show that molecular doping is a feasible and simple method to improve the efficiency of BHJ solar cells [51].

3.3 Electrochemically synthesized conducting polymeric materials for applications towards technology in electronics, optoelectronics and energy storage devices

This work done by K. Gurunathan, The state of the art of novel electronically conducting polymeric materials is presented in this review. The special emphasis is laid on the electrochemical synthesis of conducting polymers (CPs) including the choice of the monomers and solvents, supporting electrolytes and electrodes and structural aspects of these novel materials and the nature of the dopants which induce electrical conductivity in conjugated organic polymers. Finally, an overview of various technological applications of these novel polymeric materials to electronics, optoelectronics devices like electro-chromic cells, light emitting electrochemical cells and photo conducting devices, solar cells such as photovoltaic and photo electrochemical (PEC) cells, p-n-semiconductors, metal-insulator-semiconductors (MIS), laser materials and energy storage applications like solid-state rechargeable batteries and super capacitors has been presented. 1999 Elsevier Science S.A, All rights reserved. The electrochemical synthesis of novel electronic materials and their structure showed that besides the application oriented development and optimization, novel applications in more speculative ®elds such as polymer electronics or even molecular

electronics may become feasible. Thus, applications of conducting polymers as photo-conducting devices, solar energy conversion (PV) cells, in polymeric colored LEDs that could display images and form at plastic screens for computers or TVs. They could also replace traditional LCDs, which are limited to a small size. Solid-state electro-chromic cells for large area electro-chromic devices (ECDs) are being used for commercial signboards, time tables in airports and railway stations, calculators, clocks etc. In future, the world wide needs of economic fuel and pollution free environment can be met through the energy storage applications like rechargeable batteries and super-capacitors using conducting polymers as electrode material. These high-tech devices will be supercharging electronic products of the future, some of the commercial products of conducting polymers. Worldwide several companies are racing to develop ultra-capacitors with millions of times the energy storage capacity of traditional capacitors. Ultra-capacitors store and release energy like batteries, but have vastly longer lives. They can unload their energy 10 to 100 times faster than batteries. The new devices may lead to electric vehicles exhibiting superior performance of sports cars by releasing. Bursts of power when accelerating or climbing. Ultra capacitors are great use in cellular phones and supercomputers. Most of the conducting polymers that have reached the actual application stage seem to be in a production test phase and are still waiting for a greater acceptance and utilization on the current market. Therefore, it is quite unclear at the moment how much pro®t is really made with devices based on conducting polymers and whether the worldwide sales®gure of synthetic metals which was forecast as 1 billion US$ in the year 2000 will be reached [52].

3.4 Enhanced Electron Injection in Polymer Light-Emitting Diodes Polyhedraloligomericsilsesquioxanes as Dilute Additives

This work done by Xiong Gong .The molecular structures of MEH-PPV, MCC-POSS and MEH-PPV-POSS are shown in scheme 1. The MEH-PPV and MEH-PPV-POSS were provided by Organic Vision (Canada).The synthesis of MEH-PPV-POSS was reported previously. The MCC-POSS was purchased from Hybrid Plastics. By blending monochlorocyclohexyl, polyhedral- ligomericsilsesquioxanes (MCC-POSS) into poly (2-methoxy-5-(2'-ethyl-hexyloxy)-1.4-phenylenevinylene(MEH-PPV), enhanced luminous efficiency (LE, cdA−1) and brightness were observed in polymer light-emitting diodes (PLEDs) using Al as the Cathode. PLEDs made from MEH-PPV with 0.5 wt.% of MCC-POSS exhibit LE of 1 cdA−1, four times higher than that observed in simple MEH-PPV devices. X-ray diffraction studies, measurements of photovoltaic response and measurements of photoconductivity from the films of pure MEH-PPV and MEH-PPV with MCC-POSS demonstrated that the improved device performance results from mixing of MCC-POSS with MEH-PPV. The enhanced electron-injection into the emissive layer results from the effect of the ionic conductivity introduced by the addition of MCC-POSS. In summary, we have demonstrated that improved luminous efficiencies can be achieved for PLEDs with Al as the cathode by blending the emissive conjugated polymer with polyhedral-monochlorocyclohexyl- polyhedraloligomericsilsesquioxanes (MCC-POSS). XRD studies indicated thatMCC-POSS are mixed with MEH-PPV, thereby affecting the morphology of MEH-PPV films and resulting in improved device performance. Additionally, the investigation of photovoltaic devices and steady-state photoconductivity from MEH-PPV and MEH-PPV with

different concentrations of MCC-POSS demonstrated that the improvement in the device efficiency results from enhanced electron-injection associated with the ionic conductivity of MCC-POSS in the emissive layer [53].

3.5 Creation of A Gradient Polymer-Fullerene Interface in Photovoltaic Devices By Thermally Controlled Inter Diffusion

This work done by M. Drees, was supported by the National Science Foundation STTR program through Grant No. DMI-0060515.Efficient polymer-fullerene photovoltaic devices require close proximity of the two materials to

ensure photo excited electron transfer from the semiconducting polymer to the fullerene acceptor. We describe studies in which a bilayer system consisting of spin-cast 2-methoxy-5-(28-ethylhexyloxy)-1,4-phenylenevinylene copolymer ~MEH-PPV! And sublimed C60 is heated above the MEH-PPV glass transition temperature in an inert environment, inducing an inter diffusion of the polymer and the fullerene layers. With this process, a controlled, bulk, gradient hetrojunction is created bringing the fullerene molecules within the exaction diffusion radius of the MEH-PPV throughout the film to achieve highly efficient charge separation. The inter diffused devices show dramatic decrease in photoluminescence and concomitant increase in short circuit currents, demonstrating the improved interface. @DOI: 10.1063/1.1522830.

In conclusion, we have fabricated polymer-fullerene bilayer systems in which the charge transfer and charge transport have been improved by thermally controlled inter diffusion. This leads to increased proximity of C60 molecules to optical excitations throughout the bulk of the film as demonstrated by

luminescence quenching of one order of magnitude. The corresponding order of magnitude increase in photocurrent in the region of maximum absorption of the MEHPPV indicates the formation of a bulk hetrojunction due to thermally controlled inter diffusion. The optical absorption spectra of the MEH-PPV/C60 composite films before and after the inter diffusion process are indistinguishable, demonstrating that the enhanced photovoltaic efficiency is due solely to nanoscale control of the spatial locations of the two components [54].

3.6 Using Gum Arabic in Making Solar Cells by Thin Films Instead Of Polymers

In the work done by Abdelsakhi, 3 samples of Gum solar cells were made by depositing the Gum Arabic solution on ITO a glass by Spin Coating technical, and another layer was deposited from dye on a layer of Gum Arabic. Gold was fabricated on the layers to represent the anode and ITO Cathode. Gum Arabic based solar cells with Rhodamine 6G were fabricated on indium tin oxide by a spin coater position. Microstructure and cell performance of the solar cells with ITO/ Rhodamine 6G/ Gum Arabic structures were investigated. Photovoltaic devices based on the Rhodamine 6G / Gum Arabic hetrojunction structures provided photovoltaic properties under illumination. Absorption and energy gap measurement of the Rhodamine 6G / Gum Arabic hetrojunction were studied by using UV-VS mini 1240 spectrophotometer and light current-voltage characteristics. The energy levels of the present solar cells were also discussed. The three ITO/Gum/Rhodamine/Au solar cells were produced and characterized, which provided efficiency (η) is (3.8 - 5.1 and 5.2) %. Fill factor (FF) is (0.964 - 0.9462 and 0.973), current density (J_{sc}) is

(2.22 - 4.31 and 4.4) mAcm-2 and Open – circuit voltage (V_{oc}) is (1.22 -1.25 and 1.209) V. This could be used at larger scale in promoting efficiency of solar cells. The application of conducting Arabic Gum to optoelectronic devices such as solar cell, light emitting diodes, and electrochemical sensors are of practical significance, because the Arabic Gum mixture can be easily prepared and modified by rich chemical procedures to meet optical and electronic requirements .This solar cell is cheap can be easily fabricated. It efficiency is relatively large [55].

3.7 Comparison of Transparent Conductive Indium Tin Oxide, Titanium-Doped Indium Oxide, and Fluorine-Doped Tin Oxide Films for Dye-Sensitized Solar Cell Application

In the work done by Dong-Joo Kwak .The TCO materials investigated in this study are ITiO, ITO, and FTO. The FTO glass is commercially available from Pilkington Co., whereas the thin films of ITiO and ITO are prepared using RF magnetron sputtering. In this study, we investigate the photovoltaic performance of transparent conductive indium tin oxide (ITO), titanium-doped indium oxide (ITiO), and fluorine-doped tin oxide (FTO) films. ITO and ITiO films are prepared by radio frequency magnetron sputtering on soda-lime glass substrate at 300 °C, and the FTO film used is a commercial product. We measure the X-ray diffraction patterns, AFM micrographs, transmittance, sheet resistances after heat treatment, and transparent conductive characteristics of each film. The value of electrical resistivity and optical transmittance of the ITiO films was 4.15×10-4 Ω-cm. The near-infrared ray transmittance of ITiO is the highest for wavelengths over 1,000 nm, which can increase dye sensitization compared to ITO and FTO. The

photo conversion efficiency (η) of the dye-sensitized solar cell (DSC) sample using ITiO was 5.64%, whereas it was 2.73% and 6.47% for DSC samples with ITO and FTO, respectively, both at 100mW/cm^2 light intensity. In this study, we investigate the photovoltaic performance of transparent conductive ITiO, FTO, and ITO thin films. ITiO and ITO thin films are deposited on a soda-lime glass substrate by RF magnetron sputter method at relatively low substrate temperature (~300 °C) and at high rate (~10 nm/minutes), whereas the FTO film used is commercial FTO glass. We investigate the electrical and optical properties of these films such as X-ray diffraction patterns, AFM micrographs, optical transmittance, sheet resistances, and photovoltaic characteristics. The near-IR transmittance of ITiO is the highest for wavelengths over 1,000 nm, which can increase dye sensitization in DSC compared to ITO and FTO. The photo conversion efficiency (η) of the DSC sample using ITiO was 5.64%, whereas it was 2.73% and 6.47% from DSCs using ITO and FTO, respectively, both at 100 mW/cm2 light intensity [56].

3.8 The Relationship between Energy Gab & Efficiency in Dye Solar Cells

This work done by Sakina Ibrahim Ali, Four samples of (Ecrchrom Black T, DDTTC, Rohadamin B, Coumarin 500) solar cells were made by depositing the solution of Day sensitized on ITO Aluminum electrodes by Spin Coating technique and another layer was deposited from dye on a layer of (MEH-PPV).Al was used on the layers to act as anode and ITO as Cathode. A clean glass plate with a thin layer of ITO (Indium Tin Oxide) was needed. The ITO acts as the first part of the solar cell, the first electrode. In this work dye sensitized solar cells made from: Ecrchrom Black T, DDTTC, Rohadamin B, and

Coumarin 500,with Al and TTO electrodes were fabricated. The energy gab of these dyes were found using UV Spectrometer. The energy gap for: Ecrchrom Black T, Rohadamin B, and Coumarin 500 ; were found 2.16 eV ,2.20 eV ,3.27 eV and 3,60 respectively . The V- I characteristics for these cells and their performance were also found. The efficiency, Ecrchrom Black T, DDTTC, Rohadamin B, Coumarin 500 were found 1.66, 1.62, 1.49 and 1.31. It is realized that; the efficiency increased when energy gab decreased. Ecrchrom Black T, DDTTC, Rohadamin B, Coumarin 500 was found 1.66, 1.62, 1.49 and 1.31. It is realized that; the efficiency increased when energy gab decreased. This work shows that the energy gap of the dyes used in dye sensitized solar cell affect the performance and efficiency of the solar cell [57].

3.9 Solar Storm Threat Analysis

This work done by James A. Marusek, Most solar storms produce only minor disquieting affects on Earth. Typically one might expect short-term electrical power blackouts, short lived communication outages, rerouting of aircraft, loss of a few satellites and a beautiful “aurora borealis” in the nights sky from a large solar storm .But as the intensity of a solar storm increases like a wild beast, the storm can begin to develop the capacity to create a major disaster on Earth. The difference in solar storm intensity is like the difference between being hit with a tropical rainstorm and being devastated by a Category 5 hurricane. The solar storm of 1-2 September 1859, which began with a solar flare so strong that it was subsequently named the Carrington Flare, was such a beast. Oak Ridge National Laboratories estimated that only a solar storm just slightly stronger than the 13 March 1989 storm (Dst = 589 nT) would

have the capacity to produce a cascading blackout involving the entire Northeastern sector of the United States. So the question is "What damage would a spawned geomagnetic storm like the one of 2 September 1859 (Dst = 1,760 nT) bring?" Would it simultaneously degrade and damage several unique large electrical transformers at key electrical generating stations taking down the massive power grid? Would the long lead-time required to manufacture and install replacement equipment result in major yearlong electrical blackouts, rolling blackouts and brownouts? How would a long-term lack of stable electricity affect advanced civilization? This work dissects and analyzes the various threats created by Great solar storms. Most solar storms produce only minor disquieting affects on Earth. Typically one might expect short-term electrical power blackouts, short-lived communication outages, rerouting of aircraft, loss of a few satellites and a beautiful "aurora borealis" in the nights sky from a large solar storm. But as the intensity of a solar storm increases it develops the capacity to create a major disaster on Earth. A Great solar storm has the potential of seriously damaging the North American electrical power grid. The resulting blackout will be focused on the northern tier of states and the East and West coast of the U.S. and throughout Canada. The damaged equipment in the power infrastructure would generally have a replacement lead time of over year due to its uniqueness. But the scope of the outage will be so great that governments will quickly elevate its repair to the level of a national imperative. As a result, restoration that might normally take over a year wills occur a matter of weeks. Critical elements affected by the blackout will include water, sewage, commerce, industry, banking, transportation, communications, and in the winter, heating. Because modern society rely so heavily unsophisticated technology, a long-term blackout will have a very profound effect on the fabric of society. Many

satellites will be destroyed or severely degraded. The loss will primarily target communications. The lead-time to construct and replace these assets will be measured in terms of years [57].

3.10 Structure, Properties and Applications of Fullerenes

This work done by B.C. Yadav (Nanomaterials and Sensors Research Laboratory, Department of Physics, University of Lucknow) this study reports about fullerenes its structure, properties and applications. Fullerenes are the third allotropic form of carbon material after graphite and diamond. These were discovered in 1985 by Harold. W. Kroto, Robert F. Curl and Richard E. Smalley. Fullerenes consist of 20 hexagonal and 12 pentagonal rings as the basis of an icosahedral symmetry closed cage structure. Each carbon atom is bonded to three others and is sp2 hybridized. The C60 molecule has two bond lengths, the 6:6 ring bonds can be considered" double bonds" and are shorter than the 6:5 bonds. C60 is not "super aromatic" as it tends to avoid double bonds in the pentagonal rings, resulting in poor electron delocalization. As a result, C60 behaves like an electron deficient alkenes and reacts readily with electron rich species. The geodesic and electronic bonding factors in the structure account for the stability of the molecule. Fullerenes can be used as organic photovoltaic's (OPV), these are powerful antioxidants, reacting readily and at a high rate with free radicals which are often the cause of cell damage or death. Other uses of C60 like catalysts, in water purification and biohazard protection, portable power, vehicles and medical.

Thus this study gives the basic knowledge of structure of fullerenes and their applications. The fullerenes can be used as organic photovoltaic's (OPV).

Other uses of C60 like catalysts, in water purification and biohazard protection, portable power, Vehicles and medical [58].

3.11 Organic Semiconductor/Insulator Polymer Blends for High-Performance Organic Transistors

This work done by Wi Hyoung Lee (Department of Organic and Nano System Engineering, Konkuk University, Seoul 143-701, Korea) .In this study we reviewed recent advances in high-performance organic field-effect transistors (OFETs) based on organic semiconductor/insulator polymer blends. Fundamental aspects of phase separation in binary blends are discussed with special attention to phase-separated microstructures. Strategies for constructing semiconductor, semiconductor/dielectric, or semiconductor/passivation layers in OFETs by blending organic semiconductors with an insulating polymer are discussed. Representative studies that utilized such blended films in the following categories are covered: vertical phase-separation, processing additives, embedded semiconductor nanowires. We reviewed recent results with regard to organic semiconductor/insulator polymer blends for high-performance OFETs. The current pathway in the active layer was guaranteed by inducing vertical phase-separation, whereas a phase-separated insulator polymer could be used as a gate-dielectric or passivating layer. In contrast, an insulator polymer played a role as a processing additive for small molecular organic semiconductors. Embedded semiconductor nanowires are quite attractive for reducing semiconductor content and enhancing environmental stability, except for vertical phase-separation. Because phase separation is a complicated process that depends on molecular and processing parameters,

appropriate selection of materials and processing conditions is essential for achieving high performance of organic semiconductor/insulator polymer blends [59].

3.12 Role of TiO_2 Nanotubes on Improvement of Performance of Hybrid Photovoltaic Devices

This work done by SHI Quan-Min (Key Laboratory of Luminescence and Optical Information (Ministry of Education), Institute of Optoelectronic Technology, Beijing Jiaotong University, Beijing 100044) .The performance of TiO_2 nanotubes in bulk hetrojunction of poly (2-methoxy-5-(2'-ethylhexyloxy)-1,4-phenylenevinylene) (MEH-PPV)/TiO_2 nanotubes is investigated. The transport properties are studied by using the time-of-flight technique (TOF). The carrier motilities of both holes and electrons are not improved for the MEH-PPV:TiO_2 composites compared with the pristine MEH-PPV. However, photoluminescence under the influence of the electric field indicates that the dissociation of exactions in the MEH-PPV:TiO_2 composites, which is facilitated by photoinduced charge transfer, only requires a smaller electric field. In summary, the dissociation process and transport properties are investigated in MEH-PPV:TiO_2bulk hetrojunction. Compared to the pristine MEH-PPV, no transport improvement is observed for theMEH-PPV:TiO_2 bulk hetrojunction. Charge transfer occurs at the TiO2 nanotube/polymer interfaces due to the PL quenching. However, the transfer efficiency for MEH-PPV/TiO_2 interfaces is much lowerthan MEH-PPV/C60 interfaces. The dopant ofTiO2 makes exaction dissociation more facilitated. The dissociation of exactions in the MEH-PPV:TiO_2composites only requires a smaller electric field. The improved performance of bulk-hetrojunction solar

cells of MEH-PPV:TiO_2 can be attributed to the facility of exaction dissociation at TiO_2 interface[60].

3.13 Non-Linear I-V Characteristics of MEH-PPV Patterned On Sub-Micrometer Electrodes

This work done by J.H. Parka (a School of Physics and Condensed Matter Research Institute, Seoul National University, Seoul, 151-747, South Korea).The heavily doped Si substrate was thermally oxidizedand was spin-coated by an e-beam resistor ŽPMMA. on the oxidized substrate. A sub-micrometer-wide line of a conjugated polymer MEH-PPV (2-methoxy-5-(2'-ethylhexyloxy)-1,4-phenylenevinylene).-p-phenylene vinylene. was patterned using a scanning electron microscope ŽSEM.. The spin-coated thin MEH-PPV film was exposed to the electron beam in SEM, resulting in an increase in cross-linking, which reduced the solubility of the MEH-PPV film. The polymer was developed in p-xylene to dissolve the non-irradiated part of the polymer. The width, length and thickness of the active patterned area, determined by the atomic force microscopy (AFM) image, were 500, 200 and 20 nm, respectively. The two-probe current voltage characteristics of the patterned MEH-PPV line were measured as a function of temperature. The higher field data of the non-linear I_V curves were fitted using the single carrier device model which considered the field and temperature dependent mobility with space charge limited conduction (SCLC). The estimated zero-field hole mobility was of the order of $10^{-3}cm^2/Vs$ with an activation energy of 0.038 eV. 2001 Elsevier Science B.V. All rights reserved. This method of mask less patterning to make a sub micrometer-wide line of conjugated

polymer MEH-PPV was done using SEM. The I_V characteristics of the patterned MEH-PPV line were measured as a function of temperature. Non-linear I_V curves were fitted in the high field region using a single carrier device model developed by Blom et al ,which considers field dependent mobility with space charge limited conduction (SCLC). This gives a zero-field hole mobility $\mu_E = 0$ of the order of 10^{-3} cm^2/Vs and an activation energy D of 0.038 eV. As the temperature increases, the voltage gap of the I_V curves is decreased [61].

Chapter Four
Material and Method

4. 1 Introduction

This chapter is concerned with the experimental work. This includes sample preparation, apparatus, theory and the experimental work set up. In this work solar cell types with different dyes were fabricated.

4.2 Materials

4.2.1 Polymer

Polymer is a Greek phrase which means many parts. Large molecules made of repeating units of smaller molecules. Small molecules are called “monomers" monomers link together like a chain resulting in new and exciting properties [62].

Conjugated polymers are organic macromolecules with alternating single and double bonds. Conjugated polymers are organic semiconductors; the semiconducting behavior being associated with the pi-molecular orbital’s delocalized along the polymer chain. Due to the sp2 hybridization of the electron system, conjugated polymers are mostly planar, extended macromolecules. They combine the optical and electrical properties with the mechanical advantages for preparation of optoelectronic devices .There is one unpaired pz-electron per C- atom, which forms pi-pi* conduction and valence

bands in the macromolecule due to the fact, that they describe a one-dimensional crystal[63] .The Noble Prize in Chemistry 2000 was awarded jointly to Alan J. Heeger , Alan G. MacDiarmid and Hideki Shirakawa "for the discovery and development of conductive polymers", This discovery led, subsequently, to the discovery of electroluminescence in a poly(p-phenylenevinylene) (PPV) [64].In1990 The first light-emitting products based on electroluminescence in conjugated polymers have already been launched at the consumer market by Philips (The Netherlands) in 2002, whereas light-emitting products based on conjugated molecules have been introduced by the joint venture of Kodak and Sanyo (Japan). Going from discovery to product within a little bit more than one decade truly holds a huge promise for the future of plastic electronics. Other emerging applications are coatings for electrostatic dissipation and electromagnetic-interference shielding [65].Conjugated polymers and molecules have the immense advantage of facile, chemical tailoring to alter their properties, such as the band gap. Conjugated polymers combine the electronic properties known from the traditional semiconductors and conductors with the ease of processing and mechanical flexibility of plastics. In this research we used poly (2-methoxy-5-(2'-ethyl-hexyloxy)-1.4 phenylene) (MEH-PPV) due to the corresponding internal quantum efficiency .The absorbed photons to electrons, is estimated to be nearly 100% in the short circuit case. The main limiting factor towards higher efficiencies is the spectral mismatch of the active layer absorption, with a maximum around 500 nm, to the terrestrial solar spectrum with a maximal photon flux between 600 and 800 nm [66]. Therefore, the use of low band gap {Eg~ 2.0 eV}, Polymers is a viable route to increase the amount of absorbed photons and consequently the power efficiency of solar cells [67].Characterized polymers that can be turned into

solids or semi-conductive for electricity as we mentioned earlier, and to make solar cells must first add a certain percentage of oxidizing substances or shorthand to become Article polymeric. Similar properties semiconductors inorganic and lead impurities to situations within the scope of the gap between the bands valance band conduction. Has found that the energy gap of the semiconductor in some polymers ranging from (1.5-3 eV) and thus wider than the gap in the energy inorganic materials that range where the energy gap between 0.1-2.2 eV in and fit so with photon energy in the visible range of the solar radiation [68].

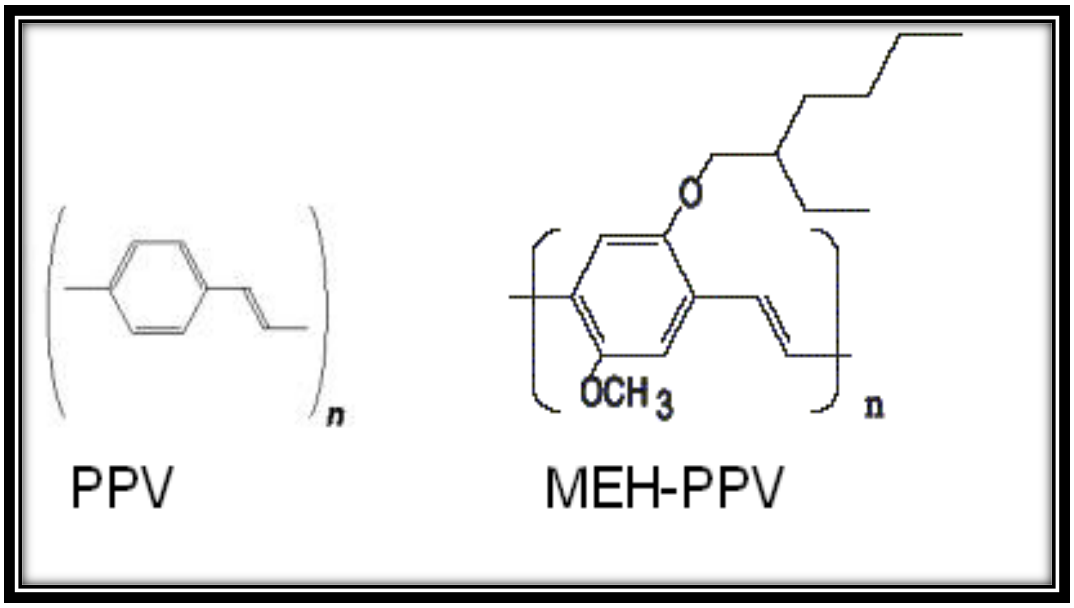

Figure (4.1) the two figures is the monomer of MEH-PPV (right) and the monomer of PPV (left)

4.2.2 ITO

ITO (Indium Tin Oxide) is a transparent conductive material. It is a mixture of indium oxide (In_2O_3) and tin oxide (SnO_2). ITO is used as one of the

electrodes in the solar cell .ITO can absorb light at the same wavelength as MEH-PPV. This is important because only the light absorbed by MEHPPV may result excitations [69].

4.2.3 Rhodamine B

Constitution 2-[6-(Diethylamino)-3-(diethylimino)-3H-xanthen-9-yl] benzoic acid Rhodamine 610 - $C28H31N2O_3Cl$ and Molecular Weight: 479.02 g/mol

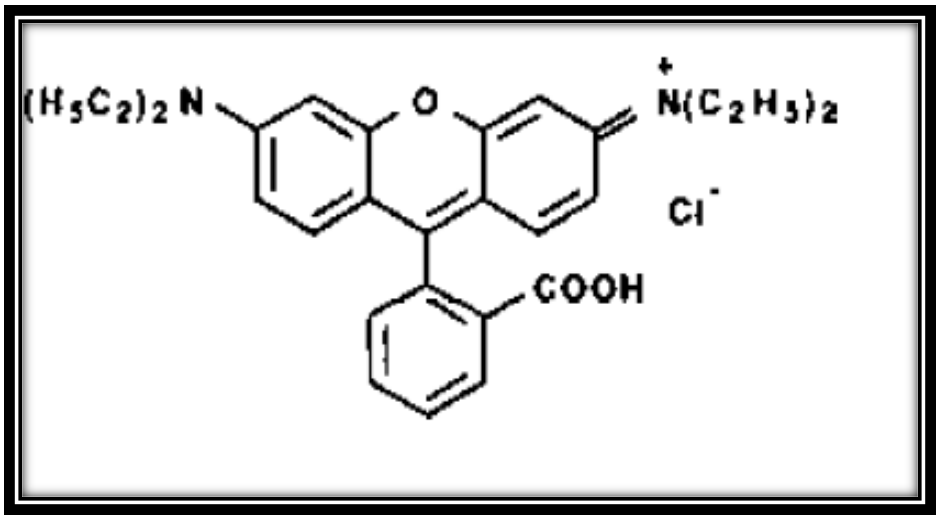

Figure (4.2) Rhodamine B

Characteristics Lambdachrome® number: 6100 CAS registry number: 81-88-9Appearance: green, crystalline solid Absorption maximum (in ethanol): 552 nm Molar absorptive: 10.7 x 10^4 L mol^{-1} cm^{-1} Fluorescence maximum (in ethanol):580 nm for research and development purposes only [70].

4.2.4 Coumarin 500

Constitution: $C_{12}H_{10}NO_2F_3$ and Molecular Weight: 257.21 g/mol

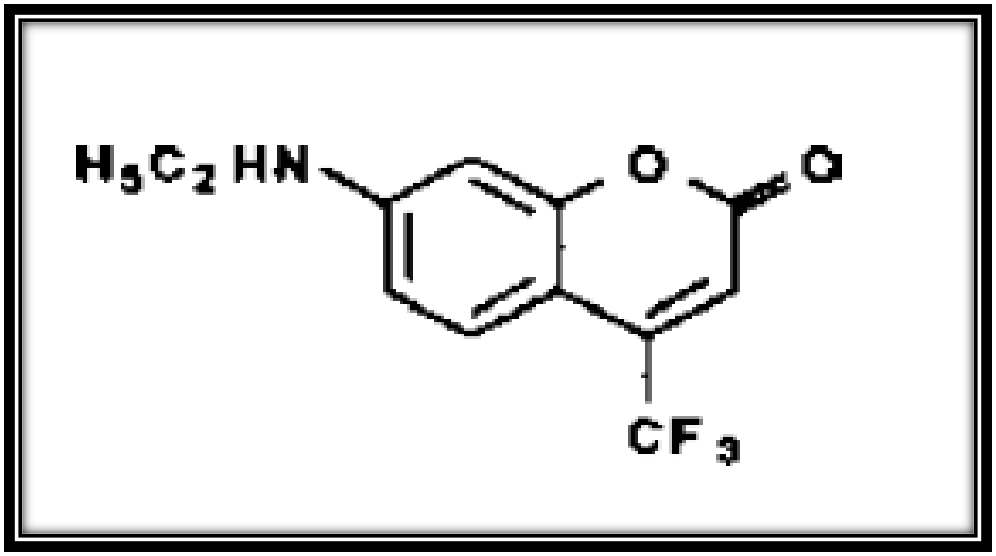

Figure (4.3) Coumarin 500

❖ **Characteristics**

Lambda chrome® number: 5010 CAS registry number: - Appearance: yellow, crystalline solid Absorption maximum (in ethanol): 395 nm Molar absorptivity: 1.85 x 10^4 L mol-1 cm^{-1} Fluorescence maximum: - For research and development purposes only [71].

4.2.5 Eriochrome black T

Constitution: $C_{20}H_{12}N_3NaO_7S$ and Molecular Weight: 461.38 g/mol

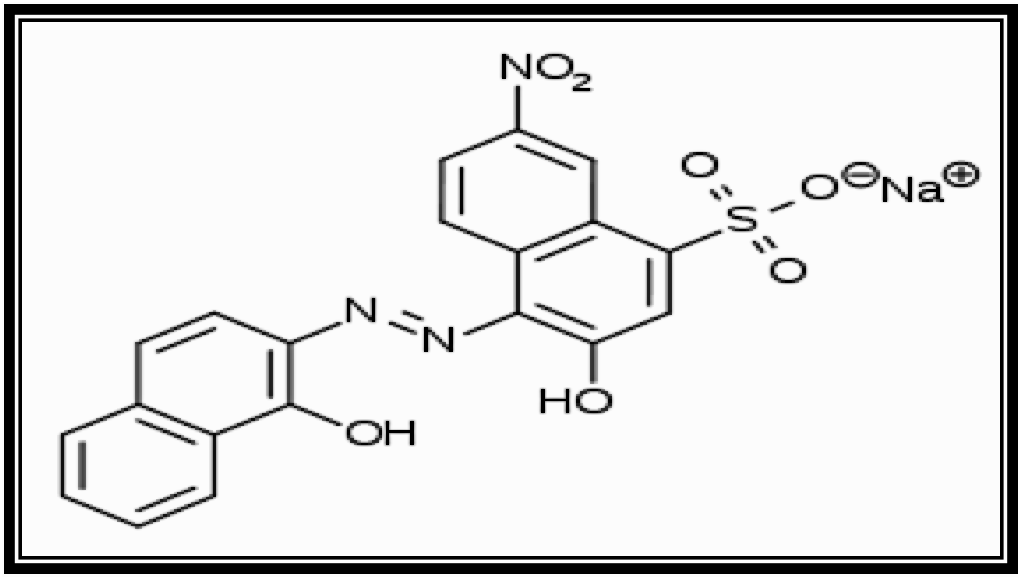

Figure (4.4) Eriochrome Black T

❖ **Characteristics**

Eriochrome Black T is a complexometric indicator that is part of the complexometric titrations, e.g. in the water hardness determination process. It is an azo dye. Eriochrome is a trademark of Huntsman Petrochemical, LLC.[1] In its protonated form, Eriochrome Black T is blue. It turns red when it forms a complex with calcium, magnesium, or other metal ions.

Grade:AR Grade, Purity:99% min, CAS Number: 1787-61-7, EC Number:217-250-3 and Molecular Formula: C20H12N3NaO7S. Eriochrome Black T has also been used to detect the presence of rare earth metals.

4.3 Experiment Setup

4.3.1 Methods

15 sample of solar cells were made(in three groups) by depositing the solution of Day (Eriochrome black T, Rohadamin B and Coumarin 500) on ITO and electrodes was silver (Ag))by Spin Coating technique, and another layer was deposited from dye on a layer of (MEH-PPV) and effected on this samples by different magnetic field (0 ,1 ,2 ,3 and 4) mT . Silver (Ag) was fabricated on the layers to act as anode and ITO Cathode. A clean glass plate with a thin layer of ITO (Indium Tin Oxide) is needed. The ITO acts as the first part of the solar cell, the first electrode. However a bit of the ITO has to be removed, to avoid short-circuiting For the purpose of the present study Day sensitized devices were made following the generally accepted methods. The fabrication process started by preparing the MEH-PPV and the dye of interest then spin coated it indium tin oxide glass. Silver (Ag) electrode was used to complete the formation of organic dye sensitized solar cell. The formed cells were characterized by Ultra violet-visible spectroscopy, Electrical circuit containing the (voltmeter and Ammeter and a light source Lamp and a solar cell). Was need to study performance .The solar cell was exposed to light and the current and voltages of the cell recorded. They were UV spectrometer was need to display absorption spectrum. 15 samples were prepared.

For the purpose of the present study effected of different magnetic field (0, 1, 2, 3 and 4) mT on the sample that was made.

The ITO glasses were firstly cleaned by ethanol and distilled water. 10mg of poly (2-methoxy-5-(2'-ethyl-hexyloxy)-1.4-phenylenevanillin) (MEH-PPV) was dissolved into 0.5ml of chloroform and 3mg of dyes dissolved into 0.5 of high pure chloroform was deposited on polymer .Been insert electrical circuit containing the (voltmeter and Ammeter and a light source "Lamp with the intensity radiological" and a solar cell).Cell was offered to light and fulfilled taking the results of the current and voltages.

4.3.2 Apparatus

*15 type of polymer solar cell (2.5×2.5) cm with different types,2 natural dyes,2 chemical dyes ,
*1 plug-in board A4 576 764,
*1 set of ten bridging plugs 501 48,
*1 pair of board holders 576 771 ,
*1 microvolt-DMM- voltmeter, KETHLEY-USA- 177 DC,
*1electrometer- ammeter, KETHLEY-USA- 642 DC, 1 halogen lamp housing, 12 V, 50/100 W 450 64, rjoostat -Albert van der perk nV Rollerdom-No-464151-27Ω-5.2A,
*light OF intensity (scouts light, power of 1000 w),
*Connecting wires shown in fig (4.4).

The purpose of this experiment is to find out the fill factor and efficiency of polymer solar cell by using 15 samples with different types of dyes. As the following steps:

1] The spin coating see fig (4.5) technique device was remove and surface was washed by distilled water and methanol,

2] Then rinsed with Acetone and dried, the ITO Glass was put in spin coating. The prepared of polymer (MEH–PPV) solution was spin coated on the ITO glass substrate for 60 sec, and prepared of dye solution was spin coated on the polymer at about 600 rpm for 60 sec in order to yield a thin uniform film .

3] Finally Aluminum strips were evaporated on top of the thin film.

4] Measures for absorbance, absorption coefficient, extinction coefficient and optical energy band gap were taken

* UV mini 1240 spectrophotometer made in a Japanese company called Shimadzu measures two types of fluids and can measure the solids in the form of slides.

4.3.3 The device components are:

Light source– a cell sample – uniform wavelength – Scout – Screen.

4.3.4 The working principle of the device:

Each of the articles has a characteristic absorption of a specific wavelength. Any material have a certain extent of absorption to unchangeable but the material properties change works on the principle Ber-lambert based on assumptions:

*Absorbance is directly proportional to the concentration.

*Absorbance is directly proportional to the length of the optical path within the sample see fig (4.6).

Figure (4.5) Spin Coating

Figure (4.6) UV spectrometer device

4.4 Theory

A polymer solar cell has p/n transition the radiation energy of incoming sun light is directly converted into electrical energy. Polymer Solar look like photodiode with a large surface area constructed so that the Light can penetrate the p/n transition through a thin n or p conducting layer (see Fig 4.8) and then creates electron-hole pairs. These are separated by the intrinsic electric field in the barrier layer and can migrate in the reverse direction. Electrons migrate into the n-doped region, and the holes migrate into the p-doped region [73].

If the external metal contacts are shorted, short-circuit current I_{sc} flows in the reverse direction of the photodiode. This current is substantially proportional to the number of electron-hole pairs created per unit time, i.e. it is proportional to the irradiance of the incoming light and the surface area of the solar cell. If the metal contacts are open, this reverse current leads to a open-circuit voltage V_{oc}, which in turn leads to an equal diffusion current I_D in the forward direction of the diode so that no current flows at all. If a load with an arbitrary resistance R is connected, the current I flowing through the load depends on the resultant voltage V between the metal contacts [74].

In a simplified manner, in can be considered to be the difference between the current I_{sc} in the reverse direction, which depends on the irradiance Φ, and the current I_D of the non-irradiated semiconductor diode in forward direction, which depend on the terminal voltage (V):

$$I = I_{sc}(\Phi) - I_D(V) \qquad (4.1)$$

In this way, the current-voltage characteristics typical of Solar cell are obtained (see Fig.4.10). In the case of small load resistances, the solar cell Behaves like a constant-current source as the forward current I_D can be neglected. In the case of greater load resistances, the behavior corresponds approximately to that of a constant-voltage source because then the current $I_D(V)$ increases quickly if the voltage changes slightly.At a fixed irradiance, the power supplied by the solar cell Depends on the load resistance R. The solar cell reaches its maximum power P_{max} at a load Resistance R_{max} which, to a good approximation, is equal to the so-called internal resistance.

$$R_i = V_{oc} / I_{sc} \qquad (4.2)$$

The maximum power:

$$P_{max} = I_{max}.V_{max} \qquad (4.3)$$

This maximum power is smaller than the product of the open circuit voltage and the short-circuit current. The ratio:

$$FF = P_{max}/V_{oc}I_{sc} \qquad (4.4)$$

FF is often called fill factor.

The efficiency η is given by:

$$\eta = I_{sc} \times FF \times V_{oc} / I_n \qquad (4.5)$$

Where I_n is the intensity of incident light. The short circuit Current density depends directly on the external quantum efficiency, the number of carriers collected/number of incident Photons [75].

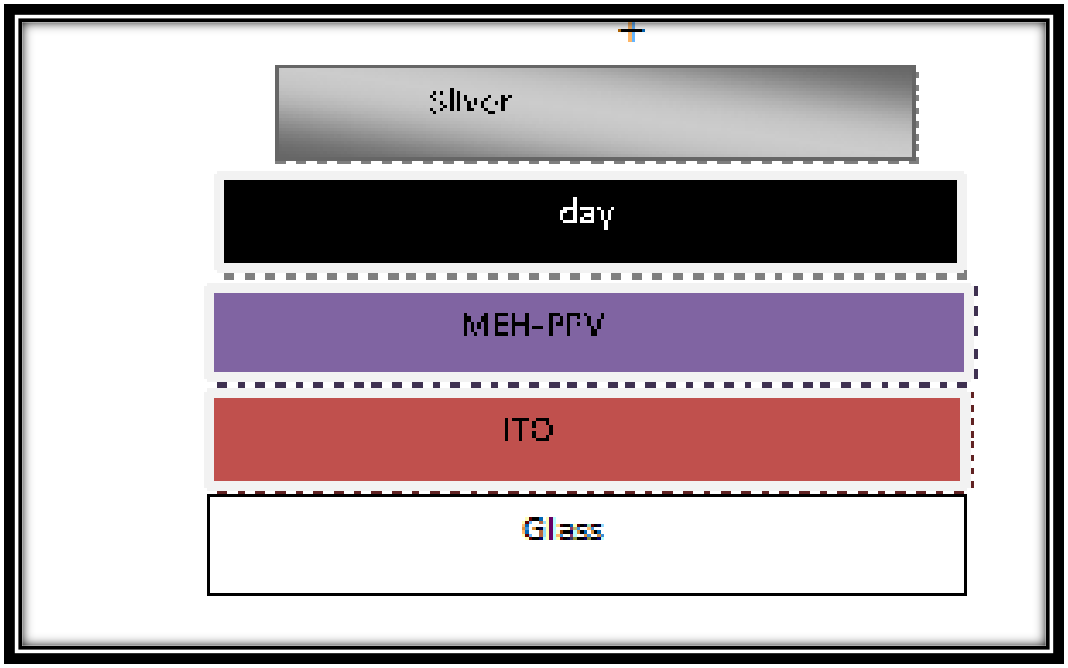

Figure (4.7) schematic structure of polymer solar cell formed with a single organic layer of MEH-PPV

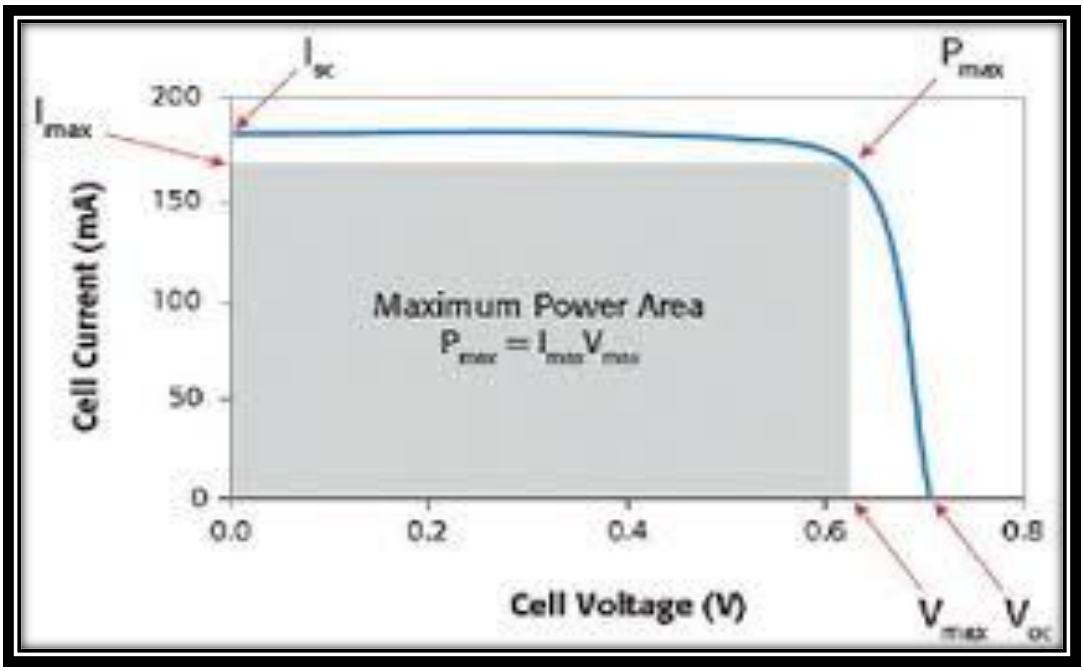

Figure (4.8) Current-voltage characteristic of a solar cell

4.5 Setup

- The STE solar cell into the plug-in board was plugged, and the upper negative pole to the lower positive pole were connected using two bridging plugs (series connection of four solar cells).
- The STE potentiometer as a variable resistor was plugged, and connected it to the solar battery using bridging plugs.
- The ammeter was connected in series with the solar battery and the variable resistor. The measuring range was selected 100 10^{-11}A DC.
- The micro voltmeter was connected in parallel to the solar cell.
- The scouts light lamp was connected to the transformer, and aligned it So that the solar cell is uniformly irradiated.

4.6 Carrying Out Of the Experiment

- The circuit was closed, first shorting the variable resistor with an additional bridging plug, and choose the distance of the halogen lamp so that the short circuit current was determined.
- The shorting bridging plug was removed, and increases the terminal voltage or decrease the current, respectively, step by step by changing the load resistance. For each step the current and the voltage were read, and take them down.
- Then interrupt the circuit, and measured the open-circuit voltage.
- Repeat the series of measurements by change load resistance.

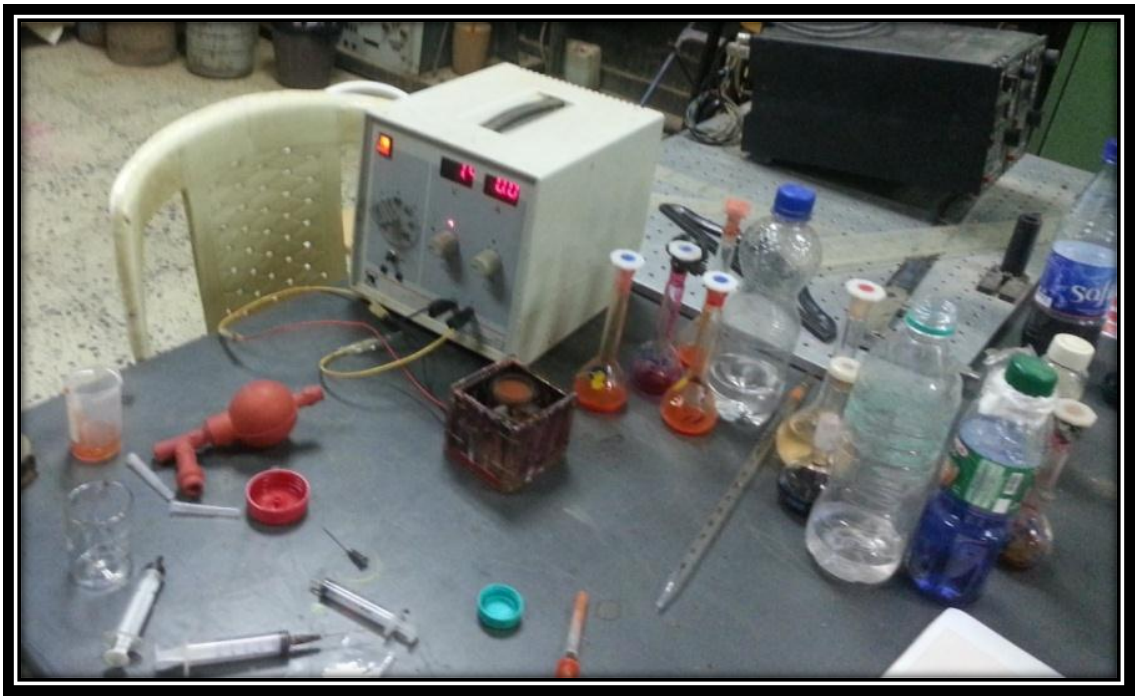

Figure (4.9) Some Materials and Apparatus That Used In the Study

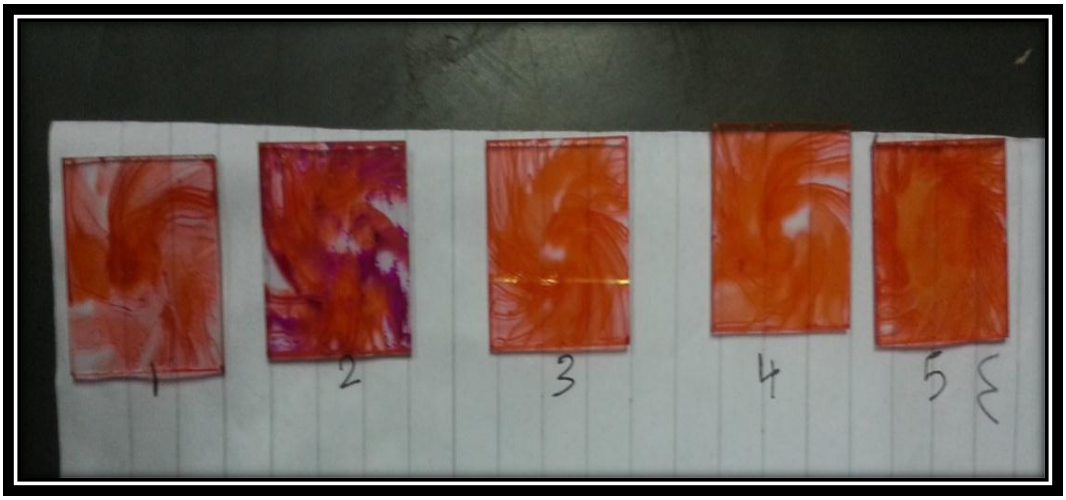

Figure (4.10) one groups of samples

Chapter Five
Results and Discussion

5.1 Introduction

This chapter concerned with results and discussion. The results consist of three groups of dye Solar cell (2.5×2.5) cm^2 with three different types of dyes. The purpose of this experiment is find out the effect on this cells by four of magnetic field intensity (1, 2, 3, and 4 mT)and find out, the fill factor and efficiency, open-circuit voltage, short-circuit current, maximum voltage and maximum current values.

5.1.1 Results of Rhodamine B

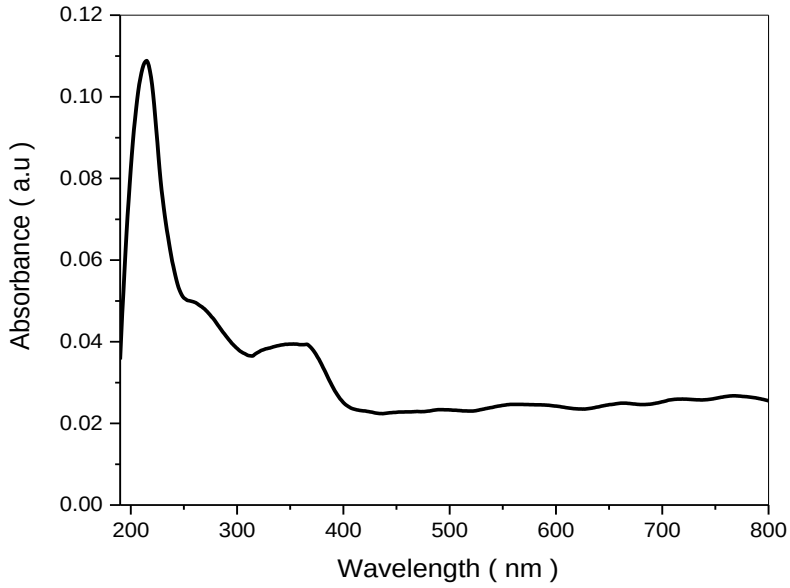

Figure (5.1) the Optical Absorption Spectra for the Rhodamine B Dye

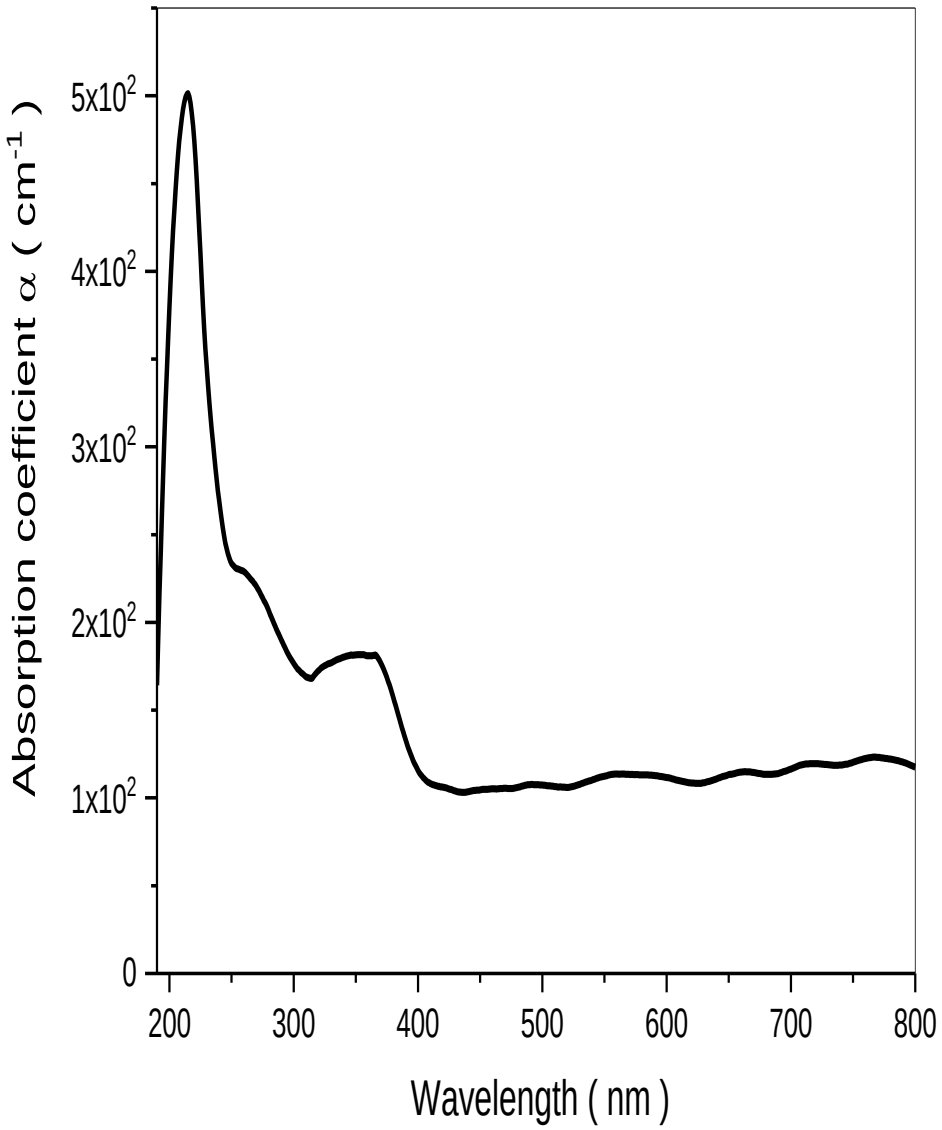

Figure (5.2) the Optical Absorption Coefficient Spectra for the Rhodamine B Dye

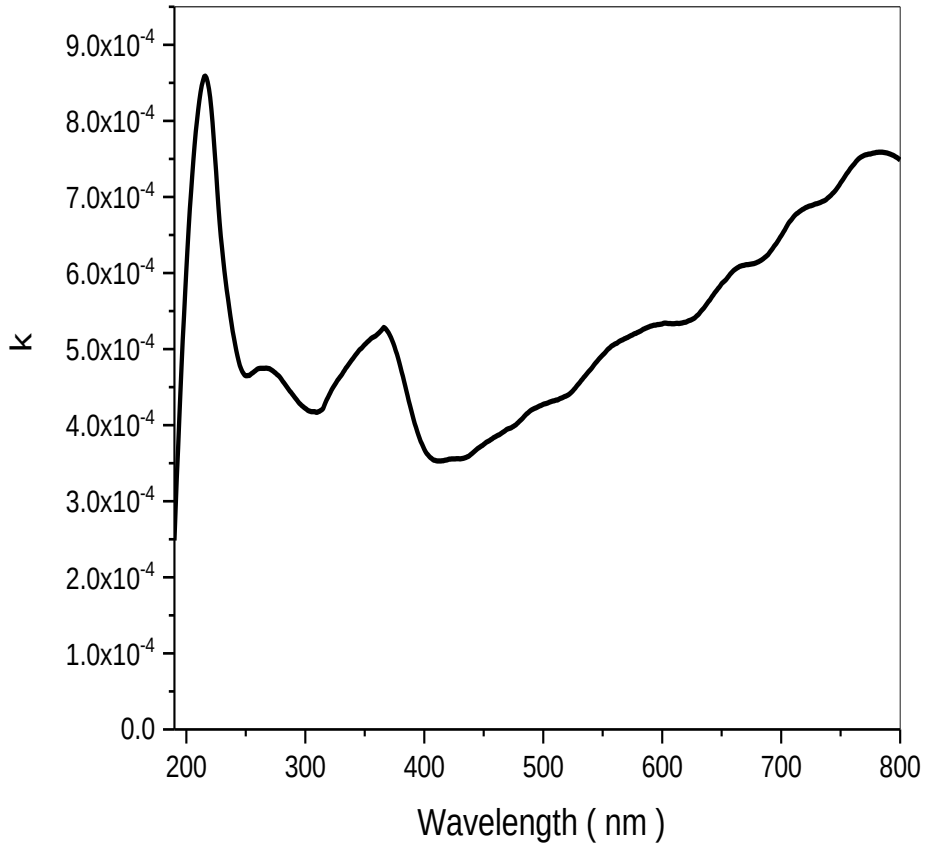

Figure (5.3) the Exaction Coefficient Spectra for the Rhodamine B Dye

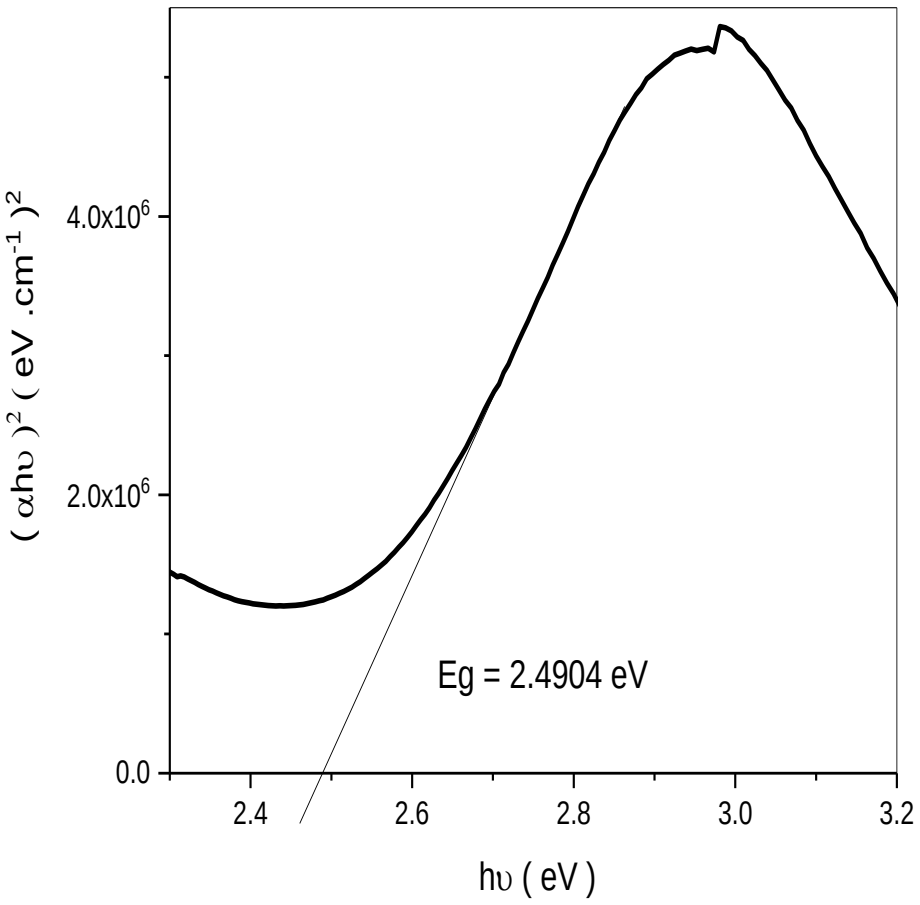

Figure (5.4) the Optical Energy Band Gap Spectra for the Rhodamine B Dye

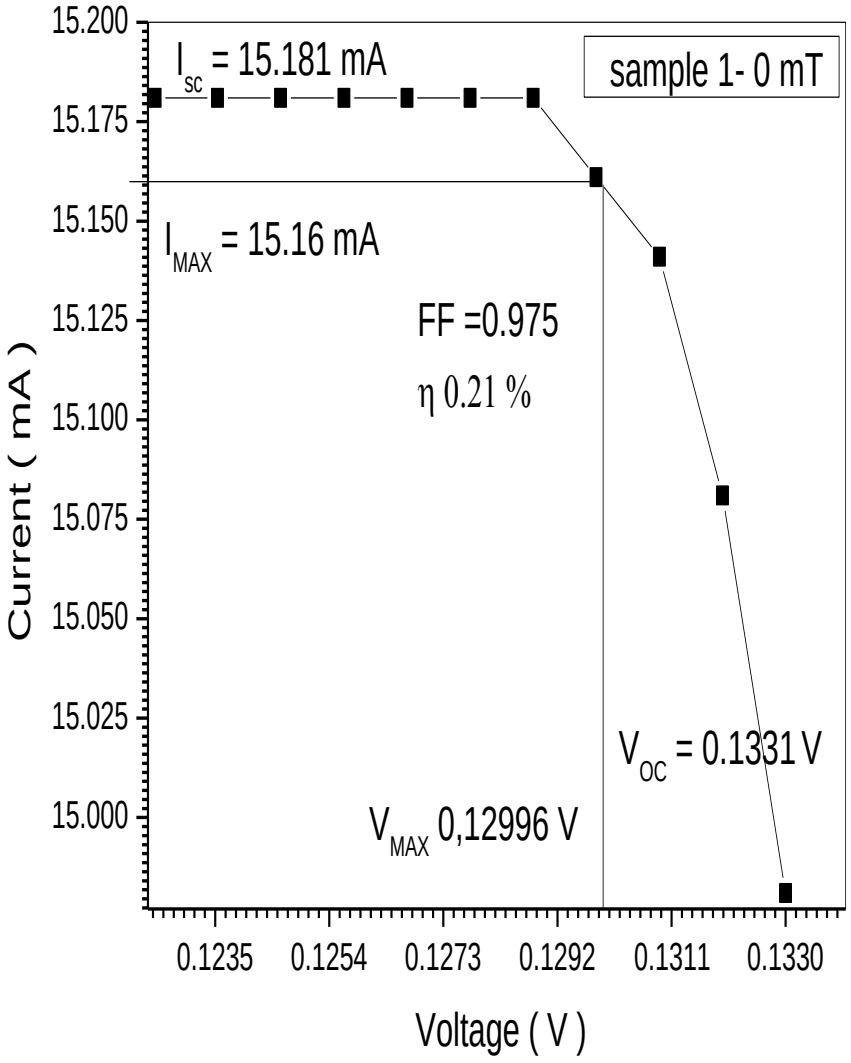

Figure (5.5) I–V Curves of Rhodamine B SC for The 0 mT

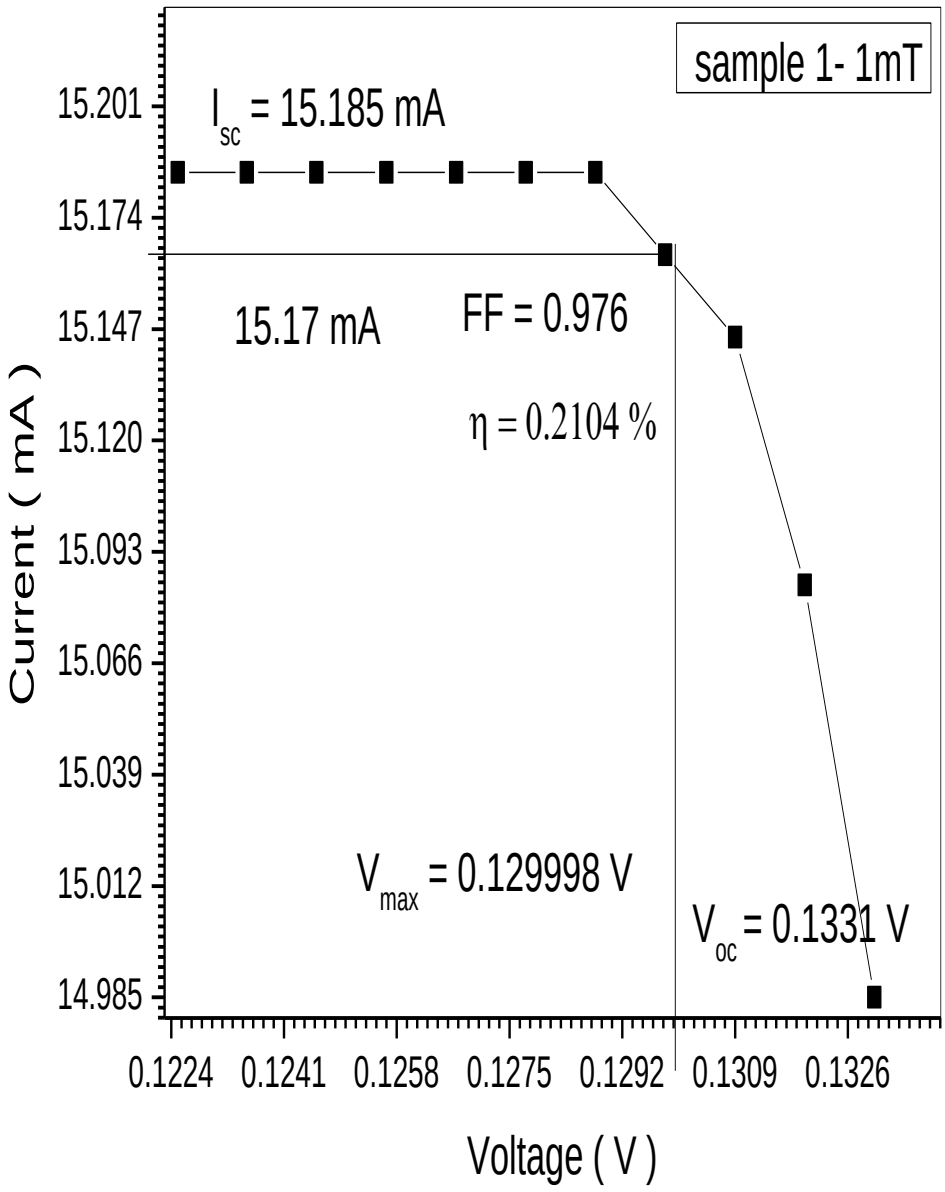

Figure (5.6) I–V curves of Rhodamine B SC for the 1 mT

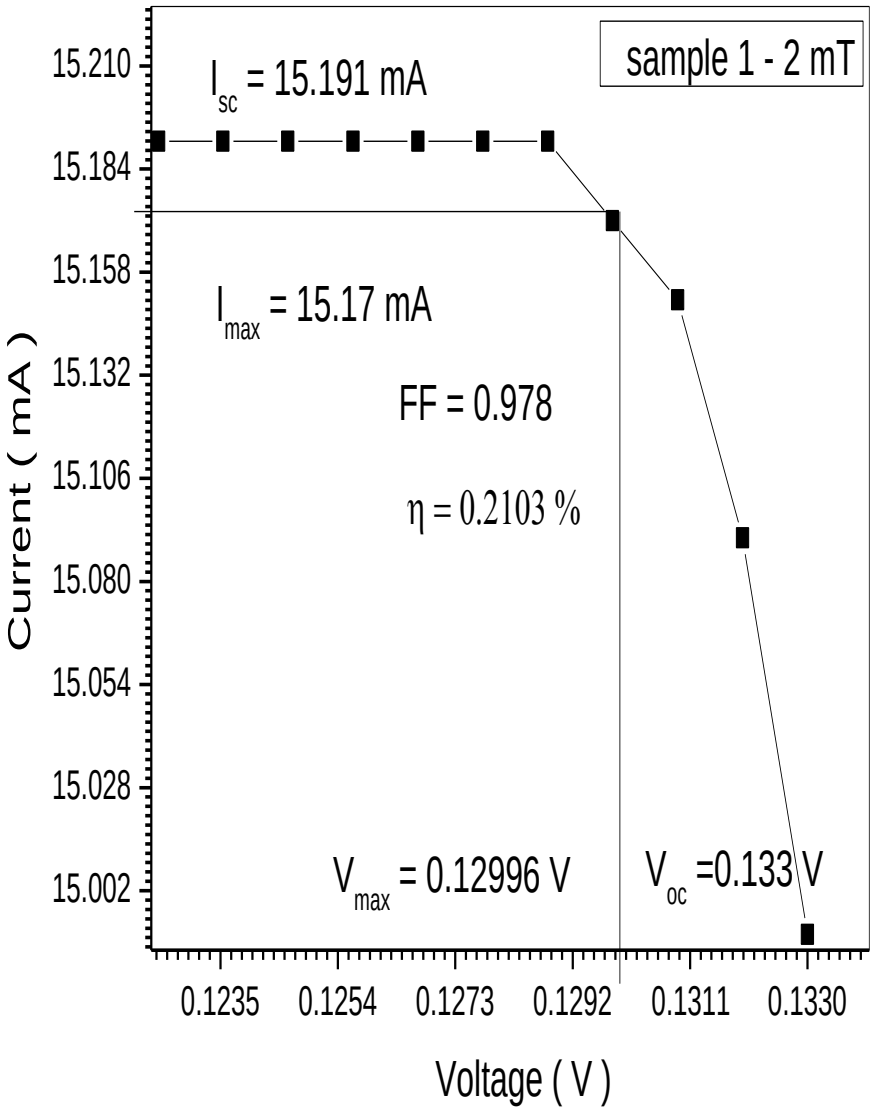

Figure (5.7) I–V curves of Rhodamine B SC for the 2 mT

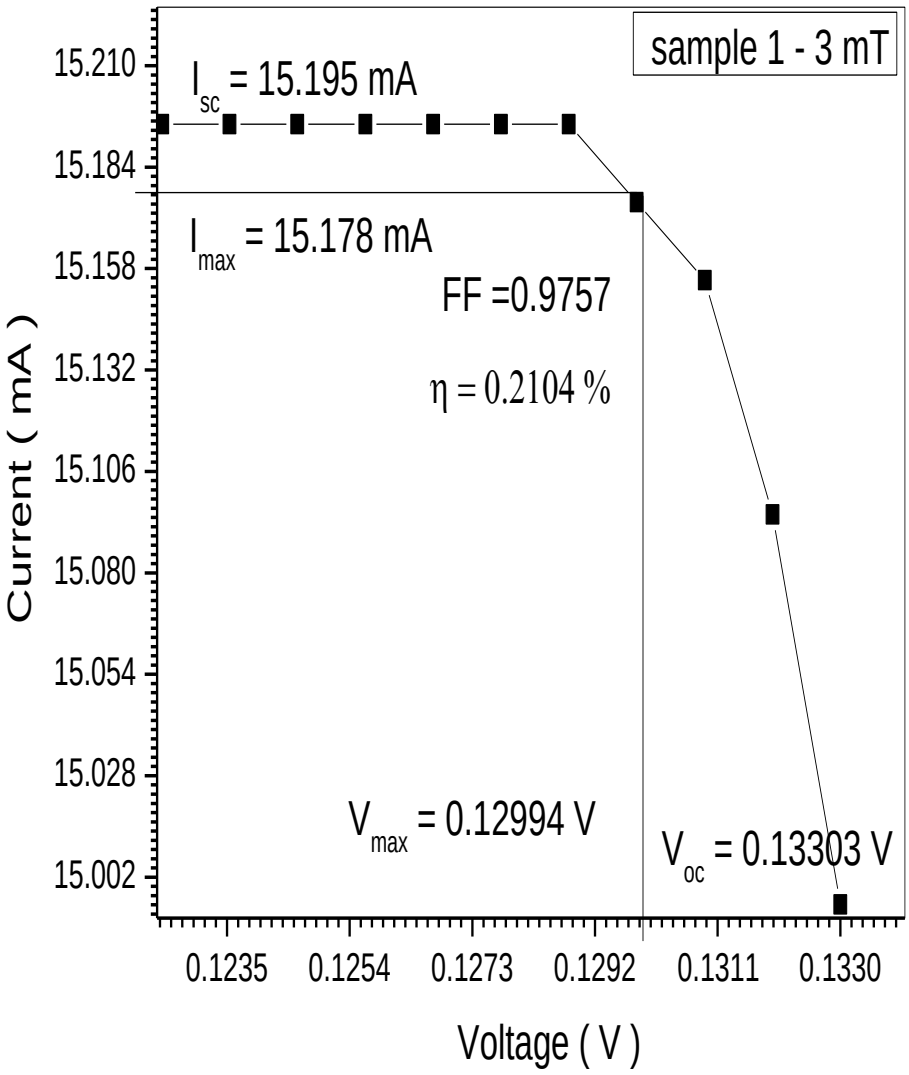

Figure (5.8) I–V Curves of Rhodamine B SC for the 3 mT

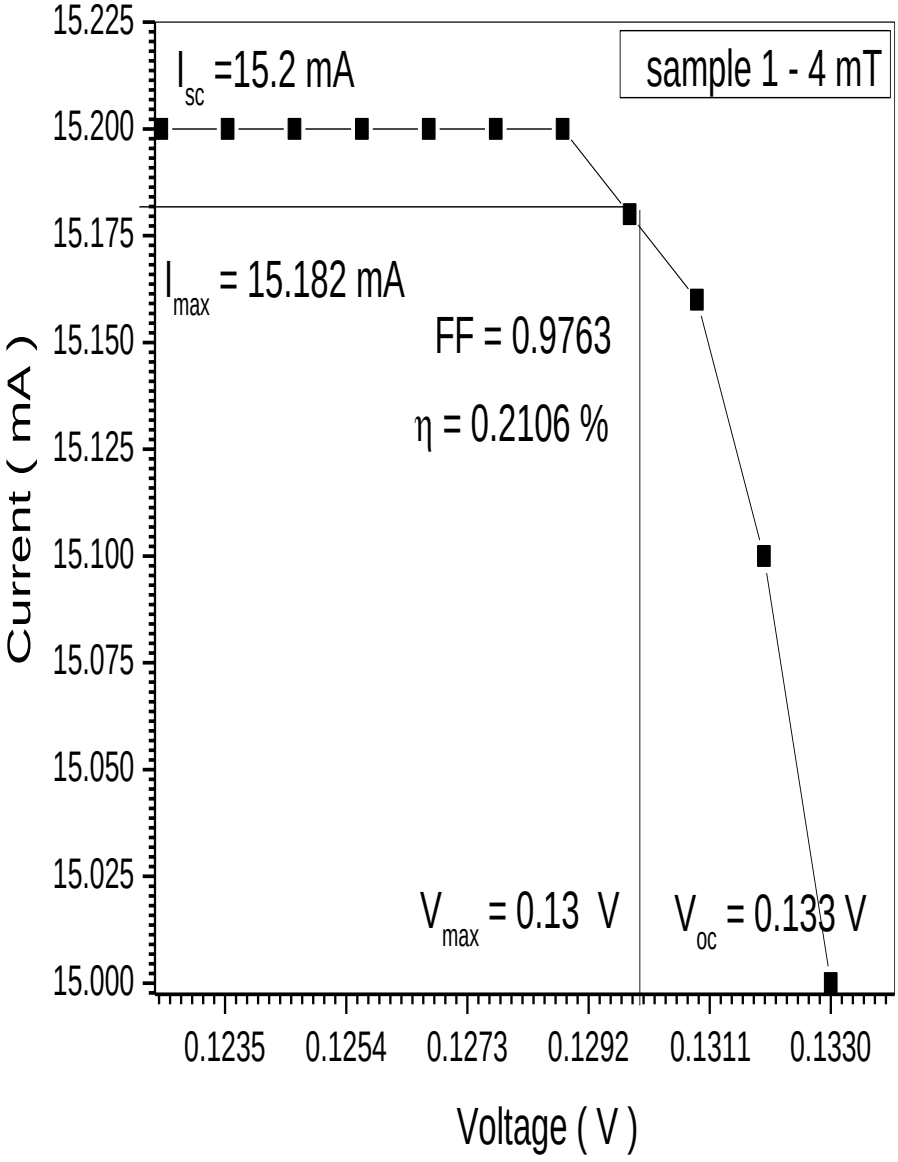

Figure (5.9) I–V curves of Rhodamine B SC for the 4 mT

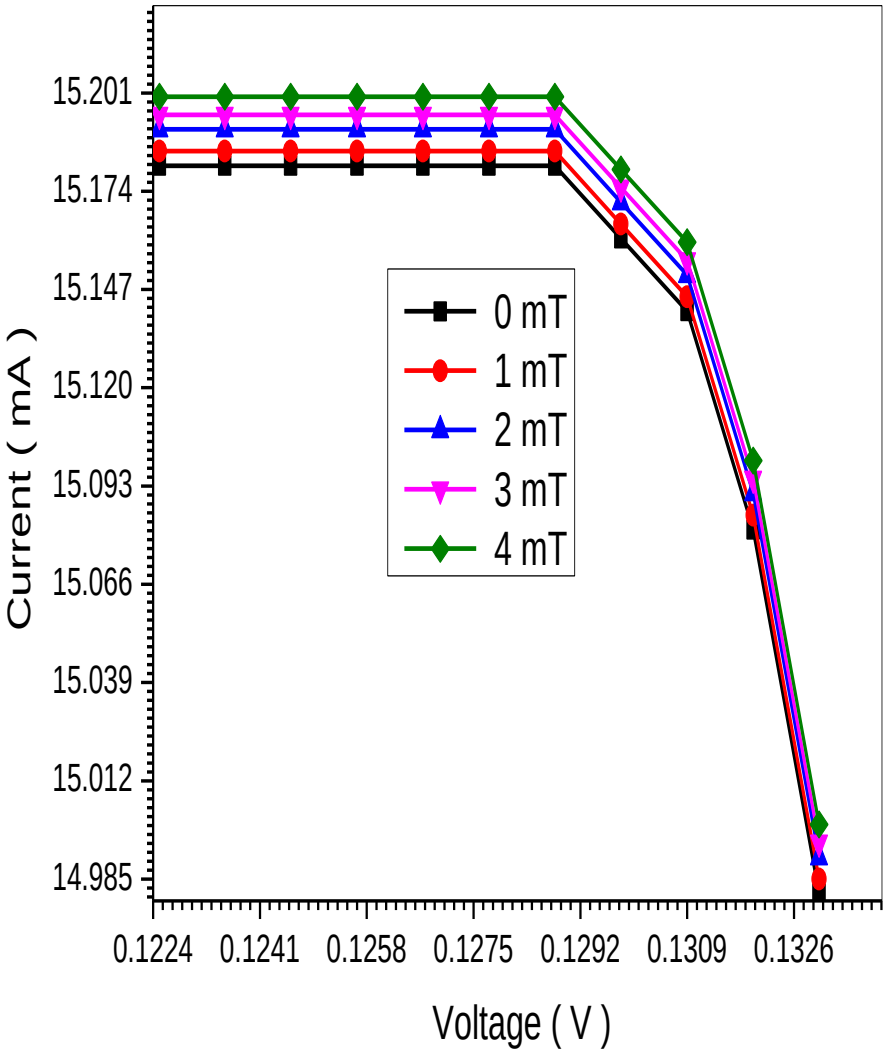

Figure (5.10) I–V curves of Rhodamine B SCs with different magnetic field (0, 1, 2, 3 and 4) mT

Table (5.1) I–V reading of Rhodamine B SCs with different magnetic field intensity (0, 1, 2, 3 and 4) mT

Sample No	**I_{sc} (mA)**	**I_{max} (mA)**	**V_{max}(V)**	**V_{oc}(V)**	**FF**	**J_{sc}(mA.cm^{-2})**	**η**	**Bm T**
1	15.181	15.16	0.12996	0.1331	0.975	2.4289	0.21	0
2	15.185	15.17	0.19998	0.1331	0.976	2.4296	0.2101	1
3	15.191	15.17	0.12996	0.133	0.978	2.43056	0.2103	2
4	15.195	15.18	0.12994	0.1333	0.976	2.4312	0.2104	3
5	15.200	15.18	0.13	0.133	0.976	2.432	0.2106	4

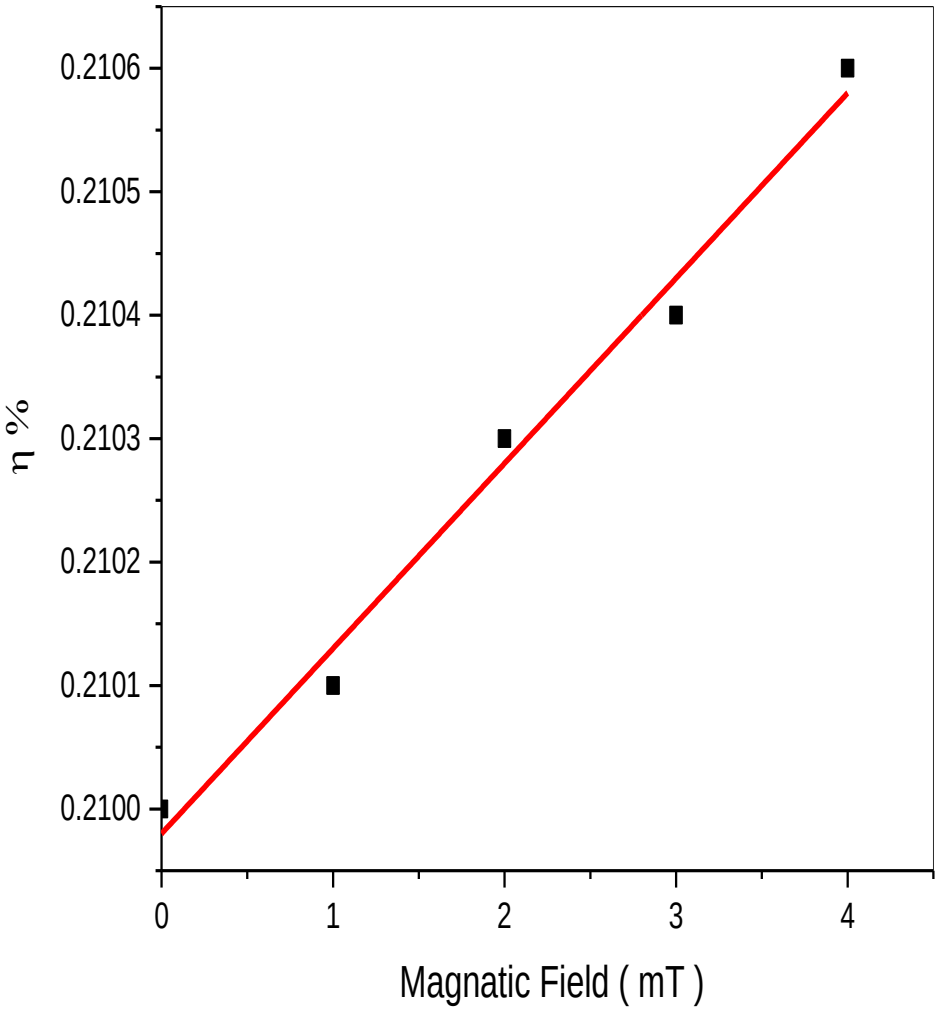

Figure (5.11) Relationship between Efficiencies versus Magnetic Field of Rhodamine B SCs

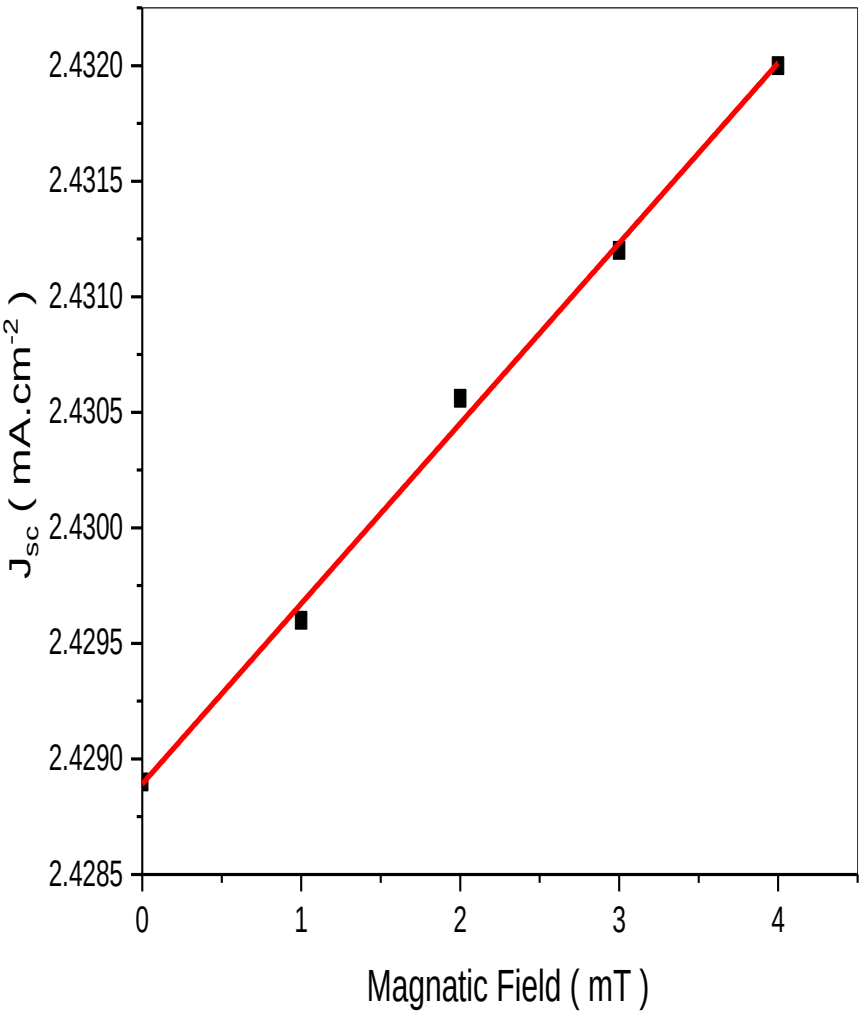

Figure (5.12) relationship between densities of current versus magnetic field of Rhodamine B (DSCs)

5.1.2 Discussion of Rhodamine B

- The optical absorption spectra in the (250 - 800) nm wavelength range for the Rhodamine B dye are depicted in Fig (5.1). They are three high absorption region is observed at wavelength (255nm is 4 a.u, 421 nm is 1.7 a.u and 600 nm equal 1.5 a.u), the absorption edge of the Rhodamine B dye corresponding to photon energy (4.9 eV, 2.9 eV and 2.1 eV).
- Fig (5.2) shows the relation between absorption coefficient and wavelengths, one found rapid decrease at 255 nm and sudden increase at 327 nm with continuous increase after 500 nm wavelength.
- In fig (5.3) show that relation between excitation coefficient and wavelengths it the same as absorption coefficient .And in fig (5.3) show that high value of excitation coefficient equal $3.2x10^{-3}$ at wavelength 600 nm .
- The energy band gap of Rhodamine B is determined using the absorption spectra. According to the absorption coefficient (α) for direct band gap material is given by the relation

$$\alpha h\nu = B(h\nu - E_g)^n \qquad (5.1)$$

Where E_g the energy gap, constant B is different for different transitions, (hv) is energy of photon and (n) is an index which assumes the values 1/2, 3/2, 2 and 3 depending on the nature of the electronic transition responsible for the reflection. And by extrapolating the straight thin portion of the curve to

intercept the energy axis, the value of the energy gap has been to found be (2.49 eV) as show in fig (5.4).

- Fig(5.5) shows the current-voltage characteristics obtained from the measured values this measurement was taken from solar cell of the structure (ITO/ Rhodamine B dye / MEH-PPV/Ag) at 0 mT effect , the short-circuit current (I_{sc}) is 15.181 mA , the open-circuit voltage (V_{oc}) is 0.1331 V, fill factor (FF) is 0.975, and the efficiency is 0.21 %.
- Fig(5.6) shows the current-voltage characteristics obtained from the measured values this measurement was taken from solar cell of the structure (ITO/ Rhodamine B dye / MEH-PPV/Ag) at 1 mT effect , the short-circuit current (I_{sc}) is 15.185 mA , the open-circuit voltage (V_{oc}) is 0.1331 V, fill factor (FF) is 0.976, and the efficiency is 0.2101 %.
- Fig(5.7) shows the current-voltage characteristics obtained from the measured values this measurement was taken from solar cell of the structure (ITO/ Rhodamine B dye / MEH-PPV/Ag) at 2 mT effect , the short-circuit current (I_{sc}) is 15.191 mA , the open-circuit voltage (V_{oc}) is 0.133 V, fill factor (FF) is 0.978 , and the efficiency is 0.2103 %.
- Fig(5.8) shows the current-voltage characteristics obtained from the measured values this measurement was taken from solar cell of the structure (ITO/ Rhodamine B dye / MEH-PPV/Ag) at 3 mT effect , the short-circuit current (I_{sc}) is 15.195 mA , the open-circuit voltage (V_{oc}) is 0.1333 V, fill factor (FF) is 0.976, and the efficiency is 0.2104 %.
- Fig(5.9) shows the current-voltage characteristics obtained from the measured values this measurement was taken from solar cell of the structure (ITO/ Rhodamine B dye / MEH-PPV/Ag) at 4 mT effect , the short-circuit current (I_{sc}) is 15.20 mA , the open-circuit voltage (V_{oc}) is 0.133 V, fill factor (FF) is 0.976, and the efficiency is 0.2106 %.

- Fig (5.10) show that the relation between current and voltage characteristics for the five samples of Rhodamine B solar cells when effect by deferent magnetic field (0, 1, 2, 3 and 4) mT . In fig (4.10) show that magnetic field increases the efficiency increase.
- The magmatic field effect on the efficiency it is very interesting to note that table (4.1) indicates the increase of magmatic field and the increases of the solar cell efficiency in general. This is since the magmatic field increase enables electrons having lower excitation energy to become free electron in a conduction band thus increasing the electric solar efficiency (by rated $1.5x10^{-4}$ % $.mT^{-1}$) as show in fig (5.11).
- The magmatic field also effect Solar Cells densities of current the results recorded in table (5.1) shows that increase of magmatic field increases densities of current. This can be under stood if one take into account the fact that according to number of electron increase on the area of solar cell and increase chances for electrons transfer from valence to conduction(by rated $7.8x10^{-4}$ $mA.cm^{-2}$ $.mT^{-1}$) show fig (5.12).

5.1.3 Results of Coumarin 500

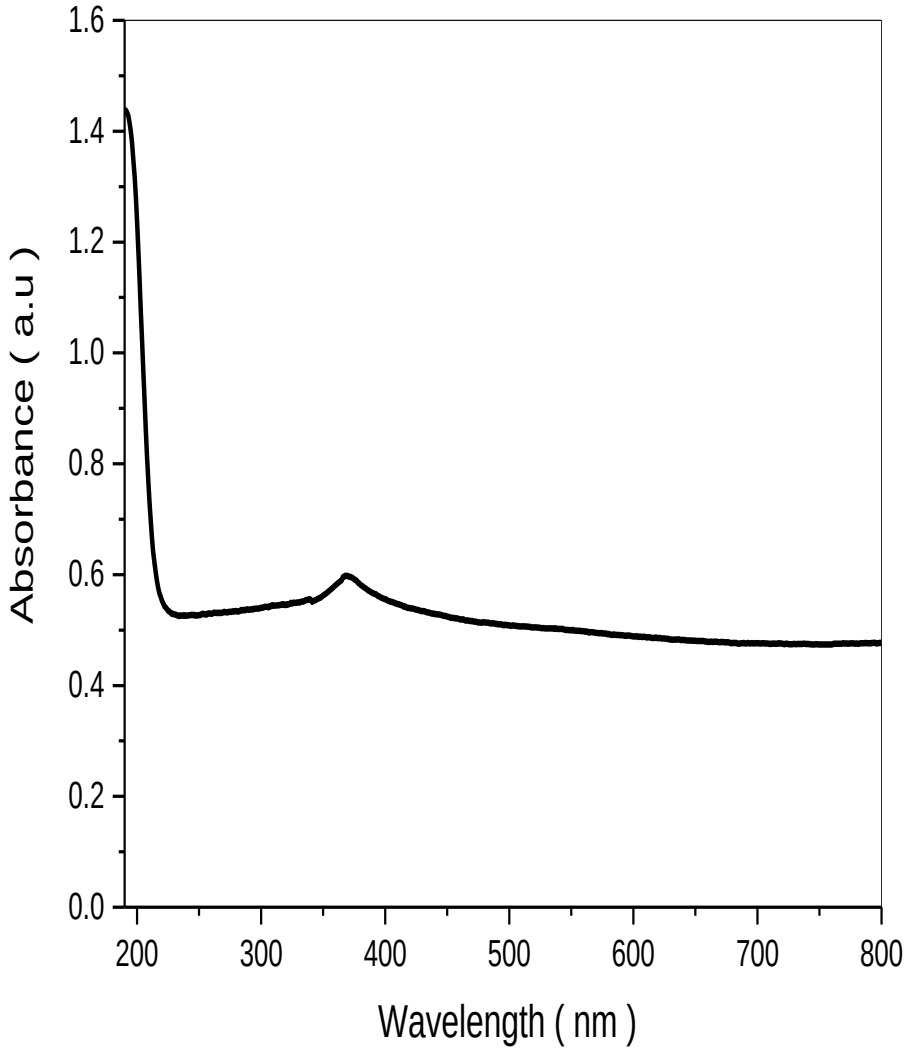

Figure (5.13) relationship between efficiencies versus magnetic field of Coumarin 500 Dye

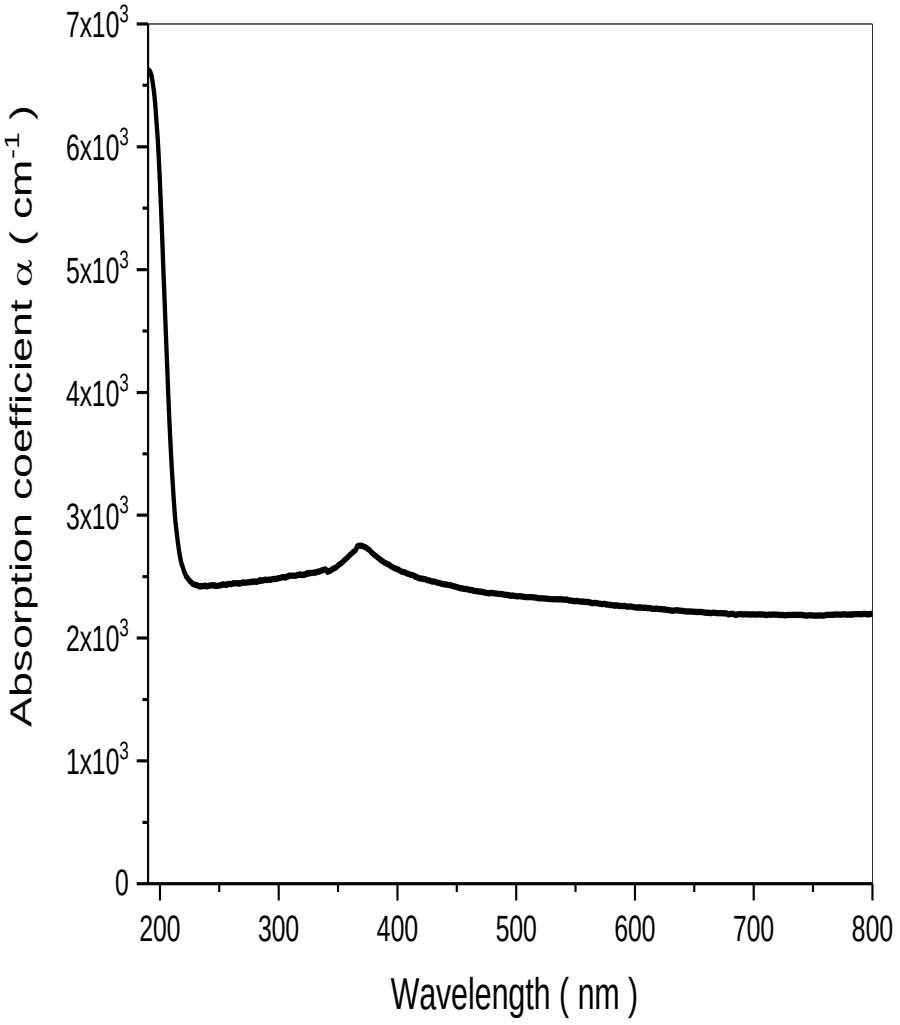

Figure (5.14) the optical absorption coefficient spectra for the Coumarin 500 Dye

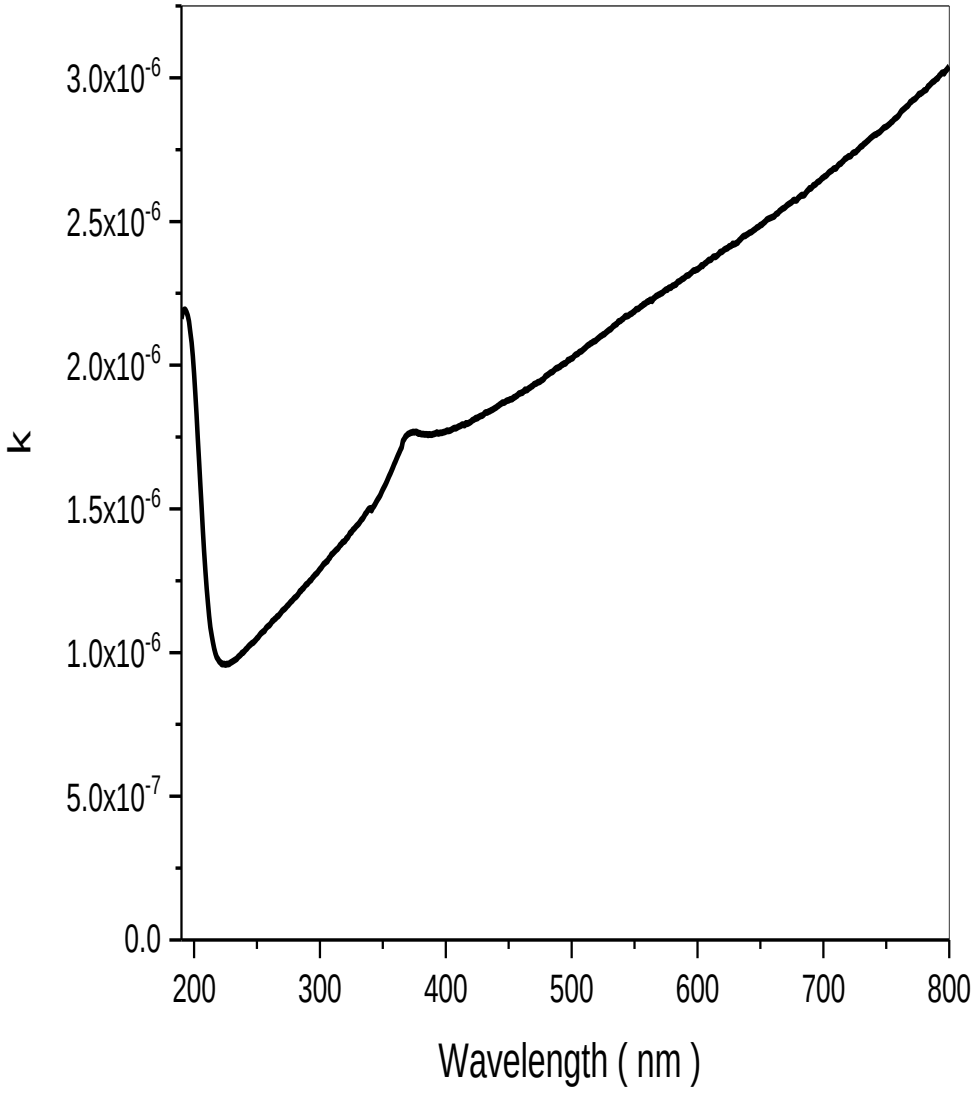

Figure (5.15) the Exaction Coefficient Spectra for the Coumarin 500 Dye

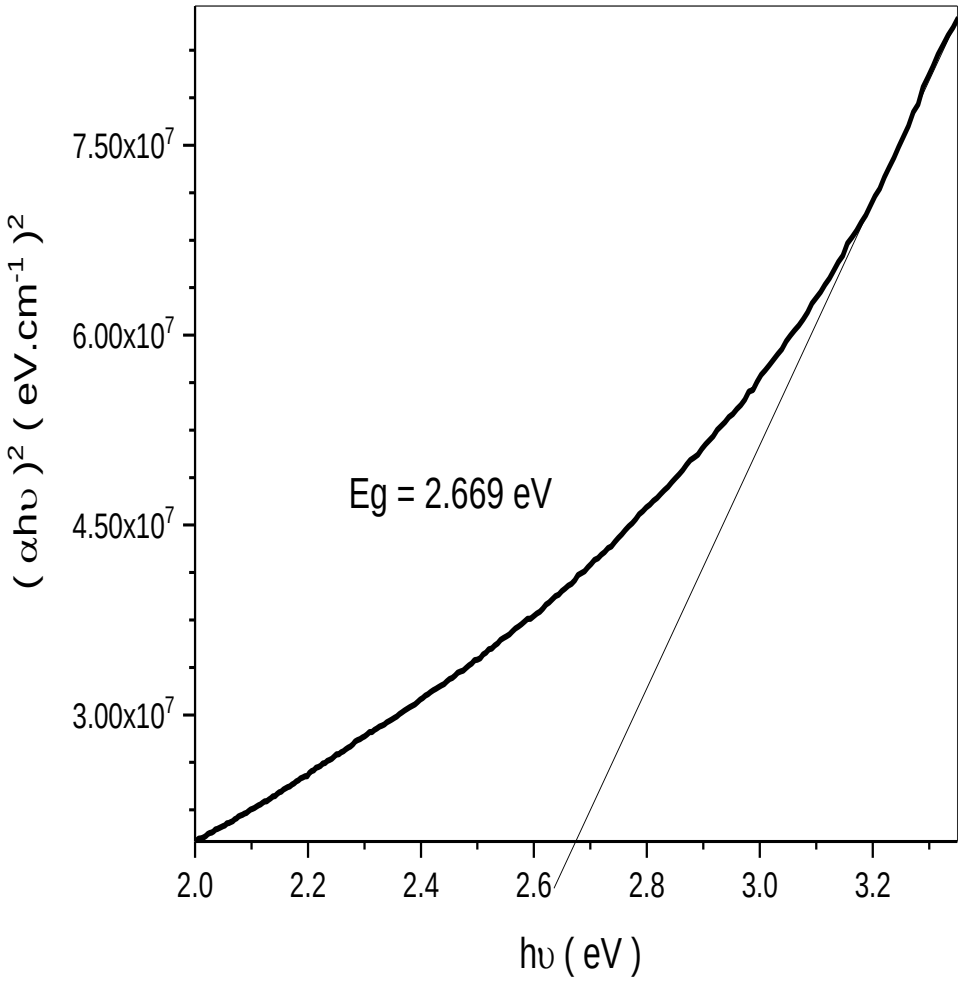

Figure (5.16) the Optical Energy Band Gap Spectra for the Coumarin 500 Dye

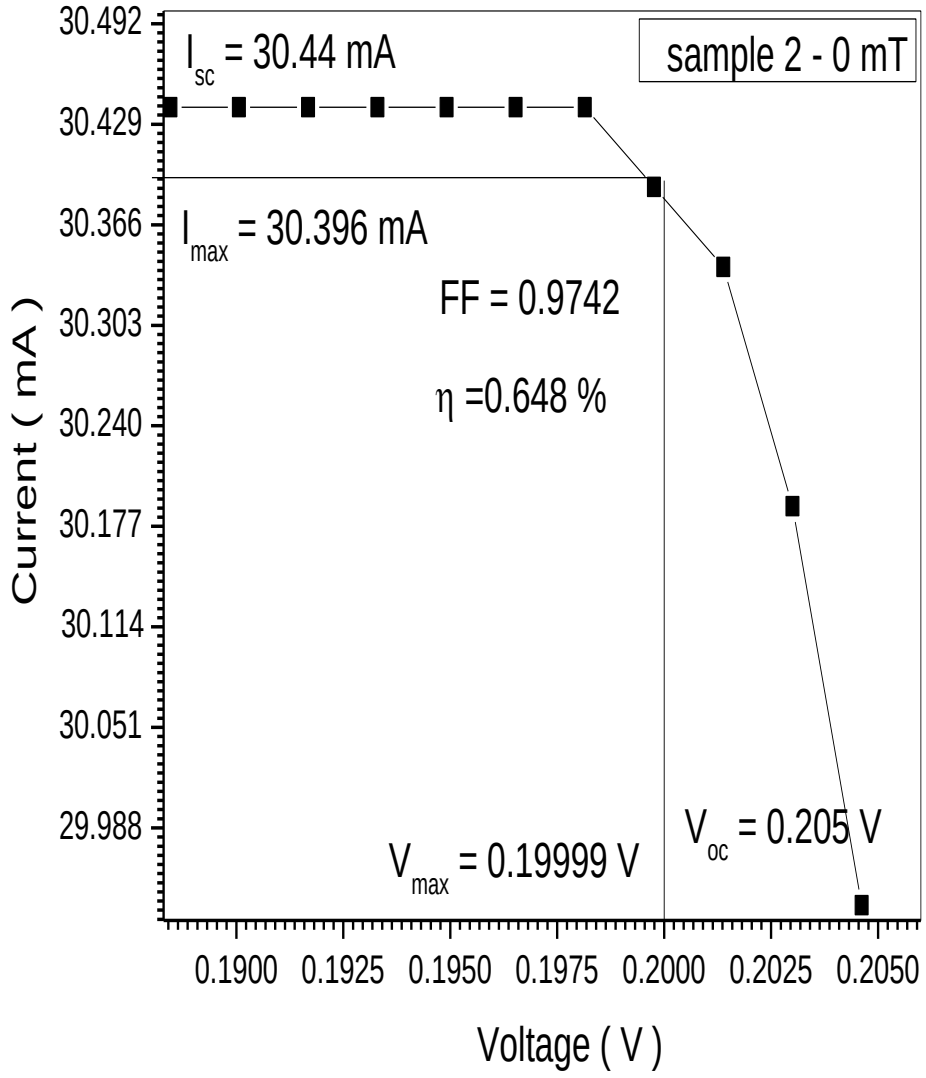

Figure (5.17) I–V curves of Coumarin 500 SC for the 0 mT

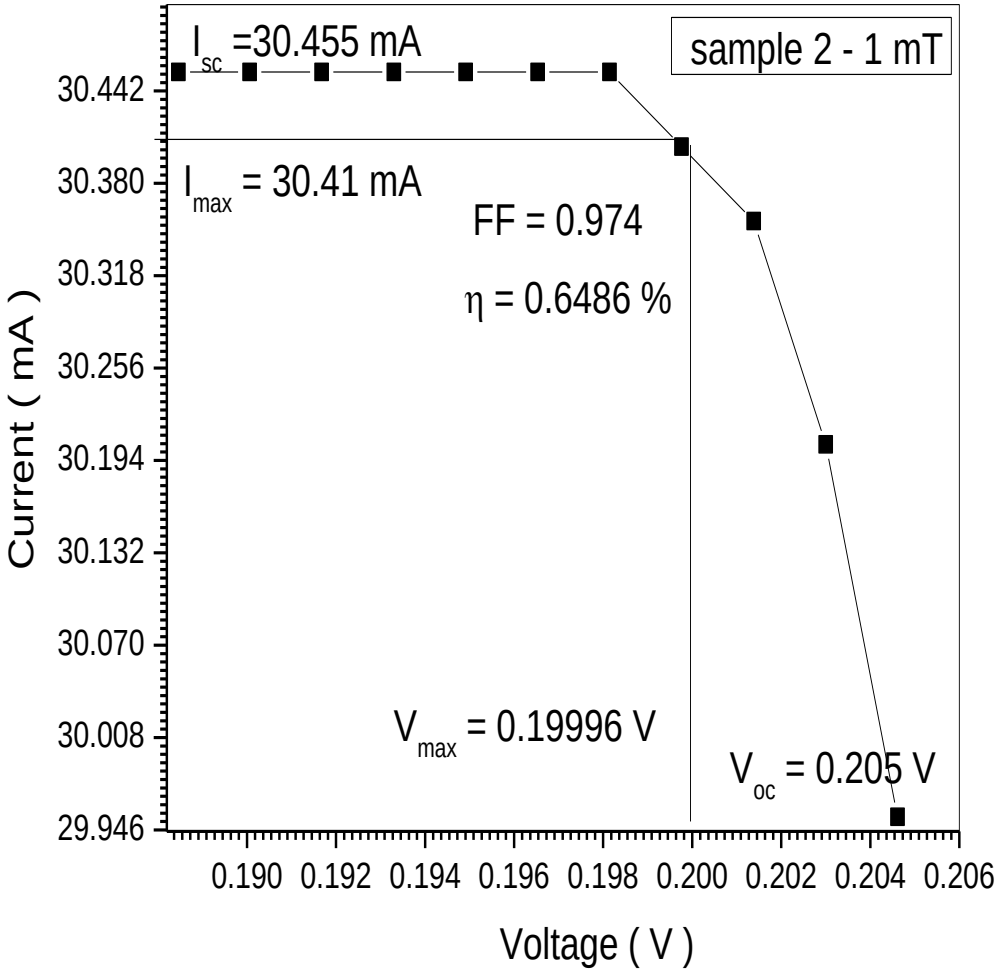

Figure (5.18) I–V curves of Coumarin 500 SC for the 1 mT

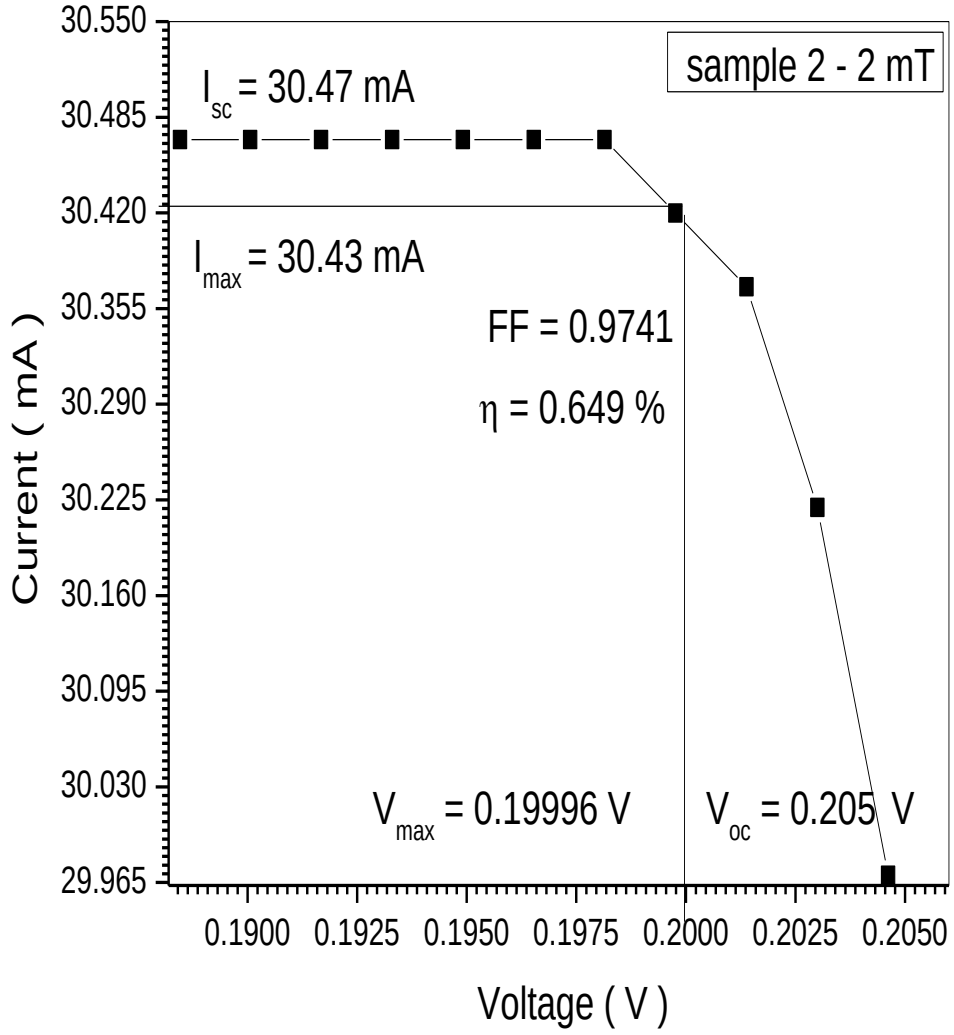

Figure (5.19) I–V curves of Coumarin 500 SC for the 2 mT

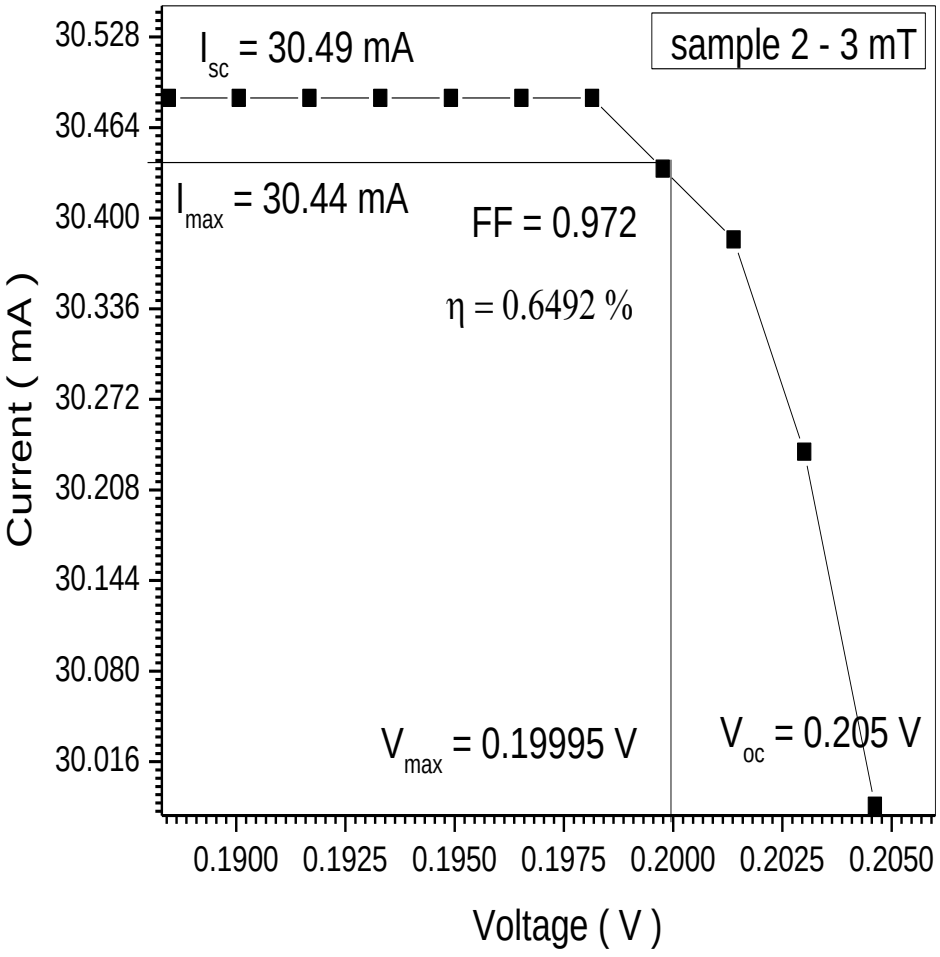

Figure (5.20) I–V curves of Coumarin 500 SC for the 3 mT

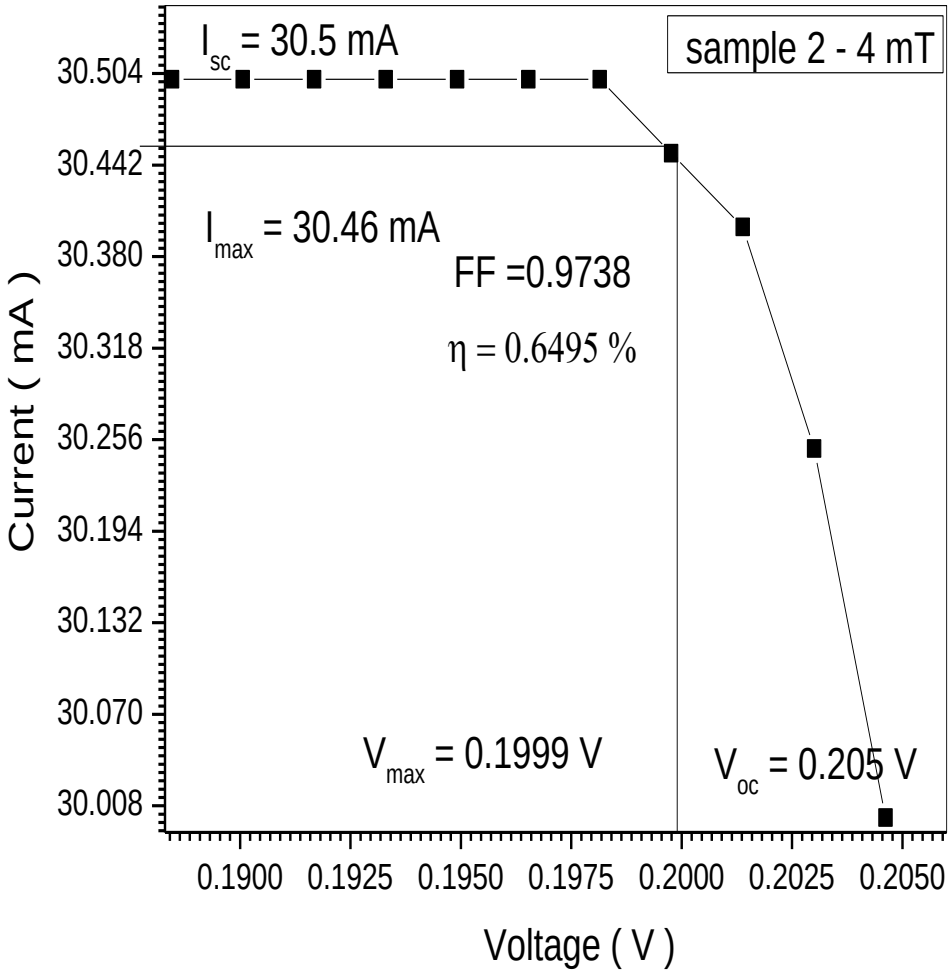

Figure (5.21) I–V curves of Coumarin 500 SC for the 4 mT

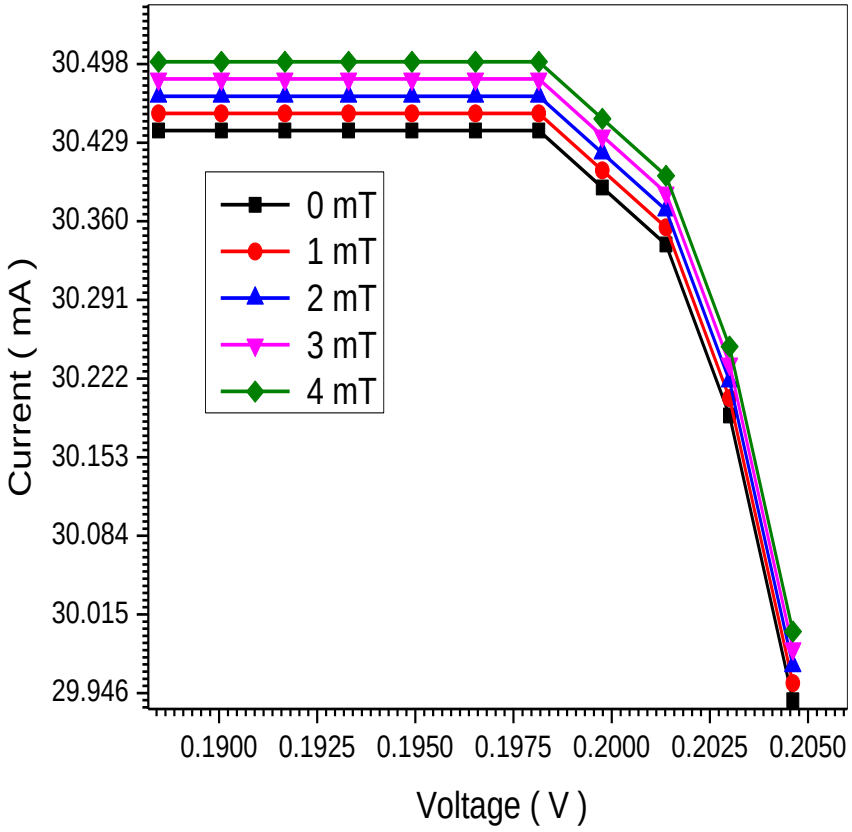

Figure (5.22) I–V curves of Coumarin 500 SCs with different magnetic field (0, 1, 2, 3 and 4) mT

Table (5.2) I–V reading of Coumarin 500 SCs with different magnetic field (0, 1, 2, 3 and 4) mT

Sample No	**I_{sc} (mA)**	**I_{max} (mA)**	**V_{max} (V)**	**V_{OC} (V)**	**FF**	**J_{sc} ($mA.cm^{-2}$)**	**η**	**B mT**
1	30.44	30.396	0.19999	0.205	0.9742	4.8704	0.648	0
2	30.455	30.41	0.19996	0.205	0.974	4.8728	0.6486	1
3	30.47	30.43	0.19996	0.205	0.9741	4.8752	0.649	2
4	30.49	30.44	0.19995	0.205	0.972	4.8784	0.6492	3
5	30.50	30.46	0.1999	0.205	0.9738	4.88	0.6495	4

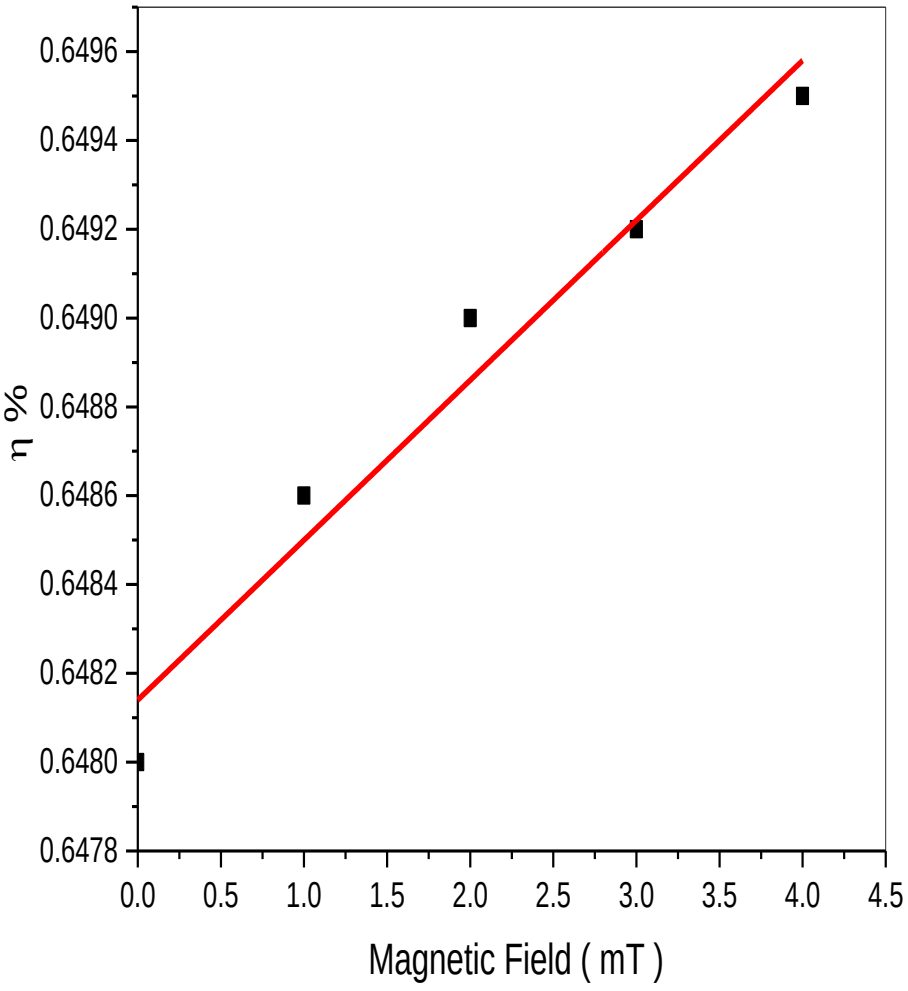

Figure (5.23) Relationship between Densities of Current versus Magnetic Field of Coumarin 500 (DSCs)

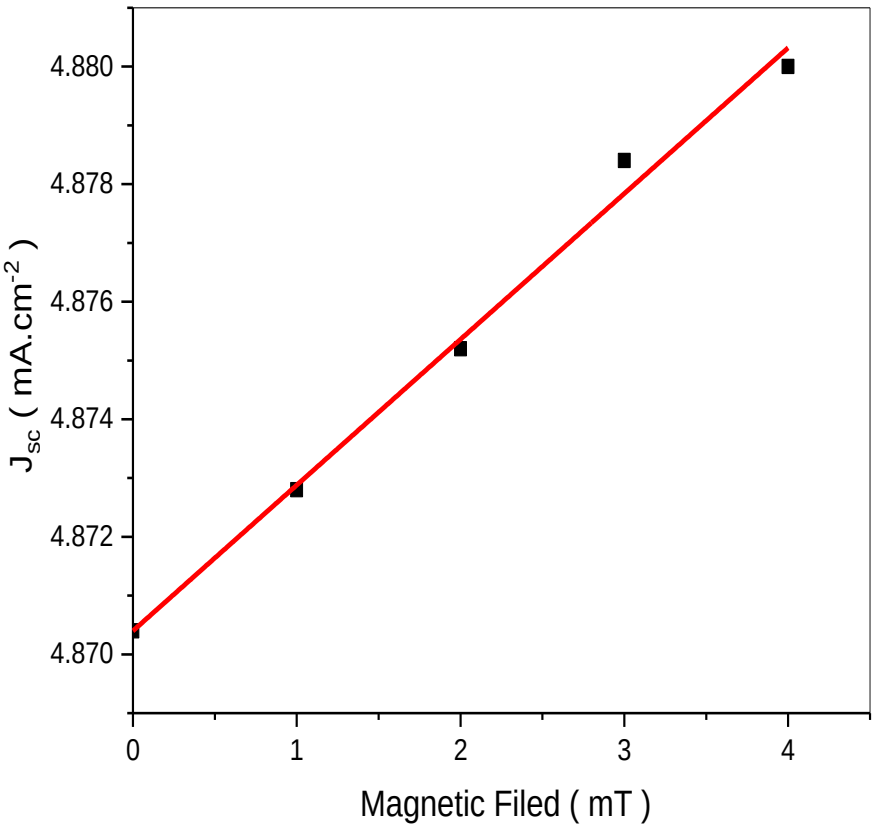

Figure (5.24) relationship between efficiencies versus magnetic field of Coumarin 500 SCs

5.1.4 Discussion of Coumarin 500

- The optical absorption spectra in the (190 - 800) nm wavelength range for the Coumarin 500 Dye is depicted in Fig (5.13). The high absorption region is observed at wavelength (225nm is 0.12 a.u), the absorption edge of the Coumarin 500 dye corresponding to photon energy (5.5 eV).
- Fig (5.14) shows the relation between absorption coefficient and wavelengths, one found rapid decrease at 225 nm and sudden increase at 360 nm with continuous decrease after 360 nm wavelength.
- In fig (5.15) show that relation between excitation coefficient and wavelengths it the same as absorption coefficient .And in fig (5.15) show that high value of excitation coefficient equal 8.66×10^{-4} at wavelength 225 nm .
- The optical energy band gap of Coumarin 500 is determined using the absorption spectra. According to the absorption coefficient (α) for direct band gap material is given by the relation

$$\alpha h\nu = B(h\nu - E_g)^n \qquad (5.1)$$

Where E_g the energy gap, constant B is different for different transitions, (hv) is energy of photon and (n) is an index which assumes the values 1/2, 3/2, 2 and 3 depending on the nature of the electronic transition responsible for the reflection. And by extrapolating the straight thin portion of the curve to intercept the energy axis, the value of the energy gap has been to found be (3.001 eV) as show in fig (5.16).

- Fig(5.17) shows the current-voltage characteristics obtained from the measured values this measurement was taken from solar cell of the structure (ITO/Coumarin 500 dye / MEH-PPV/Ag) at 0 mT effect , the short-circuit current (I_{sc}) is 30.44 mA , the open-circuit voltage (V_{oc}) is 0.205 V, fill factor (FF) is 0.9742, and the efficiency is 0.648 %.
- Fig(5.18) shows the current-voltage characteristics obtained from the measured values this measurement was taken from solar cell of the structure (ITO/ Coumarin 500 dye / MEH-PPV/Ag) at 1 mT effect , the short-circuit current (I_{sc}) is 30.455 mA , the open-circuit voltage (V_{oc}) is 0.205 V, fill factor (FF) is 0.974, and the efficiency is 0.6486 %.
- Fig(5.19) shows the current-voltage characteristics obtained from the measured values this measurement was taken from solar cell of the structure (ITO/ Coumarin 500 dye / MEH-PPV/Ag) at 2 mT effect , the short-circuit current (I_{sc}) is 30.47 mA , the open-circuit voltage (V_{oc}) is 0.205 V, fill factor (FF) is 0.9741 , and the efficiency is 0.649 %.
- Fig(5.20) shows the current-voltage characteristics obtained from the measured values this measurement was taken from solar cell of the structure (ITO/ Coumarin 500 dye / MEH-PPV/Ag) at 3 mT effect , the short-circuit current (I_{sc}) is 30.49 mA , the open-circuit voltage (V_{oc}) is 0.205 V, fill factor (FF) is 0.972, and the efficiency is 0.6492 %.
- Fig(5.21) shows the current-voltage characteristics obtained from the measured values this measurement was taken from solar cell of the structure (ITO/ Coumarin 500 dye / MEH-PPV/Ag) at 4 mT effect , the short-circuit current (I_{sc}) is 30.50 mA , the open-circuit voltage (V_{oc}) is 0.205 V, fill factor (FF) is 0.9738, and the efficiency is 0.6495 %.
- Fig (5.22) show that the relation between current and voltage characteristics for the five samples of Rhodamine B solar cells when effect

by deferent magnetic field (0, 1, 2, 3 and 4) mT. In fig (5.22) show that magnetic field increases the efficiency increase.

- The magmatic field effect on the efficiency it is very interesting to note that table (5.2) indicates the increase of magmatic field and the increases of the solar cell efficiency in general. This is since the magmatic field increase enables electrons having lower excitation energy to become free electron in a conduction band thus increasing the electric solar efficiency (by rated $6.6x10^{-4}$ % $.mT^{-1}$) as show in fig (5.23).
- The magmatic field also effect Solar Cells densities of current the results recorded in table (5.2) shows that increase of magmatic field increases densities of current. This can be under stood if one takes into account the fact that according to number of electron increase on the area of solar cell and increase chances for electrons transfer from valence to conduction(by rated $4.48x10^{-7}$ $mA.cm^{-2}$ $.mT^{-1}$) show fig (5.24).

5.1.5 Results of Eriochrome black T

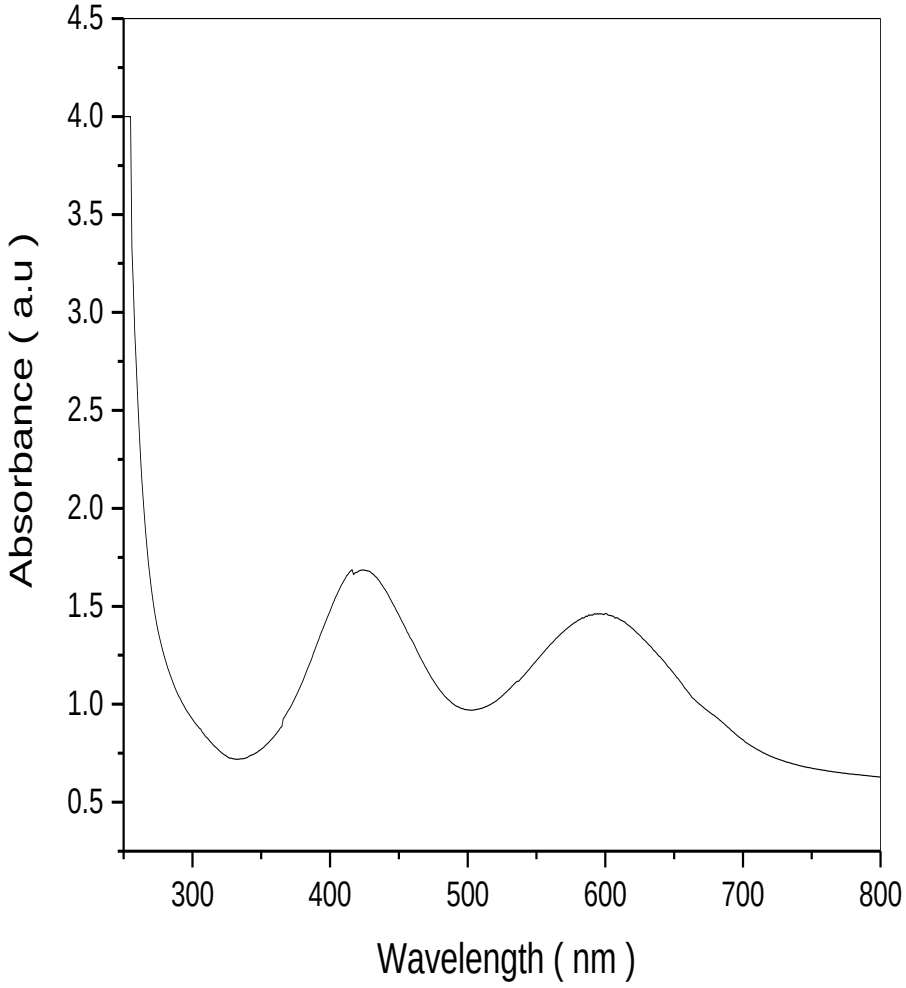

Figure (5.25) the Optical Absorption Spectra for the Eriochrome black T Dye

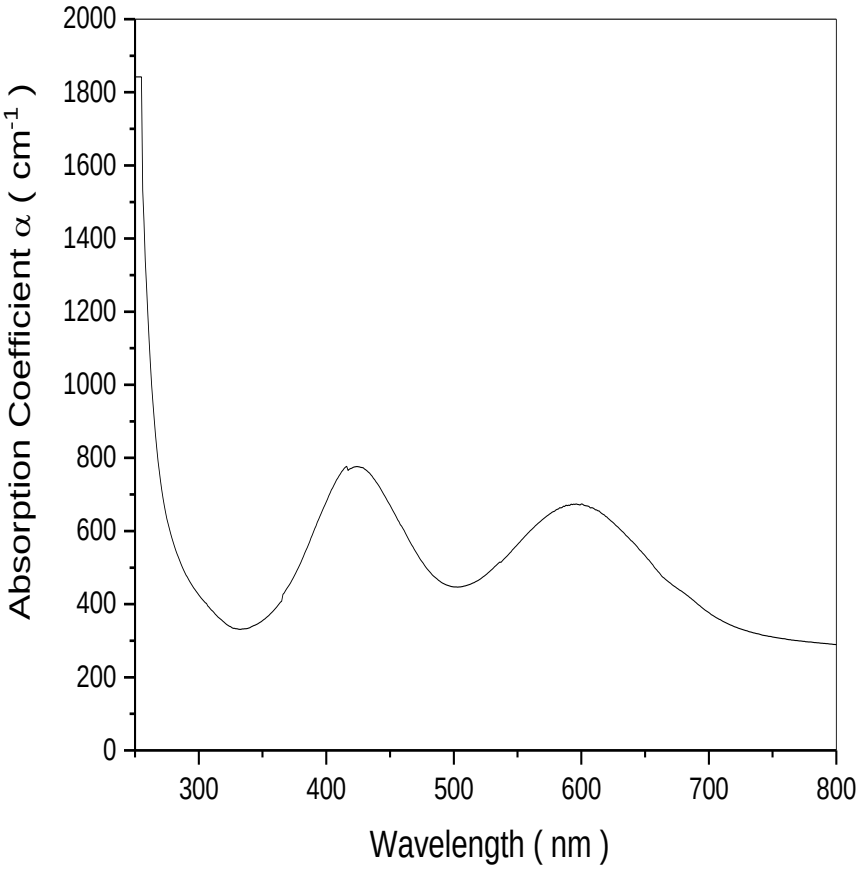

Figure (5.26) the Optical Absorption Coefficient Spectra for the Eriochrome black T Dye

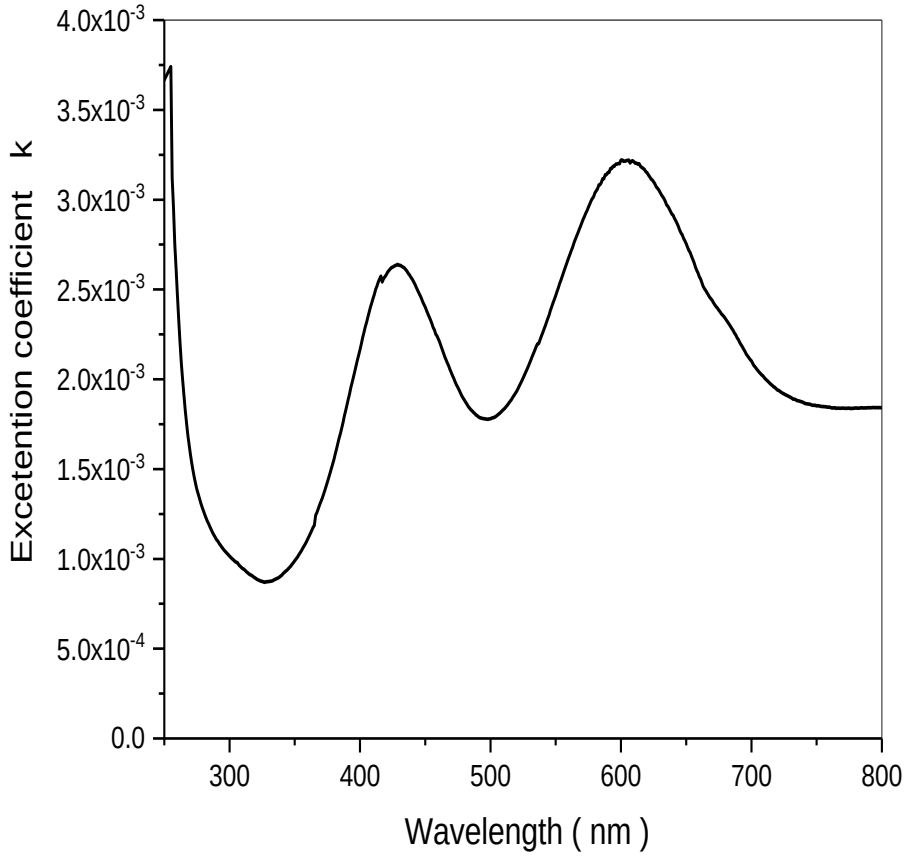

Figure (5.27) the Exaction Coefficient Spectra for the Eriochrome black T Dye

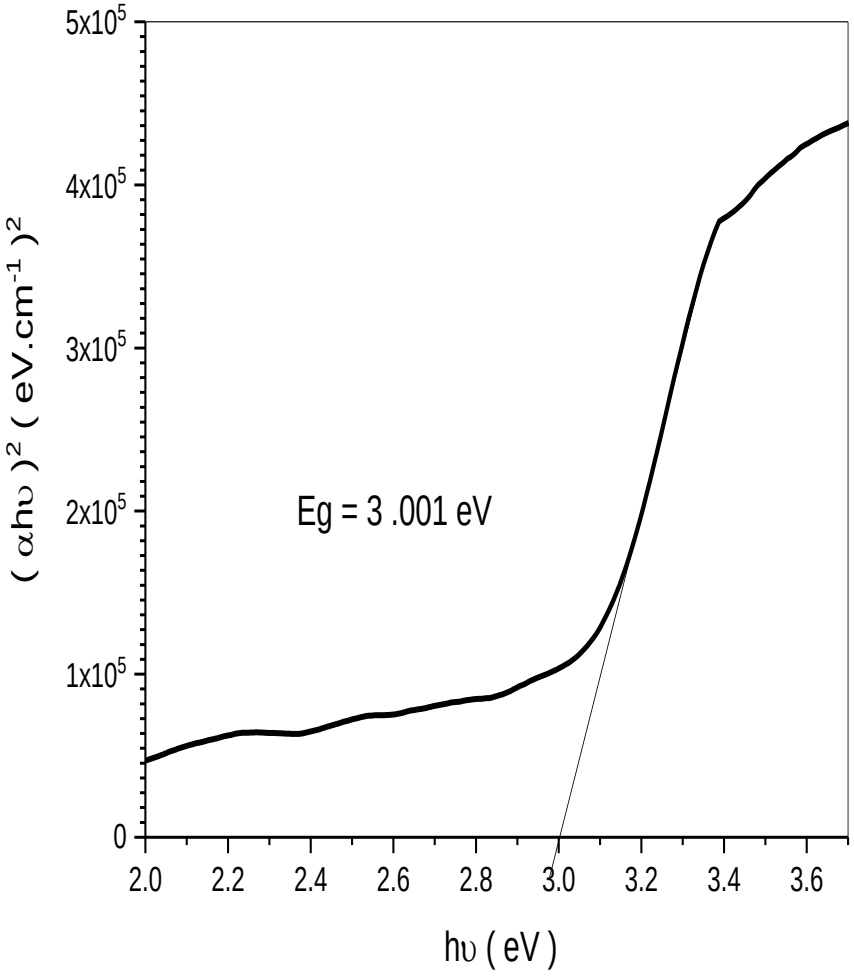

Figure (5.28) the Optical Energy Band Gap Spectra for the Eriochrome black T Dye

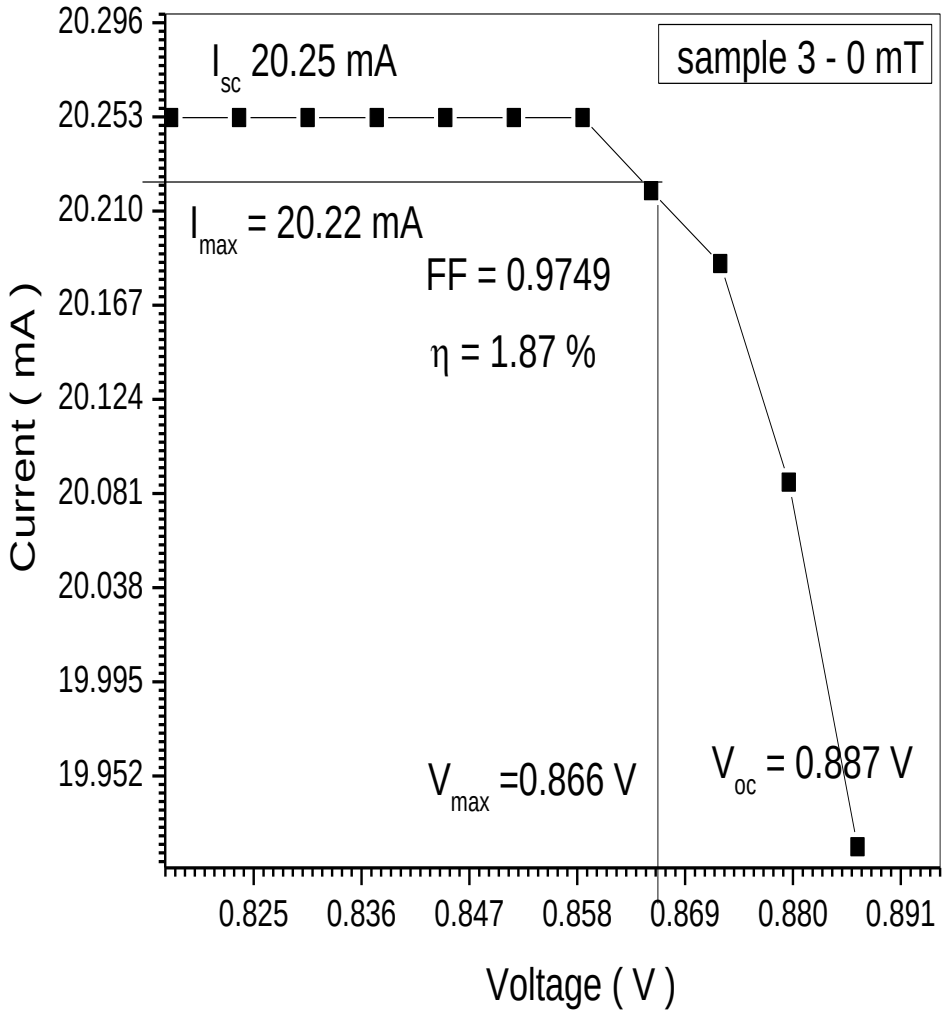

Figure (5.29) I–V curves of Eriochrome black T SC for the 0 mT

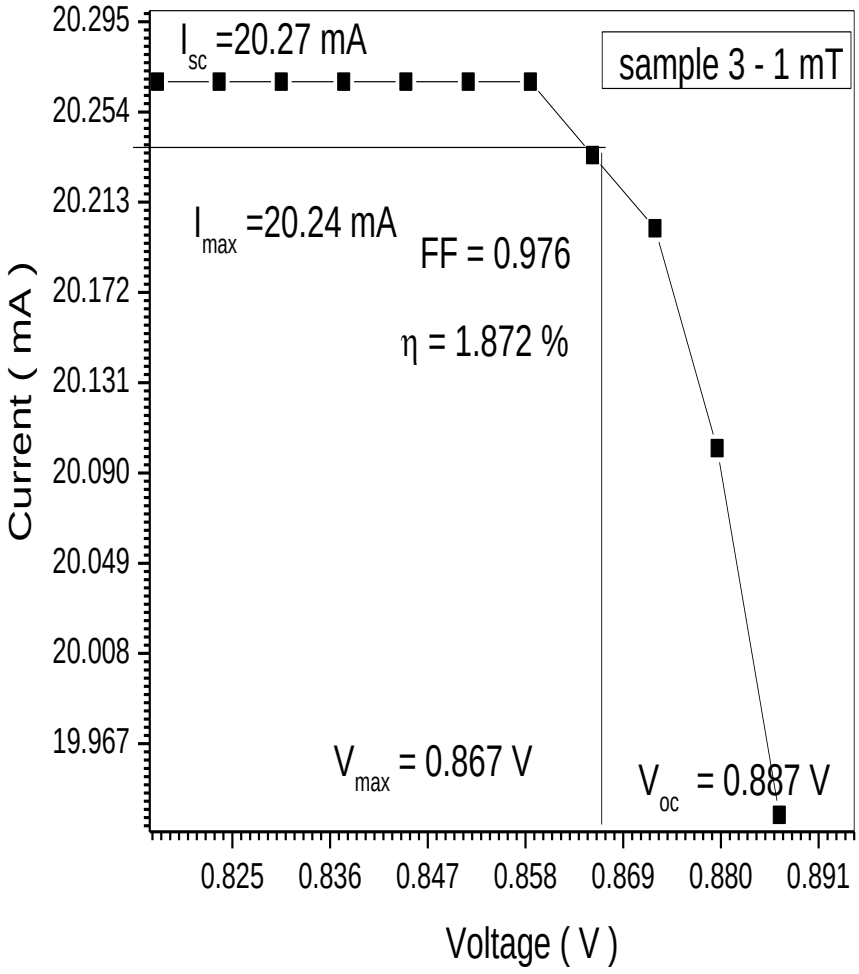

Figure (5.30) I–V curves of Eriochrome black T T SC for the 1 mT

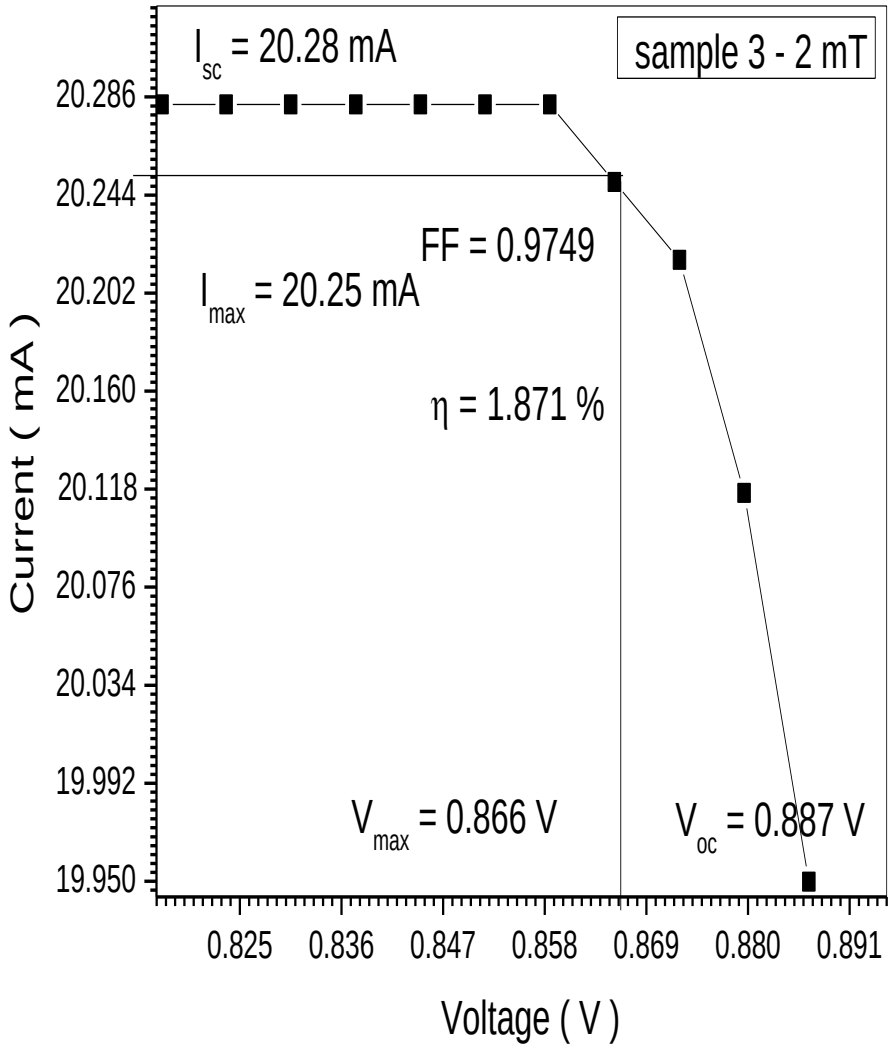

Figure (5.31) I–V curves of Eriochrome black T SC for the 2mT

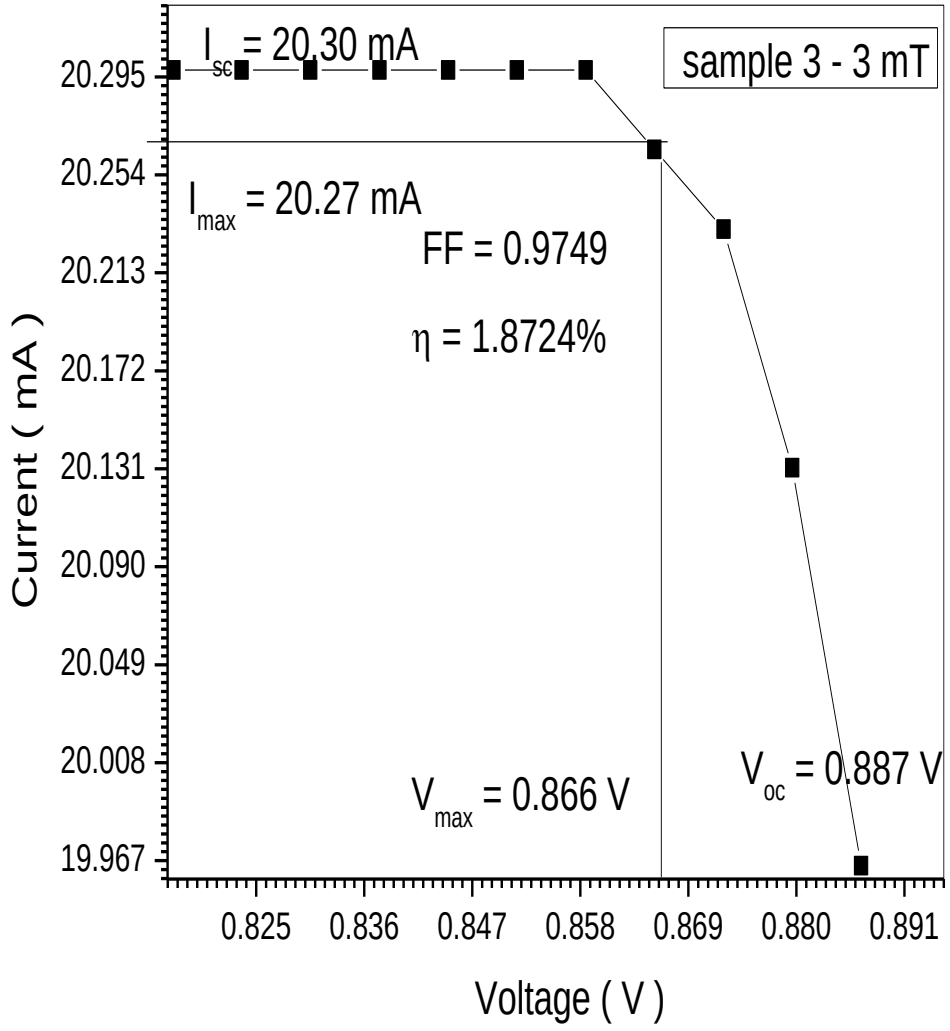

Figure (5.32) I–V curves of Eriochrome black T SC for the 3mT

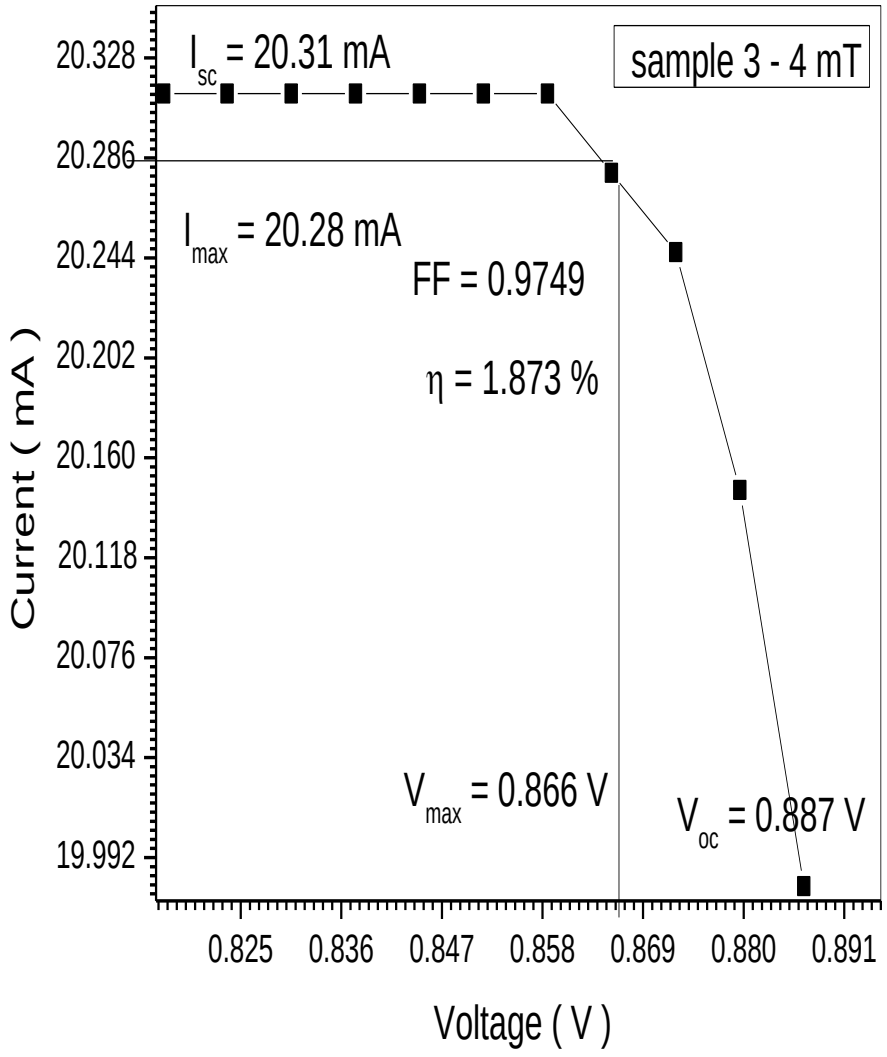

Figure (5.33) I–V curves of Eriochrome black T SC for the 4 mT

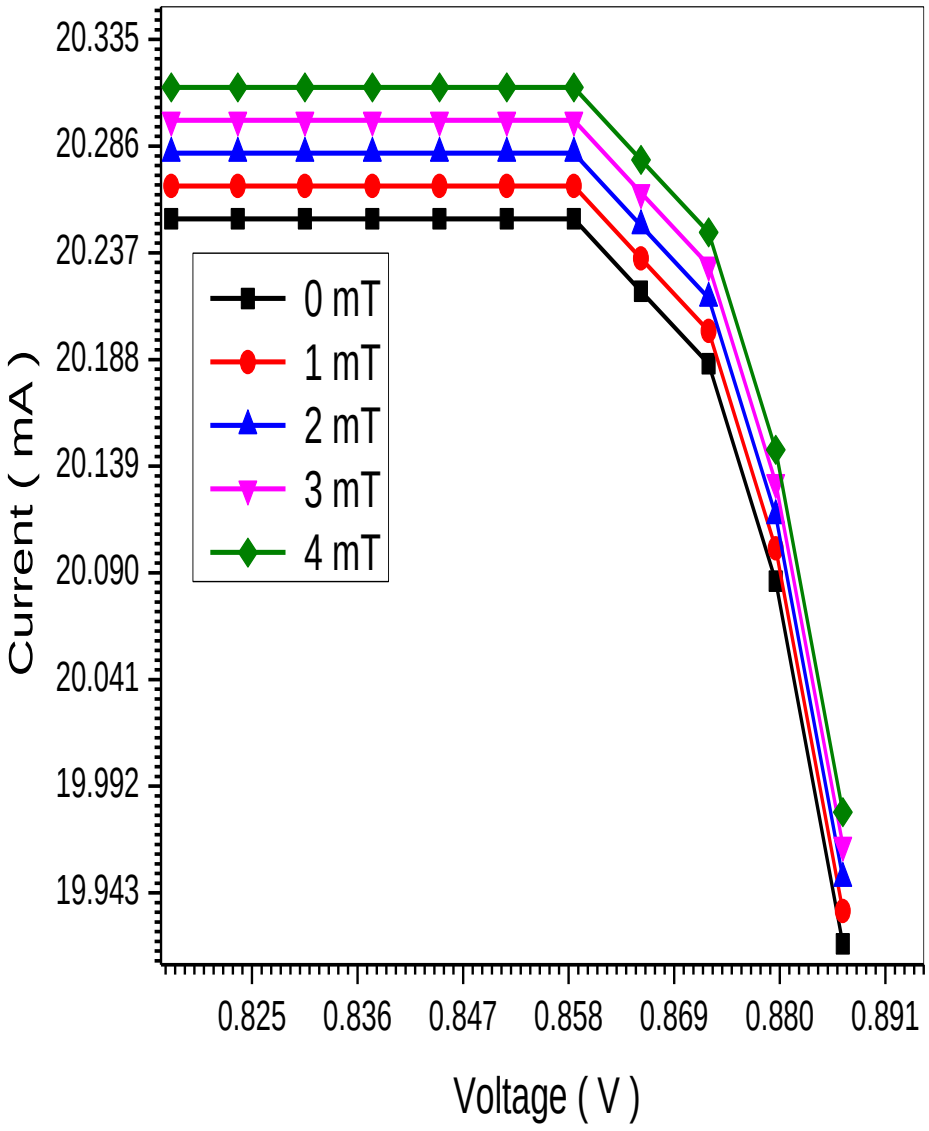

Figure (5.34) I–V curves of Eriochrome black T SCs with different magnetic field intensity (0, 1, 2, 3 and 4) mT

Table (5.3) I–V reading of Eriochrome black T SCs with different magnetic field (0, 1, 2, 3 and 4) mT

Sample No	I_{sc} (mA)	I_{max} (mA)	V_{max} (V)	V_{OC} (V)	FF	J_{sc} (mA.cm^{-2})	η%	B mT
1	20.25	20.22	0.866	0.8887	0.9749	3.24	1.87	0
2	20.27	20.24	0.867	0.887	0.976	3.2432	1.871	1
3	20.28	20.25	0.866	0.887	0.9749	3.2448	1.872	2
4	20.30	20.27	0.866	0.887	0.9749	3.248	1.8724	3
5	20.31	20.28	0.866	0.887	0.9749	3.2496	1.873	4

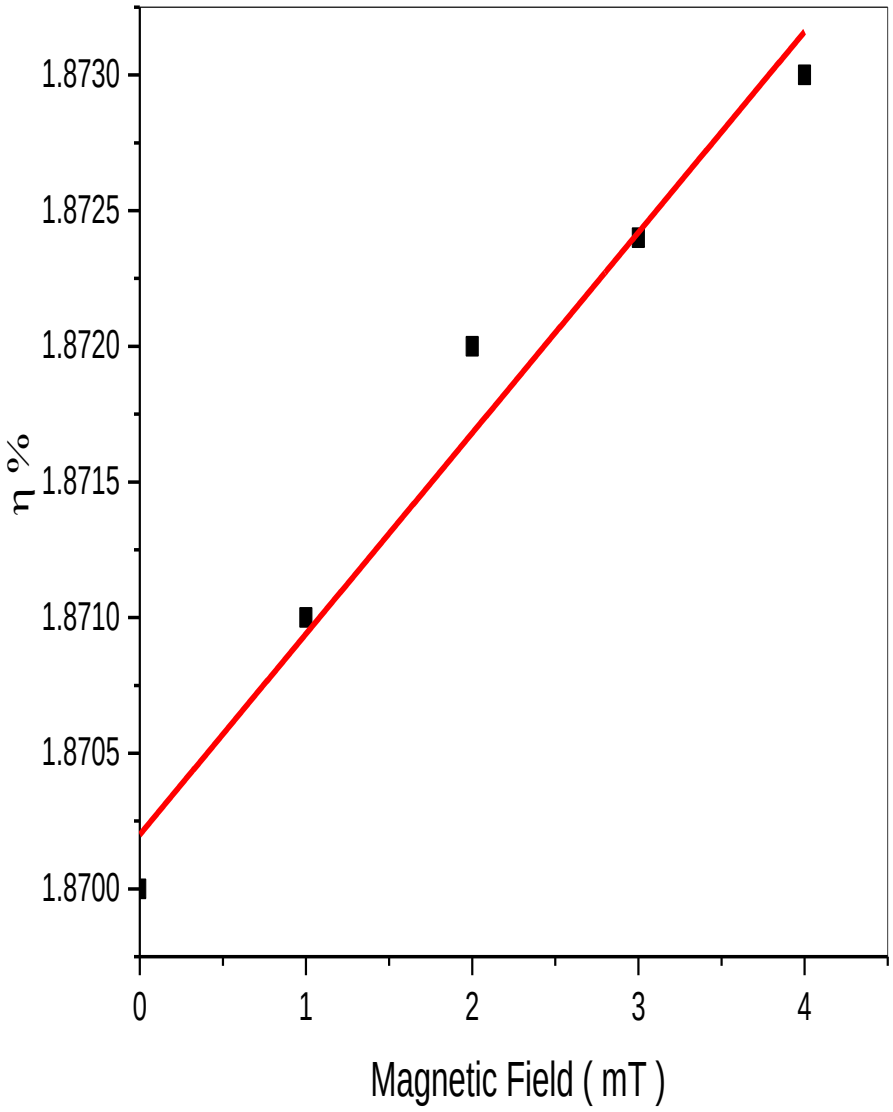

Figure (5.35) relationship between densities of current versus magnetic field of Eriochrome black T SCs

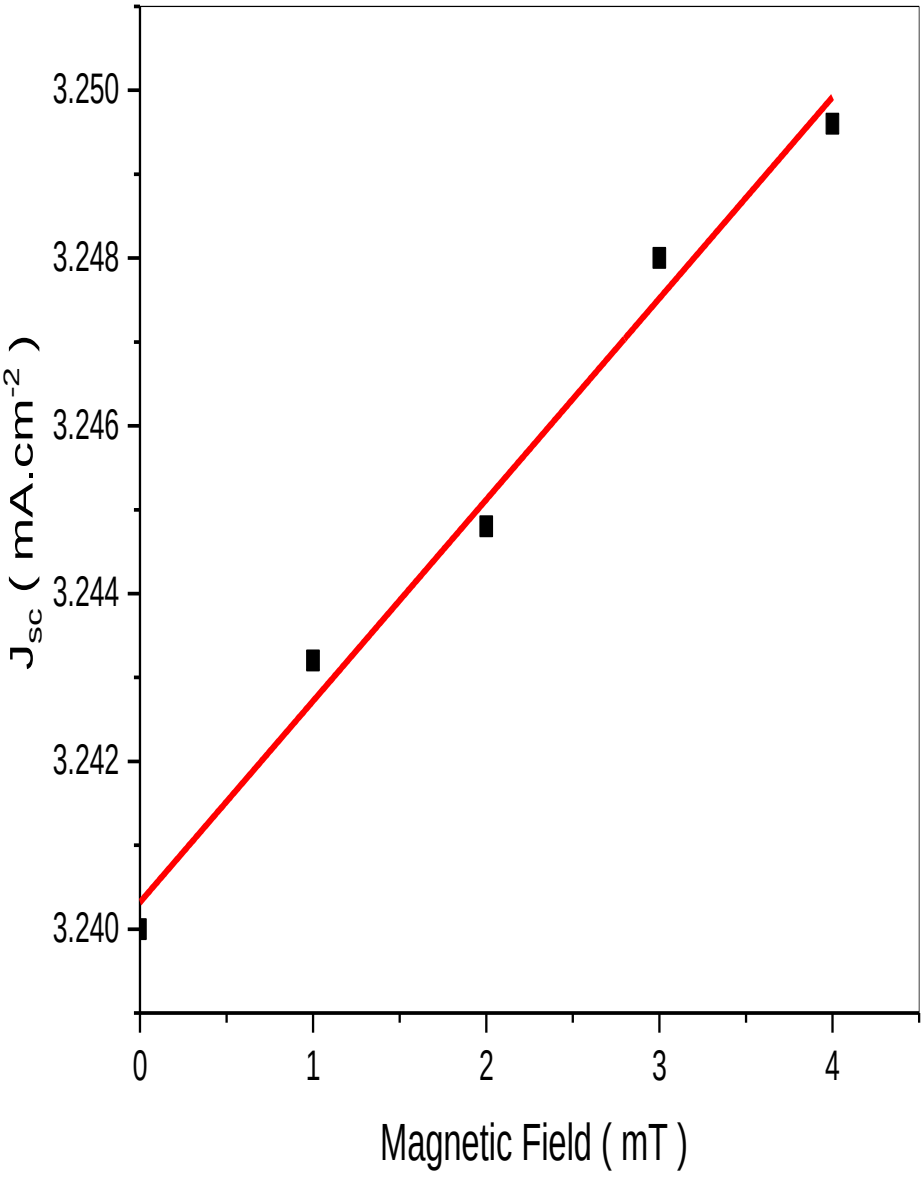

Figure (5.36) the optical absorption spectra for the Eriochrome black T (DSCs)

5.1.6 Discussion of Eriochrome black T

- The optical absorption spectra in the (190 - 800) nm wavelength range for the Eriochrome black T Dye is depicted in Fig (5.25). The high absorption region is observed at wavelength (191nm is 1.4 a.u), the absorption edge of the Eriochrome black T dye corresponding to photon energy (6.5 eV).
- Fig (5.26) shows the relation between absorption coefficient and wavelengths, one found rapid decrease at 191 nm continuous decrease.
- In fig (5.27) show that relation between excitation coefficient and wavelengths it the same as absorption coefficient .And in fig (5.27) show that high value of excitation coefficient equal 3.026×10^{-6} at wavelength 797 nm .
- The optical energy band gap of Eriochrome black T was determined using the absorption spectra. According to the absorption coefficient (α) for direct band gap material is given by the relation

$$\alpha h\nu = B(h\nu - E_g)^n \qquad (5.1)$$

Where E_g the energy gap, constant B is different for different transitions, (hv) is energy of photon and (n) is an index which assumes the values 1/2, 3/2, 2 and 3 depending on the nature of the electronic transition responsible for the reflection. And by extrapolating the straight thin portion of the curve to intercept the energy axis, the value of the energy gap has been to found be (2.669 eV) as show in fig (5.28).

- Fig(5.29) shows the current-voltage characteristics obtained from the measured values this measurement was taken from solar cell of the structure (ITO/ Eriochrome black T Dye / MEH-PPV/Ag) at 0 mT effect ,

the short-circuit current (I_{sc}) is 20.25 mA , the open-circuit voltage (V_{oc}) is 0.8887 V, fill factor (FF) is 0.9749, and the efficiency is 1.87 %.

- Fig(5.30) shows the current-voltage characteristics obtained from the measured values this measurement was taken from solar cell of the structure (ITO/Ecrchrom Black T Dye / MEH-PPV/Ag) at 1 mT effect , the short-circuit current (I_{sc}) is 20.27 mA , the open-circuit voltage (V_{oc}) is 0.887 V, fill factor (FF) is 0.976, and the efficiency is 1.872 %.
- Fig(5.31) shows the current-voltage characteristics obtained from the measured values this measurement was taken from solar cell of the structure (ITO/Eriochrome black T/MEH-PPV/Ag) at 2 mT effect , the short-circuit current (I_{sc}) is 20.28 mA , the open-circuit voltage (V_{oc}) is 0.887 V, fill factor (FF) is 0.9749 , and the efficiency is 1.871 %.
- Fig(5.32) shows the current-voltage characteristics obtained from the measured values this measurement was taken from solar cell of the structure (ITO/Eriochrome black T Dye / MEH-PPV/Ag) at 3 mT effect , the short-circuit current (I_{sc}) is 20.30 mA , the open-circuit voltage (V_{oc}) is 0.887 V, fill factor (FF) is 0.9749, and the efficiency is 1.8724 %.
- Fig(5.33) shows the current-voltage characteristics obtained from the measured values this measurement was taken from solar cell of the structure (ITO/ Eriochrome black T Dye / MEH-PPV/Ag) at 4 mT effect , the short-circuit current (I_{sc}) is 20.31 mA , the open-circuit voltage (V_{oc}) is 0.887 V, fill factor (FF) is 0.9749, and the efficiency is 1.873 %.
- Fig (5.34) show that the relation between current and voltage characteristics for the five samples of Ecrchrom Black T solar cells when effect by deferent magnetic field (0, 1, 2, 3 and 4) mT . In fig (5.34) show that magnetic field increases the efficiency increase.

- The magmatic field effect on the efficiency it is very interesting to note that table (5.3) indicates the increase of magmatic field and the increases of the solar cell efficiency in general. This is since the magmatic field increase enables electrons having lower excitation energy to become free electron in a conduction band thus increasing the electric solar efficiency (by rated $7.4x10^{-7}$ % $.mT^{-1}$) as show in fig (5.35).
- The magmatic field also effect Solar Cells densities of current the results recorded in table (4.3) shows that increase of magmatic field increases densities of current. This can be under stood if one takes into account the fact that according to number of electron increase on the area of solar cell and increase chances for electrons transfer from valence to conduction(by rated $2.4x10^{-3}$ $mA.cm^{-2}$ $.mT^{-1}$) show fig (5.36).

Chapter Six
Conclusion and Recommendation

6.1 Conclusion

- This work shows that the magnetic field affects polymer solar cell performance. This performance depends on the magnetic field value.
- The energy gap of the dyes used in dye sensitized solar cell affects the performance and efficiency of the solar cell.
- The energy gab of the dyes also effect to the performance and efficiency polymer Solar cells.
- Main work was make three gropes of dye Solar cell (2.5×2.5) cm^2 with three different types of dyes.
- The purpose of this experiment is effect on these cells by four type of magnetic field for three groups (1, 2, 3, and 4 mT) and find out, the fill factor, efficiency, open-circuit voltage, short-circuit current, maximum voltage and maximum current, compare this reading with control cell at 0 mT.
- The optical absorption spectra of Rhodamine B in the range (250 - 800) nm, the absorption edge of the Rhodamine B dye corresponding to photon energy (4.9 eV, 2.9 eV and 2.1 eV). But the optical absorption spectra of Coumarin 500 and Ecrchrom Black T in the range (190 - 800) nm, the absorption edge of the Coumarin 500 dye corresponding to photon energy (5.5 eV) and the absorption edge of the Eriochrome black T dye corresponding to photon energy (6.5 eV).

- The magmatic magnetic field effect on the efficiency it is indicated that increase of magnetic field increases of the solar cell efficiency in general. This is since the magnetic field increase enables electrons having lower excitation energy to become free electron in a conduction band thus increasing the electric solar efficiency rated $1.5x10^{-4}$ % $.mT^{-1}$, $6.6x10^{-4}$ % $.mT^{-1}$ and $7.4x10^{-7}$ % mT^{-1} respectively for Rhodamine B, Coumarin 500 and Eriochrome black T
- The magnetic field also effects Solar Cells densities of current, that increase of magnetic field increases densities of current. This can be understood if one takes into account the fact that according to number of electron increase on the area of solar cell and increase chances for electrons transfer from valence to conduction rated $7.8x10^{-4}$ $mA.cm^{-2}$ $.mT^{-1}$, $4.48x10^{-7}$ $mA.cm^{-2}$ $.mT^{-1}$ and $2.4x10^{-3}$ $mA.cm^{-2}$ $.mT^{-1}$, respectively for Rhodamine B, Coumarin 500 and Eriochrome black T.
- The value of the energy gab has been to found be (3.001 eV) as Ecrchrom Black T, and (2.669 eV) for Coumarin 500 and (2.49 eV) Rhodamine B.
- The energy gap effects on Solar Cells efficiency, that decrease of energy gap increases efficiency of Solar Cells.
- Structure (ITO/ Rhodamine B dye / MEH-PPV/Ag) at 0 mT effect, the short-circuit current (I_{sc}) is 15.181 mA, the open-circuit voltage (V_{oc}) is 0.1331 V, fill factor (FF) is 0.975, and the efficiency is 0.21 %.
- (ITO/Coumarin 500 dye / MEH-PPV/Ag) at 0 mT effect, the short-circuit current (I_{sc}) is 30.44 mA, the open-circuit voltage (V_{oc}) is 0.205 V, fill factor (FF) is 0.9742, and the efficiency is 0.648 %.
- The current-voltage characteristics obtained from the measured values this measurement was taken from solar cell of the structure (ITO/

Ecrchrom Black T Dye / MEH-PPV/Ag) at 0 mT effect, the efficiency is 1.87 %.

6.2 Recommendation

- We recommend further work in this area to enhance the dye structure and produce and adjust concentration to produce good performance by finding a common solvent to the dye and the fullerene so that the solvent can be easily evaporated and yield efficient cells.
- The magnetic field must be increased then become thinness for more efficiency.
- The temperature effect on the cells properties could be further investigated as well. Other do pant materials can be used to increase the dye photoconductivity.
- More study on the solar cells as Structure by (XRD dives, SEM or TEM).
- Study faction groups by (FTIR).

References

[1] Grätzel, M. (2003) Dye-sensitized solar cells. *Journal of Photochemistry and Photobiology*.

[2] Sule Erten-Ela. (2014) Characterization and Performance Evaluation of Dye Sensitized Solar Cell Using Nanostructured TiO_2 Electrode. *International Journal of Photoenergy*, pp 6.

[3] Grätzel, M. (2003) Review Dye-sensitized solar cells. *Journal of Photochemistry and Photobiology C: Photochemistry Reviews*, 9.

[4] Kohjiro Hara, H. A. (2003) Dye-sensitized Solar Cells. *International Journal of* 2.

[5] Kohjiro Hara, H. A. (2003) Dye-Sensitized Solar Cells. *International Journal of* 3.

[6] Kohjiro Hara, H. A. (2005) Dye-sensitized Solar Cells. *Energy and Power*, 3, 4, 5, 6.

[7] Kohjiro Hara, H. A. (2005) Dye-sensitized Solar Cells. *Energy and Power*, 2.

[8] Monzir S. Abdel-Latif, M. B.A. (2015) Dye-Sensitized Solar Cells Using natural dyes. *International Journal of Renewable Energy Research*.

[9] Sathyanarayana P et al (2015) Effect of Shading on the Performance of Solar PV Panel. *Energy and Power*. Vol 5, pp1-4, doi:10.5923/c.ep.201501.01.

[10] Sofyan A. et al. (2013) Dye-sensitized solar cells using fresh and dried natural. *International Journal of Materials Science and Applications.*

[11] Sujata Saxena, A. S. (2004) Natural Dyes: Sources, Chemistry. *Natural.*

[12] A. DUMBRAVĂa, A. G. (2008) Dye-sensitized solar cells based on nanocrystalline, *Journal of Optoelectronics and Advanced Materials.*

[13] Jun Hyuk Yang, et al. (2014) Characteristics of the Dye-Sensitized Solar Cells Using TiO2 Nanotubes Treated with TiCl4. *Materials*, Vol 7, pp 3522-3532.

[14] Oluwaseun Adedokun et al. (2014) Vol. 2, No.2, 201, Review on Natural Dye-Sensitized Solar Cells (DSSCs. *International Journal of Engineering Technologies*.

[15] Al, Q. W. (2006) Enhancement of Dye-Sensitized Solar Cells by using Graphene-TiO2 Composites as Photoelectrochemical Working Electrode. *Electrochemical*.

[16] Amaresh Mishra and M. K.-c. (2003) Metal-Free organic dyes for dyes sensitized solar cell. *Angewandte chemie International Edition*.

[17] Amaresh Mishra and M. K.-c. (2009) Metal-Free organic dyes for Dyes-sensitized solar cells. *Angewandte chemie Interrnational edition*.

[19] Berkovski, B. (1996) Magnetic Fluids and Applications Handbook. Begell House, Inc, New York, U.S.A.

[20] Piso, M. I. J. et al. (1999) *Mater* 201, 380.

[21] Yamaguchi, H et al (1999) *Mater* 201, 260.

[22] Rosensweig, R. E. *Nature* (1966), 210, 613.

[23] Horng, H. E, et al. (2001) *Phys. Chem. Solids*, Vol 62, 1749.

[24] Hong, C. Y. et al. (2001). Appl. Phys. Letter. 79, 2360.

[25] Tsebers, A. O. Magn. Gidro. (1982), Vol 18, 42 in Russian, English translation: Magnetohydrodynamics, (1983), Vol 18, 345.

[26] Sano, K.; Doi, M. (1983) *J. Phys. Soc. Jpn*. Vol 52, 2810.

[27] Yusuf, N. A. (1989) *J. Phys. D: Appl. Phys.* Vol 22, 1916.

[28] Hong, C. Y. R, et al. U. S. Pat. No 5948321.

[29] Horng, H. E et al (1999), pp 201, 215.

[30] Hong, C.Y., J. Appl. Phys. (1999), Vol 85, 5962.

[31] Wanquan Jiang, et al. (2004) Preparation and properties of superparamagnetic nanoparticles with narrow size distribution and biocompatible. Journal of Magnetism and Magnetic Materials,Vol 283, pp 5, 210-214.

[32] Jones, G. A. and Niedoba, H. J. Magn. Magn.Mater. (1988), 73, 33.

[33] Jones, G. A and Moman, A. IEEE Trans. Magn.(1990), 26, 1849.

[34] Cernak J.; Macko, P. J. Magn. Magn. Mater.(1993), 123, 107.

[35] Wang, Hao. (1994) Periodic branched structures in a phase-separated magnetic colloid *Phys. Rev. Lett*. 72, 1929.

[36] Ytreberg, F.; Marty, M.; *Susan R. Phys. Rev. E* (2000), 61, 4107.

[37] Hong, C. Y, et al. (1997) *J. Appl. Phys.* 81, 4275.

[38] Shieh-Yueh Yang, et al. (2002) Structures, Optical Properties and Potentially Electro-Optical Applications of Magnetic Fluid Films *Tamkang Journal of Science and Engineering*, Vol. 5, No. 2, pp. 85-93.

[39] A. J. Epstein, Y. Yang, (1997) Polymeric and Organic Electronic Materials: from Scientific Curiosity to Applications, MRS Bull. 22, 13.

[40] Ma, Z. et al (2012) Synthesis and characterization of benzodithiophene–isoindigo polymers for solar cells. *J. Mater. Chem*, 22, 2306–2314.

[41]Ali VeyselTunc et al, (2011) Molecular doping of low-bandgap-polymer fullerene solar cells. Effects on transport and solar cells. 1435 No. pp 7, Model 3G 6.

[42]K. Gurunathan et al. (1999) Electrochemically synthesised conducting polymeric materials for applications towards technology in electronics,

optoelectronics and energy storage devices. *Materials Chemistry and Physics* 61 pp 173, 191.

[43] Xiong Gong1, et al, (2006) Enhanced electron injection in polymer light-emitting diodes: polyhedral oligomericsilsesquioxanes. *Journal of physics d*: Appl. Phys. 39 2048–2052.

[44] M. Drees, et al (2002) Creation of a gradient polymer-fullerene interface in photovoltaic devices by thermally controlled interdiffusion Applied Physics letters v 81.

[45] Abdelsakhi .S.M. (2016) Using Gum Arabic in Making Solar Cells by Thin Films Instead Of Polymers - IOSR Journal of Applied Physics (IOSR-JAP) ISSN: 2278-4861.Volume 8, Issue 1 Ver. III, PP 27-32.

[46] Dong-JooKwak, Byung-Ho Moon, Don-Kyu Lee, Cha-Soo Park and Youl-Moon Sung - Journal of Electrical Engineering & Technology Vol. 6, No. 5, pp. 684~687, 2011

[47] Sakina Ibrahim Ali , Mubarak Dirar Abdallah and Sawsan Ahmed Elhouri Ahmed. (2016) *International Journal of Current Trends in Engineering & Research* (IJCTER) e-ISSN 2455–1392 Vol 2, 7, pp. 82 – 89.

[48] James A. Marusek (2007) Impact. *Solar Storm Threat Analysis.*

[49] B.C. Yadav and Ritesh Kumar (2008) Structure, properties and applications of fullerenes . *International Journal of Nanotechnology and Applications* ISSN 0973-631X, V 2, No 1, pp. 15–24 © Research India Publications.

[50] WiHyoung Lee and Yeong Don Park (2014) Organic Semiconductor, Insulator Polymer Blends for High-Performance Organic Transistors, Polymers 6, 1057-1073; doi: 10.3390. polym 6041057-ISSN-2073-60.

[51] SHI Quan-Min. (2009) Role of TiO2 Nanotube on Improvement of Performance of Hybrid Photovoltaic Devices. *PHYS. LETT*. Vol. 26, No.1- 017202.

[52] J.H. Parka and Non-linear (2001) I_V characteristics of MEH-PPV patterned on sub-micrometer electrodes. Thin Solid Films 393 pp 129_131. DOI: 10.1016/S0040-6090(01)01118-X.

[53] A. Mayer, et al. (2007) Polymer-based solar cells Materials. *SienceDirect*, Vol 10, 11, pp 28-33, https://doi.org/10.1016/S1369-7021(07)70276-6.

[54] Ma, Z, et al (2012) Synthesis and characterization of benzodithiophene–isoindigo polymers for solar cells. *J. Mater. Chem*. 22-2306–2314.

[55]Kang B. et al. (2008) Fluoropolymer indium-tin-oxide buffer layers for improved power conversion in organic photovoltaics Appl. Phys. Lett. 93, 133302, https://doi.org/10.1063/1.2983742.

[54] Yoo I. et al. (2005) The effect of a buffer layer on the photovoltaic properties of solar cells with P3OT. *Synth. Met.* 153 pp 97.

[56] Tao C. (2009) Role of tungsten oxide in inverted polymer solar cells. *Appl. Phys. Lett*. 94 043311.

[57] A. Bewick, M. Fleischmann, H.R. Thirsk, Trans. Faraday Soc., 58 (1962) 2200.

[58] S. Bijani, R. Schrebler, E.A. Dalchiele, M. Gabás, L. Martínez, and J. R. Ramos-Barrado, J. Phys. Chem. C, 115 (2011) 21373.

[59] T.L. Barr and Y.L. Liu,(1989) *J. Phys. Chem. Solids*, 50 pp 657.

[60] B.D. Cullity.(1978) Elements of X-ray Diffraction 2nd Ed. Addi-son-Wesley, Reading MA.

[61] W. Vallejo and J. Clavijo, Brazilian. (2010) Journal of Physics, Vol 40, 30.

[62] P. O'Brien, D. J. Otway, and J. R.Walsh. (1998) Thin Solid Films, Vol 315, 57.

[63] R. Henríquez, et al. (2010) Thin Solid Films, Vol 518, 1774.

[64] R. Yoosuf and M.K. Jayaraj. (2005) Sol Energy Mater Sol Cells, Vol 89, 85.

[65] R.E. Marotti, et al. (2008)Thin Solid Films, Vol 517, 1077.

[66] A. Akkari, et al (2011) Sci. Vol 46, 6285.

[67] M. Klein el al. (2016) Magnetic field effects in dye sensitized solar cells controlled by different cell architecture, Vol 6, 30077, DOI:10.1038/srep30077.

List of Publications

1- **[Ragab, 5(8): August 2018]** THE VALUE OF EFFICIENCY & ENERGY GAP FOR DIFFERENT DYE SOLAR CELLS, GLOBAL JOURNAL OF ENGINEERING SCIENCE AND RESEARCHES DOI- 10.5281/zenodo.1343451

2- **[Ragab, 5(8): August 2018]** THE EFFECT OF MAGNETIC FIELD INTENSITY ON THE EFFICIENCY OF DYE SOLAR CELLS , GLOBAL JOURNAL OF ENGINEERING SCIENCE AND RESEARCHES, DOI- 10.5281/zenodo.1343453